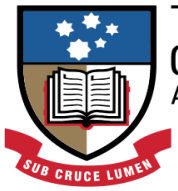

THE UNIVERSITY OF ADELAIDE
AUSTRALIA

University of Nottingham
UK | CHINA | MALAYSIA

Utilising Light in Assistive Reproductive Technologies

Carl Adrian Ang Campugan

School of Biomedicine

Discipline of Reproduction and Development

Robinson Research Institute

University of Adelaide

School of Electronic and Electrical Engineering

Optics and Photonics Group

University of Nottingham

Thesis submitted to The University of Adelaide in fulfilment of the requirements for admission to the degree of Doctor of Philosophy for a joint doctoral degree between the University of Adelaide and the University of Nottingham

Table of Contents

"The difference between a successful person and others is not a lack of strength, not a lack of knowledge, but rather a lack in will."

Vince Lombardi

Abstract

Utilising light in Assistive Reproductive Technologies

Carl Adrian A. Campugan

Despite advances in assisted reproductive technologies (ART) such as in vitro fertilisation (IVF), success rates remain low at around 20% per initiated cycle. The quality of oocytes and embryos are key determinants of IVF success. During an IVF cycle, multiple oocytes are harvested, and several embryos generated. Accurate assessment and ranking of these to identify those with the highest developmental potential would assist in patients achieving pregnancy in fewer IVF cycles. However, current assessments are subjective or invasive and importantly, do not improve live birth rate. This highlights the need for objective methods for evaluating oocyte and embryo quality. Light-based technologies, such as optical imaging, show promise in assessing intrinsic indicators of quality including metabolic activity. Beyond this, light can also be innovatively applied to measure the viscous properties of the microenvironment surrounding oocytes and embryos—an area previously unexplored in IVF but known to correlate with health in other cell types. This thesis investigates the use of optical tweezers for passive microrheology to measure viscosity in the oocyte and embryo microenvironment, examining its potential relationship with viability. Furthermore, as light-based technologies increase in prominence, I also investigated how light exposure affects embryos.

The first part of this thesis demonstrated the utility of optical tweezers to quantify the viscosity of the cumulus-oocyte extracellular matrix (ECM). I found that the viscosity of the ECM positively correlated with oocyte viability. This approach has the potential to become an objective and reliable method for assessing oocyte quality in the future.

This thesis then explored how optical tweezers can measure the viscosity of the microenvironment surrounding 4 cell- and blastocyst-stage embryos. Here, I report that the viscosity of the blastocyst

microenvironment was significantly higher than that of the earlier 4 cell-stage embryo. The findings of this study were the first to show a developmental-stage difference in the viscosity of the embryo microenvironment. These findings provide novel insights into extracellular changes that accompany pre-implantation development and dynamic shifts in metabolism.

Finally, this thesis investigated the impact of light exposure on embryo development, a crucial but often overlooked aspect of IVF. Using standardised experimental conditions, I assessed how exposure to specific wavelengths of light—common in optical imaging systems—affects embryo development, cell lineage allocation, DNA integrity, lipid abundance, and post-transfer outcomes. The findings show that morphological evaluation alone fails to capture wavelength-specific effects of light exposure on embryos. This underscores the critical importance of controlling light exposure during IVF procedures.

Collectively, Chapter 2 and 3 introduce a novel use of light, via optical tweezers, to quantitatively measure the viscosity of the microenvironment surrounding the oocyte and embryo. These studies highlight the potential for microrheology with optical tweezers to non-invasively measure viability- and developmental stage-specific differences in viscosity. While the use of light is essential in ART, Chapter 4 highlights the importance of managing the exposure of embryos to specific wavelengths during handling or imaging. Certain wavelengths may need to be avoided, or their effects mitigated to safeguard embryo viability.

Declaration

I certify that this work contains no material which has been accepted for the award of any other degree or diploma in my name, in any university or other tertiary institution and, to the best of my knowledge and belief, contains no material previously published or written by another person, except where due reference has been made in the text. In addition, I certify that no part of this work will, in the future, be used in a submission in my name, for any other degree or diploma in any university or other tertiary institution without the prior approval of the University of Adelaide and where applicable, any partner institution responsible for the joint award of this degree.

The author acknowledges that copyright of published works contained within the thesis resides with the copyright holder(s) of those works.

I give permission for the digital version of my thesis to be made available on the web, via the University's digital research repository, the Library Search, and also through web search engines, unless permission has been granted by the University to restrict access for a period of time.

I acknowledge the support I have received for my research through the provision of an Australian Government Research Training Program Scholarship.

Carl Adrian Ang Campugan

November 2024

Acknowledgements

The work presented in this thesis is the culmination of many years of research. As such, it is important for me to properly accredit the many individuals who have contributed, influenced, inspired, and supported this work – some directly, others unapparent, but nonetheless all of equal importance. First and foremost, my sincerest gratitude to my supervisors: A/Prof Kylie Dunning, Prof. Kishan Dholakia, Prof. Amanda J Wright, and Dr Tania Mendonca. The personal and professional support, the values you instilled, and the passion for science you have all given me during my PhD has really made this journey like no other. I recognise that I have been afforded plenty of professional opportunities during the past 4 years and it is by everyone's feedback and encouragement that have allowed me to continue to develop into the person that I am.

Beyond these 4 years, it would be negligent of me not to recognise and express a special thanks to Kylie. I recall having started my academic journey with you many years ago as an honours student. You were my first exposure to an academic professional, and still to this day, you are the golden standard that I uphold other academics to. I count myself truly fortunate for having been under your tutelage. Thank you for your support and believing in me, even during times where my belief in myself faltered.

To my lab colleagues in the University of Adelaide, it feels personally wrong to even call you colleagues as you all are very much family to me. From the bottom of my heart, thank you for being the ears that listen to me, the mouths that support me, and the eyes that look at me with kindness. Tiffany, Meg, and last but never the least Darren – the passionate laughs and compassionate wisdom you have imparted to me have really brightened up my darkest of days. You have allowed me to seek help beyond myself, and I never have felt lonely since.

My lab colleagues in both Adelaide and Nottingham, in no specific order: Dr Chris Perrella, Dr. Erik Schartner, Shan and Tong Li, Kerry Setchfield, Yihan and Yujang. Though retrospectively, our time doing

research may have been brief, you all provided me various support that have really aided me during my PhD. Your patience, understanding, and friendship have been important to me during this time.

Also, in both Adelaide and Nottingham, I have been really fortunate in being able to develop and form friendships that have enriched my life within and outside of academia. My friends in Adelaide: collectively referred to as “OKRAM Group”, my high school friends Roberto and Donovan, and my friends in Nottingham affectionally referred to as “Pre pre pres” (Demi, Kevin, Leo, Ashley, Edward, Maria, Millie, Cecilia, Abi, Ryan, and Jerry). Your friendships and inputs have always been appreciated and each of you have left a remarkable impact in my life. To call each one of you my dearest friend is a real privilege of mine, know that I am and will always be there for each of you.

During my time in research, it is apparent to me that this is a real privilege that not everyone is given. This work may not exist without the generous funding of the scholarships awarded by the University of Adelaide, the University of Nottingham, the Australian Research Council, and Channel 7 Children’s Research foundation.

Finally, I may have never survived the hurdles of a PhD without the relentless love, care, and support of my family. My parents, Baltazar and Marie Campugan, it was by you instilling the importance of education and fostering such a sanctuary that I can be the person I am today. Not a day goes by where I don’t think about what my life may have been like had you chosen to not sacrifice your careers in the Philippines. It was only by your selfless love and guidance as parents that I have been able to reach and grasp the stars that have always looked so far to me. The many experiences I have been grateful to call mine, may have never been without you and this dissertation is dedicated to both of you. To my younger sister Justine, there have been many times where I question on which of us is the older sibling, you have been a kind personal councillor to me, and most importantly have become my best friend, being able to witness your continuous growth as a person over the years has brought so much pride. No matter what I am always here for you. Finally, the latest addition to the family, to Mochi, though you may be unable to

transcribe these words, you have provided the family and I countless joys over the years and no Campugan family would ever feel complete without you.

Publications arising from this thesis

1. **Campugan, C. A**., Dunning, K. R., & Dholakia, K. (2020). Optical manipulation: a step change for biomedical science. Contemporary Physics, 61(4), 1-18.
2. **Campugan, C.A**., Lim, M., Chow, D.J., Tan, T.C., Li, T., Saini, A.A., Orth, A., Reineck, P., Schartner, E.P., Thompson, J.G., Dholakia, K., and Dunning, K. R., (2022). The effect of discrete wavelengths of visible light on the developing murine embryo. *Journal of Assisted Reproduction and Genetics*, *39*(8), pp.1825-1837.

Abstracts arising from this thesis

2022

1. **Campugan C.A.,** Lim M., Chow D.J.X., Tan T.C.Y., Li T., Saini A., Orth A., Reineck P., Schartner E., Thompson J., Dholakia K., Dunning K.R. Impact of discrete wavelength of light on embryo development. Society for Reproductive Biology conference, Auckland, New Zealand
2. **Campugan C.A**., Lim M., Chow D.J.X., Tan T.C.Y., Li T., Saini A., Orth A., Reineck P., Schartner E., Thompson J., Dholakia K., Dunning K.R. *The effect of discrete wavelengths of visible light on the developing murine embryo.* Australian Institute of Physics Congress, Adelaide, Australia.
3. **Campugan C.A**., Lim M., Tan T.C.Y., Schartner E., Arita Y., Bruce G., Mendonca T., Wright A.J., Dholakia K., Dunning K.R. *Microrheology of the Cumulus-Oocyte matrix using optical tweezers.* Society for Reproductive Biology conference, Auckland, New Zealand
4. **Campugan C.A.,** Lim M., Tan T.C.Y., Schartner E., Arita Y., Bruce G., Mendonca T., Wright A.J., Dholakia K., Dunning K.R. *Microrheology of the Cumulus-Oocyte matrix using optical tweezers.* Australian Institute of Physics Congress, Adelaide, Australia.

2023

1. **Campugan C.A.,** Lim M., Tan T.C.Y., Schartner E., Arita Y., Bruce G., Mendonca T., Wright A.J., Dholakia K., Dunning K.R. *Microrheology of the Cumulus-Oocyte matrix using optical tweezers.* Biophotonics Summer School., Hven, Sweden

2024

1. **Campugan C.A**., Lim M., Tan T.C.Y., Schartner E., Arita Y., Bruce G., Mendonca T., Wright A.J., Dholakia K., Dunning K.R. *Microrheology of the Cumulus-Oocyte matrix using optical tweezers.* Robinson Research Institute Symposium, Adelaide, Australia

2. **Campugan C.A**., Lim M., Tan T.C.Y., Schartner E., Arita Y., Bruce G., Mendonca T., Wright A.J., Dholakia K., Dunning K.R. *Microrheology of the Cumulus-Oocyte matrix using optical tweezers.* Society for Reproductive Biology conference, Adelaide, Australia
3. **Campugan C.A.,** Lim M., Tan T.C.Y., Schartner E., Arita Y., Bruce G., Mendonca T., Wright A.J., Dholakia K., Dunning K.R. *Microrheology of the Cumulus-Oocyte matrix using optical tweezers.* Nanoscience + Engineering, San Diego, California, United STates

List of Acronyms and Abbreviations

ART	Assisted Reproductive Technologies
BSA	Bovine Serum Albumin
COC	Cumulus-oocyte complex
CO_2	Carbon Dioxide
ECM	Extracellular matrix
eCG	Equine chorionic gonadotrophin
hCG	Human chorionic gonadotrophin
ICM	Inner Cell Mass
IU	International units
IVF	In vitro fertilisation
Min	Minute
N_2	Nitrogen
O_2	Oxygen
PBS	Phosphate-buffered saline
PFA	Paraformaldehyde
PVA	Polyvinyl-alcohol
SEM	Standard error of the mean
3D	Three dimensions
2D	Two dimensions

Chapter 1
Introduction

1.1 Infertility and IVF

Infertility is defined as the inability to conceive after one year of regular, unprotected intercourse. This has become an increasingly prevalent global issue [1]. It is estimated that approximately 17.5% of the adult population worldwide will experience infertility [2]. In Australia and New Zealand, this rising prevalence has led to a reliance on assisted reproductive technologies, including in vitro fertilisation (IVF), as a means to overcome infertility. This rising reliance on IVF is reflected by the annual growth in the number of initiated cycles. The number of such cycles has increased by approximately 8% each year since 1999 (when such record keeping began), with an overall fourfold increase between 1999 to 2021 [3]. However, IVF success has remained stagnant for more than a decade with only ~ 20% of initiated cycles resulting in a live birth [3]. This poses significant financial, emotional, mental, and physical challenges for individuals undergoing IVF treatment. Thus, there are ongoing efforts to improve this success rate.

Clinical IVF involves the retrieval of multiple oocytes (female gamete or eggs) which are then fertilised by spermatozoa (male gametes) in vitro. The resulting fertilised embryos undergo pre-implantation development in a controlled culture environment for several days. During this period, the pre-implantation embryo undergoes significant physiological and morphological changes. This includes increasing cell numbers due to mitotic divisions [4], activation of the human embryonic genome between the 4- and 8-cell stage of development [5-7], and differentiation of cells into distinct lineages at the blastocyst-stage [8]. Following fertilisation, the pre-implantation phase of development covers the progression from a single cell-embryo, to a multicellular, blastocyst-stage embryo with two distinct cell lineages – the trophectoderm and the inner cell mass which form the placenta and the offspring, respectively [9]. In vitro, blastocyst-stage embryos are graded based on morphological features [10], where a single high-grade blastocyst is subsequently transferred into the female uterus with the hope of achieving implantation and pregnancy. In this context, the quality of both the embryo and the oocyte are key determinants for IVF success [11-14].

1.2 Assessment of oocyte and embryo quality

Presently, morphological evaluation is the primary method for assessing oocyte and embryo quality in IVF procedures [15-17]. For oocytes, assessments typically focus on characteristics such as polar body extrusion and morphology [18-20], zona pellucida appearance and thickness [21, 22], and cumulus expansion following oocyte maturation [23]. Embryo evaluation, on the other hand, considers factors such as cellular/blastomere symmetry [24], blastocyst expansion, as well as inner cell mass and trophectoderm number and organisation [10]. Although morphological evaluation is standard practice in most IVF clinics, the reliability of these assessments may be affected by variability in grading systems across clinics and the subjectivity associated with assessments performed by different embryologists [25]. Furthermore, correlation between morphological features and developmental potential of the oocyte and embryo remains contentious, with conflicting evidence that overall suggests a lack of predictive capability [26-28]. This highlights the need for more objective and reliable methods to assess oocyte and embryo quality. Light-based techniques offer a promising alternative. Recent studies using optical imaging techniques such as digital holographic microscopy, hyperspectral microscopy, and confocal microscopy have been shown to provide objective measurements of intracellular metabolism and refractive index within the oocyte and embryo [29-31]. As an example, digital holographic microscopy may distinguish between high and poor quality embryos by quantifying refractive index variations that reflect lipid content [29]. A high lipid concentration is detrimental to embryo health as it dysregulates cellular metabolism [32]. Light sheet microscopy has been able to record autofluorescence from metabolic cofactors such as nicotinamide adenine dinucleotide (phosphate) and flavin adenine dinucleotide, in both oocytes and embryos, which allows determination of the optical redox ratio and overall cell metabolism [30, 31]. As ATP generation is important for oocyte viability [33, 34], light-based approaches to measuring metabolism is likely predictive of developmental potential. Further, such optical approaches have demonstrated potential for non-invasively discriminating between euploid (predicted number of chromosome) and aneuploid (chromosome number deviates from expected) embryos [30]. These approaches are label-free

and demonstrate the potential of optical imaging to non-invasively assess oocyte and embryo developmental potential. However, they are not able to assess the mechanical properties of the surrounding microenvironment of these cells – a key indicator of cell function and viability in many cell types [35, 36]. Changes in the microenvironment may alter the development of oocytes and embryos. Thus, assessing the mechanical properties of the microenvironment may provide valuable insights and serve as a potential predictor of viability. In contrast to traditional morphological evaluations, understanding the properties of the surrounding microenvironment may offer a novel, objective approach to assessing oocyte and embryo quality, complementing existing methods while also advancing our understanding of the importance of these microenvironments for the developing oocyte and embryo.

1.3 The role of the microenvironment in oocyte and embryo development

The microenvironment around cells plays an integral role in regulating cellular function [37], behaviour [38], and fate [39-45]. These microenvironments are dynamic and complex, composed of both soluble components, like growth factors or cytokines, and insoluble components, like hyaluronan [46]. Considering its importance in regulating cellular health and function in other cell types, the microenvironment surrounding oocytes and embryos may provide insight into viability.

For the oocyte, formation of a specialised microenvironment occurs during the final stages of maturation – a process necessary for successful fertilisation [47]. During maturation, the somatic cells surrounding the oocyte (cumulus cells) secrete a complex extracellular matrix (ECM). This is comprised primarily of glycosaminoglycans and proteoglycans [48-51]. The predominant component of this ECM is the glycosaminoglycan, hyaluronan [48]. This is synthesised by the enzyme hyaluronan synthase 2 (Has2) in response to a surge of luteinising hormone (LH) in vivo [52]. This synthesis leads to the generation of a matrix that acts as a physical barrier, regulating the exposure of the oocyte to its environment [53] and persisting to fertilisation where it functions to regulate sperm penetration [54, 55]. In the context of clinical

fertility treatment, some patients may require the harvesting of oocytes prior to maturation due to specific medical or logistical concerns (e.g., avoiding ovarian hyperstimulation syndrome, reducing the cost of treatment and fertility preservation). Oocyte maturation in vitro however, results in the formation of a vastly different cumulus matrix and poorer quality oocytes compared to their in vivo matured counterparts [53, 56]. Oocytes matured in vitro have significantly reduced expression of ECM components, including versican (Vcan) and the enzyme Adamts1, which are highly active during oocyte maturation and ovulation in vivo [56]. In vivo, *Vcan* is expressed in response to the LH surge, with its cleavage by Adamts1 playing an important function in cumulus expansion and oocyte developmental potential [57, 58]. Interestingly, several studies have linked higher expression of cumulus matrix genes, including *HAS2* and *Vcan*, to higher fertilisation rates [59-61], better embryo quality [59-61], and increased implantation success [62, 63]. While ECM composition is associated with oocyte developmental competence, there is limited knowledge on whether the mechanical property of this ECM differs between oocytes matured in vivo and in vitro. An example of a study in this area was conducted by Chen et al (2016) who used atomic force microscopy to show that the ECM surrounding oocytes has elastic properties that may differ between in vivo and in vitro matured oocytes [64]. Though the study is the first of its kind to identify a correlation between ECM elasticity and oocyte maturation condition, it requires deformation of the intact cumulus oocyte complex which is likely not conducive with clinical practice.

Regarding the embryo, the microenvironment has an important role during pre-implantation development. In vivo, the fertilised embryo is surrounded by a complex uterine microenvironment, consisting of a unique combination of biochemical signals, nutrients, and hormones that significantly influence embryo development [65, 66]. The female reproductive tract provides a highly dynamic environment, characterised by a substrate gradient tailored to meet the changing metabolic needs of the developing embryo. In the oviduct, where early embryo development occurs (from the 1-cell to the 8-cell stage), pyruvate and lactate levels are high. These metabolites serve as the primary substrates for oxidative phosphorylation, the predominant metabolic pathway used during this stage of development [65, 67, 68].

As the embryo transits towards the uterus, pyruvate concentrations decrease, while glucose levels rise. This shift coincides with the embryo transitioning from oxidative phosphorylation to glycolysis, utilising glucose as the substrate to meet the increased metabolic demands post-compaction (8-cell to blastocyst cell stage) [68-70]. This metabolic shift, is crucial for supporting rapid cell divisions and the formation of the fluid-filled blastocoel cavity at the blastocyst stage [65, 71]. The critical role of these substrates during embryo development is underscored by studies showing that the absence of pyruvate or glucose during in vitro culture leads to developmental arrest. Specifically, a lack of pyruvate results in blocked embryo development prior to compaction, while glucose deficiency prevents progression to the blastocyst stage post-compaction [72]. Interestingly, glucose uptake is positively correlated with viability at the blastocyst stage [73]. However, the majority of this is not used for energy production via oxidation but instead converted to lactate which is secreted into the surrounding microenvironment [74]. In vivo, lactate is secreted into the surrounding fluid and may facilitate key events such as invasion, angiogenesis, and modulation of the immune response during implantation [75]. In vitro however, the amount of secreted lactate may be a useful surrogate measurement of embryo viability at this stage of development. As high concentrations of lactate in whole blood lead to an increase in viscosity [76], it would be interesting to determine if the microenvironment surrounding blastocyst stage embryos in vitro are higher in viscosity than earlier stages of pre-implantation development, that predominantly use oxidative phosphorylation rather than glycolysis. Thus, characterisation of mechanical changes of the microenvironment, that reflect metabolic activity, may provide an important predictor for embryo development and implantation success.

In summary, the oocyte and embryo are surrounded by a highly complex and dynamic environment. Whether changes in viscosity of these microenvironments are associated with viability is yet to be determined. Measuring the mechanical properties of their microenvironments may provide a diagnostic for oocyte and embryo developmental potential. However, as these cellular environments in vitro occur in a microlitre volume [64], an appropriate method for measuring viscosity at this scale is required. In this context, optical tweezers may provide a solution. In the following published review, I explore the history

and principles behind optical tweezers, highlighting its key applications in the study of various biological samples. Following the review, I describe the use of the optical tweezers for passive microrheology and how analysis of particle motion may be used to quantitatively measure the viscosity of the oocyte and embryo microenvironment. As this thesis describes the use of light in assisted reproductive technologies, the final section of this introduction aims to identify current research on the impact of light exposure on the developing embryo.

1.4 Statement of Authorship

Statement of Authorship

Title of Paper	Optical manipulation: a step change for biomedical science
Publication Status	☑ Published ☐ Accepted for Publication ☐ Submitted for Publication ☐ Unpublished and Unsubmitted w ork w ritten in manuscript style
Publication Details	Published in *Contemporary Physics*, July 2, 2021

Principal Author

Name of Principal Author (Candidate)	Carl Adrian Campugan		
Contribution to the Paper	My contributions to this paper were: • Wrote, edited, and approved the final version for publication		
Overall percentage (%)	50%		
Certification:	This paper is a literature review written during the period of my Higher Degree by Research candidature and is not subject to any obligations or contractual agreements with a third party that would constrain its inclusion in this thesis. I am the primary author of this paper.		
Signature		Date	30/10/24

Co-Author Contributions

By signing the Statement of Authorship, each author certifies that:

i. the candidate's stated contribution to the publication is accurate (as detailed above);

ii. permission is granted for the candidate in include the publication in the thesis; and

iii. the sum of all co-author contributions is equal to 100% less the candidate's stated contribution.

Name of Co-Author	Associate Prof. Kylie R. Dunning		
Contribution to the Paper	• Wrote, edited, and approved the final version for publication. • Accepts responsibility for all aspects of the work, ensuring that any questions regarding the accuracy or integrity of the content are thoroughly investigated and addressed.		
Signature		Date	19/11/2024

Name of Co-Author	Prof. Kishan Dholakia		
Contribution to the Paper	• Wrote, edited, and approved the final version for publication. • Accepts responsibility for all aspects of the work, ensuring that any questions regarding the accuracy or integrity of the content are thoroughly investigated and addressed.		
Signature	K Dholakia	Date	19/11/2024

1.5 Optical Manipulation: a step change for biomedical science

CONTEMPORARY PHYSICS
2020, VOL. 61, NO. 4, 277–294
https://doi.org/10.1080/00107514.2021.1930707

Optical manipulation: a step change for biomedical science

Carl A. Campugan [a,b], Kylie R. Dunning [a,b,c] and Kishan Dholakia [c,d,e,f]

[a]Robinson Research Institute, Adelaide Medical School, The University of Adelaide, Adelaide, Australia; [b]Australian Research Council Centre of Excellence for Nanoscale BioPhotonics, The University of Adelaide, Adelaide, Australia; [c]Institute for Photonics and Advanced Sensing, The University of Adelaide, Adelaide, Australia; [d]School of Physics and Astronomy, University of St Andrews, North Haugh, Scotland; [e]School of Biological Sciences, The University of Adelaide, Adelaide, Australia; [f]Department of Physics, College of Science, Yonsei University, Seoul, South Korea

ABSTRACT
The transfer of optical momentum can exert miniscule but important forces on biological specimens. This area of optical manipulation has been thriving for over 50 years. Its importance was recognised by the award of half of the Nobel Prize in Physics in 2018 to Arthur Ashkin for the use of a single focused light beam for manipulation, namely optical tweezers. This article reviews the basic physics of trapping and gives an overview of the basic premise of the field. We particularly focus upon its importance and impact on the biomedical sciences.

ARTICLE HISTORY
Received 24 March 2021
Accepted 29 March 2021

KEYWORDS
Optical tweezers; optical trap; biophysics

1. Introduction

In Physics, light holds a special place. Its invariance of speed in different frames of reference is key to understanding relativity. In the standard model it mediates the electromagnetic interaction. Importantly, the photon – the quantum of electromagnetic radiation – possesses momentum. Einstein's famous experiment on the photoelectric effect in 1905 was a clear indicator of the concept of light comprising of quantised units of energy, the photon. This was followed by the famous Compton effect experiment in 1922 that conclusively showed that a photon carried momentum proportional to its wave number.

The history of the momentum of light exerting a force goes back to the sixteenth century, to the German astronomer, Peter Apian. In 1531, he illustrated his observations in careful hand-coloured drawings showing the tail of Halley's Comet extending away from the sun. Johannes Kepler followed up with further thoughts on the origins of the behaviour of comet tails. In 1619 he published his view on why the tails of comets, on their highly eccentric orbits, point away from the sun. To explain his observations, Kepler invoked the notion of solar light pressure – a radical notion signifying the basis that light could exert a force. The solar interaction with such a celestial object led Kepler to believe that a space sail might one day harness sunlight, in the same manner as the sail of a boat captures the wind.

The concept of electromagnetic radiation was developed and at the beginning of the twentieth century. Nichols and Hull performed a key study of the radiation pressure of light being exerted on a macroscopic object. James Clerk Maxwell had calculated stresses in the electromagnetic field and predicted this outcome in 1873. Based on a thermodynamics viewpoint, Adolpho Bartoli also predicted the effect in 1876. Nichols and Hull circumvented shortcomings of previous attempts, due to residual gases, incorporating both the ubiquitous gas heating and ballistic effects in such a system and in this way, verified Maxwell's theory [1,2]. A separate demonstration was undertaken at that time by Pyotr Lebedev at Moscow State University in Russia [3].

Whilst important, it took a landmark discovery in optics to make an advance for optical forces: in 1960 Theodore Maiman invented the first laser, heralding a step change in the use and application of light. In the 1960s Arthur Ashkin and others started investigating the light–matter interaction in new ways, aiming to utilise of optical forces across a wide range of the sciences. This force is a result of the change of the momentum of light with matter. However, this momentum p, given by the famous de Broglie relation $p = h/\lambda$ (where λ is the wavelength and h is Planck's constant), is miniscule: for a photon of visible wavelength it is around 10^{-27} kg ms^{-1}. However, at the mesoscopic scale (nanometre to micrometre size), the mechanical effects

CONTACT Kishan Dholakia kd1@st-andrews.ac.uk

of optical fields have made a significant impact that is not restricted to biological material. They have given key insights into fundamental physics, colloidal science, chemical interactions and beyond, showing its immense reach across the sciences.

In this review, we will focus on the impact of optical forces on biomedicine. Ashkin was the key pioneer of the field of optical manipulation for mesoscopic particles. He was also passionate about trapping atoms with light which has emerged separately as a major field with impact in atomic and quantum physics. Optical manipulation has seen unprecedented expansion in the last five decades, culminating in the award of half of the Nobel Prize in Physics in 2018 to Ashkin for his work and its impact on biology. It is this latter aspect that forms the focus of this review. We note optical tweezers have made an exceptionally widespread impact across all the sciences, enhancing our understanding of the light–matter interaction, the nuances of structured light, nonequilibrium thermodynamics and even inroads into optomechanics. We are not able to cover all these topics here and refer the interested reader elsewhere [4–7]. To date, the biomedical sciences have perhaps seen the most significant impact with optical traps and this is the key topic of this article. We begin with a discussion of the basic geometries developed from a physics standpoint covering the main types of optical traps. We mention the theoretical modelling that can be applied to understand the forces on a trapped particle and then progress to focus on how this can be tailored to measure force and displacement accurately, a crucial aspect for the biological sciences. We then elucidate how optical manipulation can be used for answering key questions for single-molecule biophysics, cellular studies and *in vivo* applications.

2. The development of optical manipulation and optical tweezers

Ashkin's first study used micron-sized spheres manipulated with a visible wavelength laser source [8]. Sending the laser beam horizontally into a liquid sample medium, aligned these microspheres with the beam propagation axis. These microspheres were then seen to be propelled along the laser beam direction due to radiation pressure. This was the first demonstration of optical guiding: the relay of particles along the bright centre of a propagating light beam [8]. This may be understood as follows: the optical force from the gradient of the light field draws the object into the beam axis and a radiation pressure (scattering) component propels the particle along the beam propagation axis. This is the case for particles of higher refractive index than that of their surroundings. Ashkin added a second counter-propagating light beam (of the same power) creating a radiation pressure force in the opposite direction. Under these conditions, the particle came to rest between the two laser beams, realising the first optical trap. This was the so-termed counter-propagating dual-beam trap geometry [8]. Using single-mode optical fibres rather than free space optics makes this dual-beam trap system more practical [9]. In itself, the counter-propagating beam trap is important for the biomedical sciences and we shall discuss its particular attributes later in this article.

A milestone was reached in 1986: Ashkin and colleagues demonstrated how one light field could confine a particle using the single-beam gradient trap, known as optical tweezers [10]. This is cemented as the most widely used method for applying optical forces to hold and manipulate microscopic particles. Such optical tweezers are compatible with a standard microscope and may be implemented solely using a microscope objective with a high numerical aperture typically above unity. The laser powers needed are not high and of the order of a few mW per trap site, but the tight focusing may lead to high power densities leading to potential heating issues, which we shall discuss later.

From these early studies, optical manipulation has seen a consistent and ever-increasing impact across a variety of different fields. Although there are also several recent review papers in the general field of trapping, this paper focuses upon the impact of optical traps in biomedicine, namely cell biology, *in vivo* studies and for single-molecule biophysics, bringing to the fore the physical aspects that have underpinned these studies. This paper is organised as follows: First, we describe the theoretical basis for single-beam optical trapping, including a discussion of how the forces may be understood to operate at different size scales. We then progress to describe experiments related to single-molecule studies and cell biology. We include a discussion of laser damage and heating and conclude with advanced topics in trapping and the combination of trapping with other methodologies. Our aim is not to give a comprehensive overview but rather highlight the important physics innovations in optical manipulation used for biomedical discovery. We conclude with a brief discussion on the future applications of optical manipulation for the life sciences.

3. Theoretical basis for optical trapping

Optical manipulation is a generic phrase widely used to cover the breadth of application of the forces of light to transport and trap mesoscopic-sized objects in both two and three dimensions. Optical tweezers use a single tightly focused beam to optically trap particles in 3D and are based on an inhomogeneous optical field distribution.

In addition to scattering or refraction, laser light may be absorbed in the sample medium, trapped particle or biological specimen, resulting in thermal forces. These can often overwhelm optical forces and as such due care needs to be taken. Optical trapping is thus constrained to relatively transparent media and particles where any thermal effects are negligible. For biomedical studies, any optically induced changes in temperature can adversely affect biological viability. This may be circumvented with a judicious choice of trap laser wavelength and other parameters. We shall discuss this aspect later on in this review.

The dimensions of the trapped particle (of radius r) and those of the wavelength of the trapping laser source (λ) determines how we consider the light-particle interaction and the resultant optical forces. For the case of a dielectric particle where $r \ll \lambda$, the particle may be treated as an oscillating dipole, and is the so-termed Rayleigh limit. In this limit, we may consider the optical force comprising of a gradient force F_g and scattering forceF_s. The scattering force is proportional to the intensity gradient of the optical field (I), $F_s \propto I$. The gradient force is proportional to the polarisability α of particle and field intensity, $F_g \propto \alpha \nabla I$. This relation explains why it can be challenging to trap dielectric particles below a micron in diameter as α is proportional to particle volume. This relation also explains why though very small dielectric particles (e.g. $r \sim 100$ nm) are challenging to trap, in fact metallic nanoparticles may be readily confined, being highly polarisable. The complex nature of the refractive index of a metallic particle needs consideration as this may result in appreciable thermal effects.

For the converse case where the particle size significantly surpasses the wavelength of the trapping light, i.e. $r \gg \lambda$, the geometrical (ray) optics formalism is appropriate. This is perhaps the most evocative and accessible way to understand the operation of optical tweezers. Here the propagation of light through the trapped sphere is determined through the principles of simple ray propagation and the use of Snell's law at the interfaces between the particle and the medium. The reflection and refraction of light at the boundary of the trapped particle may be used to determine the forces exerted. Figure 1 describes how a dielectric particle may be trapped by a single focused beam: i.e. in optical tweezers. A particle of higher refractive index than its surroundings is drawn into the most intense part of the optical field. We may consider the beam as a set of individual rays, each with weighted intensity matching the beam profile and propagating in a sample medium of refractive index n. Each individual ray alters direction upon reflection or refraction as it is incident on the particle with the ray path dictated by the Fresnel equations. These result in forces to confine

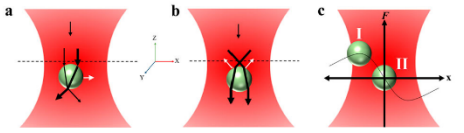

Figure 1. Ray optics model of optical tweezers for a particle of higher refractive index than its surroundings. The beam propagates in the downwards direction as indicated in (a) and (b). The trapped particle is not drawn to scale and only the refraction of the light is shown for simplicity. (a) Lateral Trapping. The particle is maintained in position by optical forces resulting from propagation of the light rays (black lines). The resultant reaction forces (white arrow) act in the x and y directions towards the field maximum. (b) Axial Trapping. The article finds an equilibrium position on the *z*-axis by axial momentum (black arrow) and reaction force (white arrow) The particle sits below beam centre (the dashed black horizontal line) as radiation pressure from photon scattering (black arrow) pushes against the particle. The position in the *x*–*y* plane is maintained by the intensity gradient of the light field. (c) An overlay of the force versus extension curve for the trapped particle. (c) I shows the particle held at the turnover point of the force-extension curve $\sim$200 nm away from the trap centre. Here, though trap stiffness is zero, a constant force is exerted. In (c) II the particle is trapped near the centre of the trap and the linear region of force versus displacement is depicted. Displacement of the bead in the *x* direction results in measurable changes in the force *F*.

the particle very close to beam focus (Figure 1). For a Gaussian trapping beam, we create a parabolic potential well (over a given distance from trap centre). Such a potential leads to a linear relationship between force and extension (Figure 1(c)) near trap centre with the force becoming independent of position at the periphery of the beam before falling rapidly at more extended distances. This force vs position dependency is used in studies in biomedicine, as we shall see later.

Experiments are often conducted with trapped particles of a size comparable to the trapping laser wavelength ($r \sim \lambda$). Such particles turn out to be near-optimal for obtaining the maximum trap stiffness with the lowest error in force measurements [11]. In this case, classical electrodynamics is required to understand the behaviour. The force exerted on an object positioned in a time-harmonic electromagnetic field may be calculated using the law of conservation of linear momentum. The linear momentum in this instance is either within the optical field or is present as the mechanical momentum of the particle. The sum of these two parts, which is the total momentum of the system, is conserved. The electromagnetic field momentum flux in a linear medium is represented mathematically by the Maxwell stress tensor. The optical force expressed in these terms is of general validity for an arbitrary (albeit rigid) body within the surface. It is entirely determined by the electric and magnetic

fields at the surface [12]. When considering deformable objects (such as a cell), both electrostrictive and magnetostrictive forces have to be considered. This approach is very general and powerful and may in fact be applied for all ratios of particle size to trapping wavelength if desired.

We also remark that the force field in optical tweezers shows both a conservative and non-conservative component: the gradient force is conservative and may be related to a potential, whereas the scattering force is non-conservative and dissipative. It is not possible to relate this to an effective potential. Its influence on particle position fluctuations is in fact to create toroidal vortex trajectories [13]. The non-conservative component to the force adds intriguing physics to optical traps but is typically not a major consideration for calibrating and using optical tweezers for biomedicine.

4. Measuring force in optical traps

Overall, optical tweezers for trapping in liquid media may be modelled as an overdamped simple harmonic oscillator. The power of optical tweezers centres upon its ability to measure the force exerted on a trapped particle and record its position variation with time. Optical tweezers act as a Hookean spring: the force F is proportional to the displacement (x) of the sample from equilibrium $F = -k_{\text{trap}}x$, with the constant of proportionality being the trap stiffness (k_{trap}). This assumption is valid for up to around 200 nm or so around the centre of the optical trap. Measuring sample position may be used to calculate the force if the system is calibrated. A prerequisite, however, is that this must be performed at nanometre and millisecond accuracy and naturally should be reproducible. Three key methods have emerged in this regard for determining trap stiffness: the drag method, the use of energy equipartition and the use of the power spectrum. We refer the reader elsewhere for a detailed discussion and comparison between these approaches which have their own attributes and drawbacks [4]. The power spectrum approach has proved popular for biomedical studies: a position histogram is recorded by imaging the trapped particle onto a quadrant photodiode. Taking the Fourier transform of particle position yields a Lorentzian-shaped power spectrum, where the roll-off frequency is related to the trap stiffness. Knowing the Stokes drag on the particle, and assuming a linear relation between particle displacement and detector voltage, are prerequisites for this approach.

For the case of many single-molecule studies, just operating in the linear region of the trap (a few hundred nm around trap centre) is not enough, as in fact we have two attached springs to consider: one of the trapped particle and the other of the molecule itself. As an example, we may consider the case for DNA adhered to an enzyme on a slide, with its other end adhered to a microparticle. Motion of the enzyme alters the extension of the DNA with the movement of the particle restricted by the trap stiffness. Overall, the result is that the motion of the particle is not the same as motion of the molecule under investigation, complicating the analysis. To tackle this limitation some innovative methods were developed. A key advance was operating at the point of trap stiffness (k_{trap}) being zero. This does not equate to a force of zero but means we are operating at a point with constant force for a range of particle displacement (see Figure 1(c)). This optical force clamp avoids the need to incorporate the compliance of the biological molecule in studies. For a constant applied force, the biological link does not vary its extension [14].

New concepts and approaches are also emerging for this area to obviate the need for frequent calibration of the trap, which may be deleterious for experimental studies. In particular, measuring the change in momentum between the incoming and outgoing light is emerging as an alternative way to look at this issue. This is not related to the specific trapping beam, particle size or particle shape [15,16]. This concept has been advanced recently to deduce individual forces for several optical traps simultaneously using the multiplexing afforded by holographic tweezers for force measurements [17]. This opens up the possibility of quantitative multipoint force measurements in complex biological settings (e.g. cell flow in the blood stream). Other notable recent work has seen the emergence of a novel route to reconstruct the microscopic force using a maximum-likelihood-estimator analysis (termed FORMA). The method may rapidly determine both conservative and non-conservative components of the force field. Such analysis may be useful for future optical traps and their use as microscopic and nanoscopic force transducers [18].

5. Molecular motors

The existence of molecular motors was first reported in 1864. Since then, a plethora of studies have led to a better understanding of the role molecular motors play in cellular function. These motors utilise chemical energy to fuel mechanical work within cells and fall within three categories:

(1) *Cytoskeleton motor proteins,* including kinesin, myosin and dynein. These are linear motors that bind to and transit along the cytoskeleton, a network of microtubule and actin filaments spread

throughout a cell. These are involved in muscle contraction, cellular transport and the segregation of chromosomes during cell division. These motor proteins are composed of two domains, the two-headed motor domain that transits along the cytoskeleton track in a 'hand-over-hand' fashion, a process akin to walking, and the 'cargo binding' domain that specifies the type of cargo it transports. Cytoskeleton motor proteins are fuelled by the hydrolysis of adenosine triphosphate (ATP) to adenosine diphosphate (ADP).

(2) *Nucleic acid motor proteins*, including DNA and RNA polymerases. These motor proteins bind DNA and RNA and are critically important for the maintenance of genetic code and for the production of all proteins within cells. Energy to fuel these motor proteins comes from polymerisation of nucleic acids, protein synthesis and/or hydrolysis of ATP to ADP. Our understanding of these motors is far less complete compared to cytoskeleton motor proteins, likely due to the complex nature of these biological processes.

(3) *Rotary motor proteins,* namely F_0F_1-ATP synthase, which synthesises cellular energy in the form of ATP and flagella, which are necessary for the movement of bacteria. These motors are embedded within cell membranes and produce torque through mechanical rotation and are powered by electrochemical potential, a proton or sodium ion gradient. As with nucleic acid motor proteins, we are less informed of their function, compared to cytoskeleton motor proteins.

The importance of molecular motors is best illustrated where mutations result in an altered function and consequently, disease. Examples include deafness (mutations in myosin VI); infertility (dynein); cardiomyopathy (cardiac myosin); and neurodegenerative diseases (kinesin). Before the advent of optical tweezers, knowledge of molecular motor function and associated pathologies was achieved using an array of *in vitro* assays. However, these were limited in their capability to quantify force and motion. This is where optical tweezers have made a significant impact.

5.1. Optical tweezers to study molecular motors – manipulating single-molecule biophysics

Our understanding of muscle contraction (e.g. energy consumption, contraction rate) had until recently come from bulk *in vitro* assays using muscle fibres. Single-molecule experiments using optical tweezers have advanced this field over the last three decades, enabling direct measurement of individual motors and answering questions such as: do they move in discrete, regular steps? Do they pause? How big is the step size? What force do they exert? We now know that molecular motor proteins act in a distinct, stepwise manner with high efficiency. The study of different molecular motors necessitates the use of an array of optical tweezers assays (Table 1, Figure 2), tailored to accurately measure force (at the piconewton level) and displacement (nanometre to Ångstrom scale).

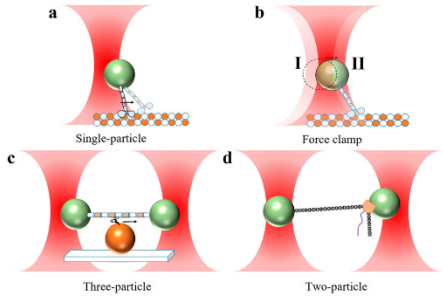

Figure 2. Common optical trapping assays for measuring single-molecule forces and displacement as described in Table 1. Particles, laser beams, molecular motors and polymers/microtubules are not drawn to scale. (a) A single-particle assay. The trap is static where particle displacement is reflective of molecular motor displacement. (b) Force clamp. A dynamic trap with the trapping position and force on the particle is maintained. Motion of the particle will accompany trap movement – point I (dotted line) to II (filled line). (c) Three-particle geometry with two static optical traps. Particle displacement on both ends directly represents molecular motor displacement. (d) Two-particle configuration. The left particle is held in a trap of high stiffness. The right particle is positioned at the turnover point as in Figure 1(c). This generates a force clamp where displacement at the right particle is accurately reflective of DNA or polymerase activity. Stands in (a) - (c), denoted by alternating colours, represent a microtubule or DNA. The black helical strand in (d) represents DNA; the purple strand indicates transcribed RNA. Schematics adapted from [108] and [4].

5.2. Cytoskeletal motor proteins: kinesin, dynein and myosin

The most frequently used optical tweezers geometry for measuring the force of a molecular motor is shown in Figure 2(a). In this design, motor proteins or a single microtubule are tethered to a particle, usually polystyrene or silica (typically $\sim$1 µm in diameter), via chemical binding (creation of a biotin–streptavidin link) [19]. The fixed surface is prepared in the opposite manner, by the binding of a microtubule or motor protein, respectively.

Table 1. Optical Trapping assays and their respective configurations for the measurement of molecular motor displacement. () indicates attachment of molecular motor to polymer. Adapted from references [108] and [4].

	Optical tweezers assay	Configuration	Molecular motor of application
Static	Single Bead Figure 2(a)	bead – molecular motor – polymer chain	Kinesin, RNA polymerase
	Three Bead Figure 2(c)	bead – polymer (molecular motor) – bead	Myosin, Kinesin, Dynein
	Two Bead Figure 2(d)	bead – DNA strand – molecular motor – bead	RNA polymerase
Dynamic	Force – Clamp Figure 2(b)	bead – molecular motor – polymer chain	Kinesin, Dynein
	Position – Clamp	bead – polymer chain (molecular motor) – bead	Myosin

The particle is then optically trapped, enabling manipulation of single molecules attached to the bead. The force applied by the trap can then be used to stall or slow the molecular motor kinesin, enabling measurement of both force and velocity and their relationship [20,21]. To measure kinesin and dynein generated forces, the bead is displaced from the centre of the trap due to the motility of the molecular motor, until a point where the bead snaps back to the trap centre. This occurs due to the stalling of the molecular motor (stall force) and its displacement from the microtubule [22,23]. Measuring these stall forces provides information on the type of load the motor protein is capable of transporting as well as conditions that affect its function (e.g. temperature and availability of chemical energy; ATP) [24,25]. This stall force may also be determined using zero-velocity plateaus before snap-back occurs [20,21]. Alternatively, measurement of stall force is achieved by lowering the force of the trap until a point where the molecular motor resumes [26].

Force clamps, which we discussed earlier are where the optical trap applies constant force (see Figure 2(b)). They are useful in measuring step size and isometric stall force [21,27]. Here the trap maintains the same trapping position of the kinesin-coated particle by responding to the movement of the motor. This geometry can also be used to apply an external force, stimulating kinesin and dynein to commence stepping/motility [27,28]. This external force can stimulate dynein to commence stepping unidirectionally along a microtubule, as occurs within a cell. While kinesin naturally transits in a forward direction along a microtubule track, an external backward load applied by a force clamp can remarkably stimulate stepping in a backward direction.

Collectively, these studies showed that kinesin advances in discrete 8 nm steps, with binding and hydrolysis of an ATP molecule required at each step. Further, these motors also show a stall force of 5–7 pN. For dynein, the reported step size varies from 8 to 32 nm, dependant on force load [29]. This extraordinary work demonstrates the power of optical tweezers to measure small changes in the biomechanics of kinesin and dynein and directly links the work performed by the motor specifically to these chemical reactions.

Due to its unique mechanism of action, a different optical tweezers assay is required to study myosin (Figure 2(c)) [30]. Here, a silica particle is attached to a fixed surface (coverslip) in order to raise a single myosin molecular motor, allowing it to come in contact with an actin fibre. The actin fibre is suspended between two particles, each individually held in a separate optical trap. As myosin interacts and moves along the actin track, force of motion can be quantified based on tension and displacement detected by the trapped beads. This tweezers assay has enabled characterisation of myosin step biomechanics including step size (11 nm), step force (3–6 pN), attachment distance ($\sim$40 nm) and travel distance ($\sim$5–10 steps prior to load detachment) [30–32].

5.3. Nucleic acid motor proteins: RNA polymerase as an example

The RNA polymerases are responsible for transcribing DNA into RNA, an essential intermediatory step in the translation of genetic code into protein, also known as gene expression. Transcription involves opening double-stranded DNA and threading the separated strands through RNA polymerase. The enzyme then moves along the DNA template, in a stepwise manner, transcribing genetic code into a complementary single-stranded messenger RNA. Single-molecule experiments with optical tweezers have significantly advanced our knowledge of the biomechanics of RNA polymerases, which work on the smaller ångström level compared to the nanometer scale of kinesin and dynein molecular motors.

The stall force for RNA polymerase was shown to range from $\sim$21–27 pN [33], considerably greater than the $\sim$5–7 pN determined for kinesin. This may reflect the requirement for RNA polymerase to separate the entangled DNA structure. This work and other studies show that RNA polymerase pauses for periods of

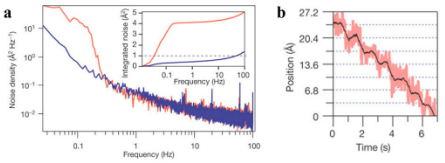

Figure 3. Forces associated with the two bead RNA polymerase optical assay described in Figure 2(d) and used in Abbondanzieri et al. [36]. (a) Power spectrum data for the stiffly trapped bead (left most bead in Figure 2(d)) in air (top trace) and helium (bottom trace). Inset: the integrated noise spectra for air (lighter, noisy trace) and helium (dark line) shows a tenfold reduction in power. (b) Displacement of resolved RNA polymerase steps in the bead-DNA-bead configuration [36]. Displacement over time is recorded by the right hand (weakly trapped) bead when the stiffly held (leftmost) bead moves in increments of 3.4 Å at 1 Hz. Data reproduced with permission from [36].

0–30 s (measured at ∼100 ms scale), necessary for the protein to backtrack as few as 2 base pairs (∼7 Å) to proofread what was already transcribed [34,35]. More recently, the step size of RNA polymerase was determined by Abbondanzieri et al. [36]. In this study, the authors describe an ultra-stable, dual-beam optical tweezers assay (Figure 2(d)). Importantly, this advance allowed a step from nanometre to ångström level position resolution in optical tweezers, crucial to resolve the minute steps taken by *E. coli* RNA polymerase during transcription. Normal force clamps may suffer from variations in signal fluctuations and beam pointing stability of the laser trap. One key part to overcome these issues was to place the optics external to the microscope in a chamber filled with helium gas rather than air. As the refractive index of helium was around an order of magnitude closer to vacuum than air, the pointing stability of the optical beam was reduced by the same level yielding an instrument with angstrom-level stability. A further important piece of physics was the use of a passive force clamp by using a bead placed at the turnover point in the force vs extension curve as described earlier (Figure 3 and see also Figure 1(c)). This obviated the need for computational correction of forces. In tandem, this led to a deeper understanding of transcription, showing that RNA polymerase has a discrete step size of 3.7 ± 0.6 Å, consistent with the size of one base pair of DNA [36].

5.4. DNA elasticity – pulling experiments

Within cells, DNA is stretched, twisted and bent in biological processes like transcription, as described above. In pioneering studies, optical tweezers have been used to stretch DNA to better understand its elastic properties and thus how it withstands the mechanical stress of various cellular processes [37,38]. In so-called pulling experiments, single-beam traps have been used where the DNA strand is tethered between an optically trapped particle and a fixed surface (coverslip) or pipette. The distance between the bead and coverslip, or pipette, is increased in order to apply increasing force/stretch. The extension of DNA under increasing force is recorded and presented as a force to extension (FE) curve. These studies show that DNA, when in its right-hand double helix configuration, has elastic characteristics that are entropic in nature when forces are below 5 pN. This elastic behaviour is best described by the worm-like chain (WLC) model which works under the assumption that DNA is a flexible rod of a particular length. When a force beyond 10 pN is applied the behaviour of DNA becomes intrinsic due to a change in DNA structure/confirmation. Interestingly, at ∼65 pN DNA undergoes the *overstretching transition* when a conformational change in structure (where the helix partially unwinds) results in DNA stretching ∼70% beyond its initial length without the need for any additional force [37,39,40]. Many studies have since investigated the intricacies of this change in DNA structure that in turn allows for such a dramatic shift in DNA elasticity [41,42].

5.5. Rotary motors: flagella

Bacteria including *E. Coli* swim using single or multiple flagella that are driven by a reversible rotary motor at its base. This molecular motor is ∼45 nm in diameter and powered by an ion gradient. The torque generated by the rotary motor is transferred to a helical filament via a hook (∼80 nm long) causing the filament to rotate in a propeller-like fashion. Optical tweezers have proven useful in measuring torque generated by flagella rotation in addition to characterising the biomechanics of motion. In seminal works by Block et al. the bacteria were tethered to a fixed surface with external torque applied by the trapping laser using beam steering optics [43]. This showed that bacterial flagella act as linear torsion springs for half of a full rotation, beyond this the flagella became more rigid. Subsequently, Berry et al. used a similar set-up with the exception that a trapped particle was used to stall the flagella. This facilitated measurement of the generated torque (∼4500 pN nm), which occurred at all angles of the flagella irrespective of whether it was stalled, or allowed to progress forwards or driven backwards [44]. This study also showed that these motors are capable of backwards rotation and thus, not directly connected to the unidirectional flow of ions that fuel this motor. This provides important insights as to how these motors function.

Others have characterised the force of flagella by optically trapping single bacteria in a microfluidic chamber and combined this with imaging (e.g. fluorescence) [45,46]. In this case, the barrel-shaped motile bacteria are held between two optical traps with monitoring of flagella position performed using both optical traps and by imaging the light from each of the tweezers beams onto two photodetectors. Using this approach, bacterial flagella were shown to exert two types of rotation: rotation of the flagella and subsequent rotation of the barrel-shaped body. The resultant motion was either progressive in nature or tumbling. Further advancements in imaging have enabled researchers to monitor multiple flagella simultaneously to determine the mechanics of rotation [45].

6. Cells

Optical tweezers have also seen use in numerous cellular assays. We describe some of the key studies enabled by optical tweezers. At the cell scale, they range from cell patterning and organisation to microrheology and controlled studies of cell migration and fusion. Several cell types have been studied including primary human cells, embryonic stem cells, bacteria and red blood cells. Optical tweezers have featured in hemorheological studies including the dynamics and biophysics of leukocytes and platelets [47].

6.1. Cell patterning

In biology, topology is a key factor in cell lineage selection and development. To study this effect, positioning and organising cells in arbitrary geometries would be advantageous. In particular, embryonic stem cells are of major interest for such studies. With optical tweezers direct organisation and manipulation of embryonic stem cells at a precise level was demonstrated (Figure 4(a–c)) [48]. Alternatively, direct optical trapping for organisation has also used a photonic-crystal platform. This has enabled trapping and cell organisation with low power requirements and improved force efficiency. Jing et al used such a system for mammalian fibroblast, yeast and *E. coli* cells. This technology inherits the versatility from conventional optical tweezers and improves trapping-force efficiency by using a photonic-crystal substrate, without compromising cell viability [48].

Multiplexed traps can enable widespread patterning of living cells. A study in 2006 showed heterotypic networks of living cells in hydrogel. The team showed cell positioning at submicron precision with an intercell separation < 400 nm, which enabled the generation of a network of mouse fibroblasts surrounded by a ring of bacteria.

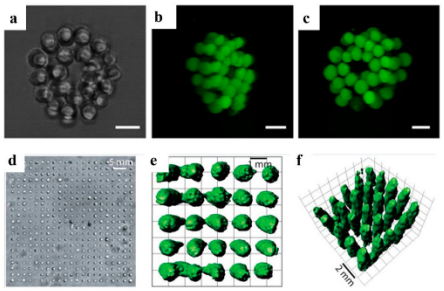

Figure 4. Cell patterning of embryonic stem cells (eSCs) ((a)–(c)) and bacterial cells ((d)–(f)). (a) A brightfield image of eSC organisation using holographic optical tweezers. (b)–(c) Fluorescent confocal images of the cells in (a) showing cell organisation. Scale bar is 12 µm. (d)–(f) Bacterial cell patterning using time multiplexed holographic traps generated by an acousto-optic deflector and spatial light modulator. (d) Micrograph of a 21×21 2D custom microarray of *P. aeruginosa* generated through optical manipulation. (e)–(f) By employing a false-colour isosurface in the confocal images, the mean distance between centres of structures is determined as 1.52 ± 0.06 µm with a mean spacing between bacterium of 354 ± 134 nm. Data in (a)–(c) reproduced with permission from [109] and data in (e)–(f) reproduced with permission from [49].

Separately hundreds of *Pseudomonas aeruginosa* were positioned in two- and three-dimensional arrays. There is promise in using such organisation for more detailed studies of cell differentiation and tissue development (Figure 4(d–f)) [49].

6.2. Microrheology

The response in terms of deformation and flow of biological material subjected to an applied force may give researchers insight into the complex mechanical properties of cells and tissue. Many show viscoelasticity: the response to strain exhibits neither liquid-like viscosity or solid-like elasticity, rather a combination of the two. Bulk rheology studies have prevailed where strain is applied to the whole sample and the bulk stress response is recorded. The drawback is that operating at such scales does not extract information relating to heterogeneities or size-dependent aspects of the sample response.

As a result, methods for microrheology have emerged to determine viscoelasticity within microlitre volumes. Passive microrheology approaches track microspheres embedded in the material that are freely diffusing, to determine both the frequency-dependent elastic modulus and viscous modulus. The Stokes–Einstein relations may be used to relate the microparticle trajectories to viscoelastic properties. In contrast to the passive approach,

we may move a microparticle through the material and perform active microrheology. This widens the applicability and parameter space of study. Optical tweezers are excellent for active microrheology, measuring miniscule forces with high precision both spatially and in time [50]. Microrheology with traps can be performed with rotating rather than translating microparticles. Notable microrheology studies with optical traps have included synthetic polymers, DNA, actin, microtubules, intermediate filaments, moving up to viscous fluids including mucus and vitreous humour.

By reconsidering the physics of the counter-propagating dual-beam trap, Guck et al. showed a new insight into the behaviour of deformable objects placed in such a system. The momentum of light is proportional to the refractive index n of the medium within which the light is travelling, according to the Minkowski formulation. This means when light passes from the sample medium to the cell (and back out again) a momentum change occurs at the interface that results in a force *away* from the medium of higher refractive index. For a deformable object such as a cell held in a counter-propagating trap system, this counter-intuitive outcome means the cell bulges outwards from the light beams [51]. The resulting deformation is also indicative of the mechanical properties of the cell which can vary from normal to neoplastic conditions. Guck et al used this *cell stretcher* (Figure 5(a,b)) to explore a range of cancer and blood cells where the very deformation of the cell within the counter-propagating beam trap was correlated with the degree of neoplasia (cancer). This label-free mechanical phenotyping approach has been applied to breast and oral cancer with encouraging results [52,53].

Turning to traditional optical tweezers, they have enabled viscoelastic measures of cell deformation through tether formation. A powerful approach has been utilising polymer microbeads to act as handles, each attached to opposing ends of cells. In this way, a cell stretching assay can be achieved in a geometry [54] that complements the counter-propagating dual-beam cell stretcher developed by Guck et al. [52]. Optical tweezers have enabled the investigation of many aspects of red blood cell mechanics and function including elasticity, shape and electrochemical charge in addition to alterations due to disease state (reviewed in [55]). As an example, Mills et al used Stokes' law of force deformation in fluid viscosity to measure extraction forces using trapped microbead handles directly attached to one or opposing ends of red blood cells (Figure 5(c,d)), in a geometry akin in appearance to the actin-myosin dumbbell assay (Figure 2(c)) [56]. By indirectly or directly trapping erythrocytes and measuring tensile forces, recent work has been able to define elasticity changes of erythrocytes following drug

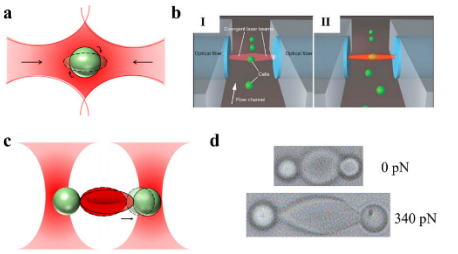

Figure 5. Cell stretching assays in optical manipulation. (a) The counter-propagating dual-beam trap acting as a cell stretcher. Two optical beams directed towards each other generate surface forces that enable both trapping and deformation of the cell outwards towards each of the two beams. (b) Optical stretching schematic reproduced with permission from [52]. (b)I Two counter-propagating beams emanating from optical fibres trap cells in a microfluidic flow channel. (b)II Deformation of the trapped cell is induced by typically increasing the laser field. (c) The bead-based cell stretcher. Trapped beads adhered to the surface of the cell act as handles. The left bead is subject to a static trapping force while the right bead (handle) is moved. The deformation of the cell for a given force may be used to determine mechanical characteristics (e.g. shear modulus). (d) Image of the bead-stretching assay on a live red blood cell showing the case of no force (top) vs a force of 340 pN (bottom) which causes stretching. Reproduced with permission from [54].

treatment or pathology onset [57,58]. Though predominantly used in erythrocytes, tether formation has been employed to measure viscoelastic changes related to cell differentiation. In studies of human and mouse stem cells, optical tweezers demonstrate changes in cell membrane tension associated with differentiation state [59–61].

6.3. Guiding cell growth

Determining what cues and factors cause directional cell growth may enable researchers to understand underlying mechanisms of cell repair, cell migration, and establishment of cell connection. Here we show examples where optical tweezers have directed such cell growth through either direct or indirect means.

By directly focusing a laser beam at the leading edges of developing growth cones of a neuronal cell, Ehrlicher and colleagues observed that lamellipodia extension could be directed towards a particular direction [62] (Figure 6(a)). This effect was attributed to how the optical gradient force of the focused beam attracts actin monomers at that particular edge. This creates a pool of monomers that are required for actin-polymerisation events key to lamellipodia growth [63]. Further studies showed filopodia alignment to an applied optical field may direct growth [64].

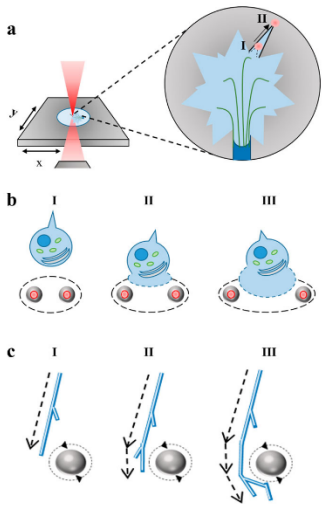

Figure 6. Optical tweezers configurations for guiding cell growth. (a) Single-beam assay for the direct guidance of neuronal cell growth (figure adapted from [62]). The laser is directed on an actively developing growth cone at a neuronal edge (position I). Translating the laser at the edge directs guidance of growth (moving the beam from I to II) (b) Indirect guidance of cell growth with optical tweezers through chemotaxis. We see precise positioning and release of a chemoattractant incorporated into a bead (grey circle within dashed oval) that are held with laser light in the proximity of leukaemia cells. Over time the cell develops a lamellipodium (extension) in the direction of the chemoattractant depicted in (b)I–(b)III. Adapted from [65]. (c) Indirect guidance of axon growth, by trapping and rotating a birefringent particle close to an axon. This exerts microfluidic-induced forces on growth cones, resulting in controlled directional axonal growth. In this case, an anticlockwise rotating vaterite particle was held adjacent to the axon causing it to change course and follow the rotation of the particle depicted in (c)I–(c)III. Adapted from [66].

Beyond direct induction of monomers, optical tweezers may be used to initiate chemotaxis for directed cell growth. Chemotaxis refers to the migration of cells toward attractant chemicals or away from repellents. Virtually all motile organisms show some form of chemotaxis. The chemotactic responses of eukaryotic cells involve the regulation of cytoskeletal elements (actin or microtubule). Optical tweezers can move engineered, micron-sized particles containing a molecular cargo to any point in a sample for controlled release [65]. This enables characterisation of a cell's response to such stimuli from various positions. Kress et al explored the motility of single human leukaemia cells in this way and showed directed migration towards the chemoattractant formyl-methionine-leucine-phenylalanine (Figure 6(b)), and repulsion from released cytochalasin D, an inhibitor of actin polymerisation (necessary for cell extension and motility).

Alternatively, rather than directly using optical forces, or tweezing such engineered particles to release molecules, traps can create specific flows and forces adjacent to cells. This can have a major impact: as an example, a rotating trapped particle held adjacent to the axonal projection of a nerve cell guided the cell's extension. The physics of how we set such particles into rotation is described in Section 8. In this case, the particle rotation created a localised microfluidic flow in turn resulting in a sub pN shear force against the growth cone. The cone in turn responds to this shear (Figure 6(c)). This light-driven micromotor demonstrated that the axonal direction and growth could be influenced in this novel manner [66]. All these examples are seen in Figure 6 and demonstrate some of the routes researchers have explored using traps for cell growth.

6.4. *Cell fusion*

Whilst we have concentrated on laser light exerting a force, laser light may also cut or surgically remove material. The details of this depend upon parameters such as the laser wavelength and whether the laser is operating in pulsed or continuous wave mode. Only a few years after their development, optical tweezers were combined with a pulsed UV laser microbeam to demonstrate laser microsurgery leading to cell fusion, in this case without invoking chemical or electrical methods. This enabled a step-change in the manner biologists considered the generation of viable hybrid cells [67]. Chen et al used this approach, successfully fusing embryonic stem cells with somatic cells. Such studies may lead to a better understanding of cell differentiation and reprogramming [68]. A more detailed discussion of this topic may be found elsewhere [69].

7. Optical manipulation at large scales and *in vivo*

The dual-beam counter-propagating geometry has found rich applications including as a cell stretcher, and trapping with other analytical modes (e.g. fluorescence or Raman detection). Studies have consistently shown it is highly favourable in trapping larger objects and can obviate laser damage issues due to its use of divergent, gently focused light beams. In particular, the absence of high numerical aperture optics, large capture range and fibre implementation mean it is compatible with higher throughput and microfluidic geometries when compared to three-dimensional optical tweezers. Beyond *in vitro*

manipulation, optical forces have also been explored as an instrument for *in vivo* manipulation and trapping assays. This counter-propagating geometry has been invigorated in the last decade due to new embodiments and applications. An example is 'macro-tweezers'. In this study, a spatial light modulator (SLM, see later) shaped the standard Gaussian beam into two beams each with a different divergence [70]. These were imaged into the probe chamber, creating two axially separated focal spots. After reflection of one of the beams at the mirror behind the sample, a light configuration – the 'macro-tweezers', similar to a counter-propagating fibre trap, was realised. Three-dimensional all-optical trapping and guiding were achieved in a volume of around 4 mm^3. The work focused upon studies of actively swimming organisms, for example, Euglena protists and dinoflagellates of up to 70 µm length. The lower power density reduced photodamage and heating issues [70].

Trapping in zebrafish, a now popular assay, obviated the need for the light field to penetrate opaque external barriers which would be the case for other organisms. This ability to manipulate exogenous particles within zebrafish with optical tweezers was reported in 2016. In that study, by injecting cell adherent nanoparticles of high refractive index, Johansen et al were able to use multiplexed optical tweezers to trap and measure deformability of internal endothelial cells, erythrocytes and macrophages [71].

Structures however need not be adhered to exogenous nanoparticles for manipulation at the *in vivo* scale. In a study by Favre-Bulle et al., optical tweezers were used to trap otoliths within zebrafish (Figure 7). These are ear stones which may produce fictive vestibular stimuli in zebrafish [72]. The ototliths were around 55 microns in diameter providing a major challenge for optical manipulation. The study calculated the optical force using the ray optics method whilst accounting for light scattering characteristics of biological tissues, refractive index. This included using a light deflection method for recording and accounting for the spatial variation in the refractive index across each otolith: This influences the locations and directions of the optical forces. The study was able to identify the corrective tail movements that accompany otolith stimulation, a mechanism produced by zebrafish to correct their spatial positioning. Although the significance in direct trapping provides a novel potential for *in vivo* targeting, accurate beam positioning is required, with beam drifts of < 2 µm away from optimal position inducing a significant drop in optical force ($\sim 20\%$). These reports show new directions for trapping and understanding *in vivo* nanoparticle-cell interaction in drug treatment or cell–cell interaction in a whole organism. Moving onto higher-order organisms, *in vivo*

Figure 7. *In vivo* optical trapping of zebrafish otoliths (ear stones). (a) Schematic showing optical trapping of otoliths (55 µm) in zebrafish. Reproduced with permission from [110]. (b) Dorsal view of otoliths (circled) in a zebrafish larva at 6 days post fertilisation (scale bar denotes 200 µm). Reproduced with permission from [72].

trapping of erythrocytes within subdermal blood capillaries of a mouse ear has also been reported [71]. The capillary depth matched the working distance for tweezers making this study feasible. In the same study, the authors used tweezers to clear a blocked microvessel. It is to be noted that standard optical tweezers are restricted to tissues that are highly vascularised, with these vessels close to the surface of the skin. More advanced *in vivo* studies in future would benefit from aberration correction to implement trapping at depth [73,74].

8. Laser heating and damage

So far, we have considered how light may exert a force on a range of mesoscopic particles including cells. Whether contact with light is direct or indirect, for all forms of optical manipulation we also need to consider the absorption, heating and subsequent potential damage that might accrue due to the application of laser light. This is particularly pertinent for sensitive molecules and cells and can be a major issue in optical tweezers where we tightly focus light. From a biological perspective there is a range of approaches to identify cell damage. The short-term (immediate) impact, cellular uptake of propidium iodide for example indicates rupture of cell membranes which can result in cell death. Longer-term damage is more challenging to measure: quantification of cell cloning efficiency as well as screening for cell anomalies in derivative populations may be effective studies in this regard [75].

Ashkin's first studies showed that cellular light exposure assays that aim to maintain biological integrity typically favoured longer wavelength light in the near infrared region (NIR) for trapping [76]. In the visible or ultraviolet region of the spectrum biological integrity may be compromised with deleterious photochemical reactions and reactive oxygen species generation [77,78]. Further studies in the literature have demonstrated that even working in the NIR may still cause significant impact on

cellular health. This may include reduced clonal growth, decline in bacterial motility and cell death [79].

Practically today, optical tweezers typically operate with laser wavelengths in the near infra-red region of the spectrum (the so-termed therapeutic window for biological studies extends from around 650–1350 nm) to minimise damage and heating. It is important to note that such damage and heating may take place within the liquid medium, within an inert trapped particle or the biological specimen itself. A rigorous evaluation of these effects is key to understanding how optical tweezers can be most effective. Optical tweezers use modest laser power but as the light is tightly focused power densities may reach $\sim$MW/cm^2. In 2002, Peterman and Schmidt developed a trapping model that incorporated heat generation due to optical absorption around a focused beam at 1064 nm. In this model, they considered the outward heat flow, and heat sinking by the glass surfaces of the sample chamber [80]. They saw that in the most common scenarios (for studies using micron-sized polystyrene or silica beads), absorption of the laser light in the liquid bath around the trapped particle, not in the particle itself, was the key contribution to heating. Experiments recorded the spectrum of the Brownian motion of trapped beads in water and in glycerol as a function of the trapping laser intensity to verify the predictions. Interestingly, heating of the medium thus has a non-negligible effect on trap calibration in typical biophysical experimental circumstances. This should be taken into consideration particularly when higher laser powers (>100 mW) are used. From a physics standpoint heating within the liquid or the trapped particle can be an issue that may deflect from the accuracy of measurement. In addition to local temperature changes, such heating would alter the local viscosity surrounding the particle. Other studies have explored heating due to translation and rotation.

Laser damage and heating considerations are not needed solely for single-beam optical tweezers. Near field traps (see Section 8.2) often use surface plasmons for enhancing optical forces. These are coherent electron oscillations moving in unison with an electromagnetic wave along the interface between a dielectric and a metal. These dissipate and lead to thermal effects that have to be considered along with optical forces. The dual-beam counter-propagating trap which we have described for cell stretching may be used to study thermal effects upon cells. A study used the spreading of cells as a novel, sensitive viability marker. The optical stretcher was used to simulate heat shocks that cells typically experience during measurements in manipulation studies. The results showed that about 60% of the cells survived the heat shocks without critical damage at temperatures of up to 58°C [81]. It is important to note the mechanical properties of a cell may change with temperature. The optical stretcher incorporated a separate laser operating at a wavelength of 1480 nm solely for heating. This allowed a study of the degree of thermal softening of cells in the passive viscoelastic regime, and observing cell contraction whenever the overall temperature exceeded 52°C [82]. Overall, these studies show optical forces normally go hand-in-hand with potential damage or thermal effects. From a biological perspective, a careful examination of these is essential for any new study to ensure the validity of the data.

9. Advanced topics in optical manipulation

9.1. Structured light

The advent of optical beam shaping both in phase, amplitude and polarisation with an array of technology has enabled this area in recent years. Multiplexing traps have been essential to perform biological studies. Indeed, for single-molecule studies, we often require two or three traps which are typically generated using acousto-optic deflectors or multiple paths in the beam geometry. These approaches are largely restricted to two dimensions. To achieve full three-dimensional control of each individual trap, we may use holographic optical tweezers [83]. These may be implemented using liquid crystal devices such as an SLM that can allow full control over the phase and amplitude of light. In turn this can allow researchers to create multiple traps in a three-dimensional space. Furthermore, the versatility of SLMs means we can shape the light to compensate for aberrations as well as create more advanced forms of propagating light fields, so-termed structured light [5]. This generally refers to a range of transverse mode profiles, moving away from a standard zeroth-order Gaussian beam. This includes vectorial fields where the polarisation of the field plays an integral role. In the last three decades, light fields possessing angular momentum (spin and orbital) have enabled trapping studies where the transfer of optical angular momentum from the beam to the trapped particle causes rotation (see later). Propagation invariant beams have shown extended transport of particles and motion of particles and cells on more complex trajectories. Structured light creates extended optical patterns in both two and three dimensions that may be termed potential energy landscapes. Particle and cell motion across such landscapes is intricately linked to the physical response of the cell to the underlying optical field resulting in a differential motion – sorting. A major body of work has looked at the use of optical forces to separate or fractionate particles, notably cells. The motion of particles over such potential energy landscapes has been a rich

playground for physics-based studies. It is reasonable to say the prospect for their use for cell separation may be hampered by throughput and selectivity though work has shown success on some cell types notably eythrocytes and leukocytes. Traps can also be used to select particles from flow cytometer type geometries. We refer the reader elsewhere for a review of this topic and its broader implications [84].

Even reverting back to a single-beam trap, the role of the polarisation state of the trapping beam can play a profound role. As a prime example, circularly polarised light is known to possess spin angular momentum of value $\pm\hbar$ per photon. Intriguingly by trapping birefringent particles one can set these into rotation due to the trapped object acting as a waveplate and a torque being exerted due to the passage of light through the object [85]. This is not the only route to implement rotation of trapped objects and we refer the reader to a comprehensive recent paper that describes rotational dynamics in more depth [86]. The original work on rotating trapped particles was performed with calcite particles. However, a large subsequent effort developed birefringent particles of known size and shape for trapping purposes. A suite of anisotropic colloids has emerged for such use including the microsphere vaterite [87]. Such crystals have been used for rotation. Upon trapping, these particles reach a terminal angular velocity due to a balance between the optical torque applied from the trapping beam and the rotational Stokes drag from the liquid environment [88,89]. From the biology perspective, we have already described the use of such rotating particles for directed cell growth. At the molecular scale, an example of a key experiment using such spinning particles was the observation of RNA polymerase translocation in real time as it worked under a defined torque. In this experiment, RNA polymerase was torsionally anchored to a coverslip. The end of the DNA template was torsionally anchored to the bottom of a nanofabricated quartz cylinder held in an angular optical trap. This study revealed that RNA polymerase adapts its biomechanical behaviour when encountering a region of supercoiled (over – or underwound) DNA. In these conditions, RNA polymerase slows and pauses more frequently than previously observed. It is also able to produce sufficient torque (11 ± 4 pN.nm) to alter DNA structure which allows transcription to continue [90]. For rotating particles, studies showed spinning vaterite may be used as a microviscometer for human tear fluid, recording a viscosity value of 1.1 ± 0.1 cP. In the absence of a tear response, between 1 and 5 µl of eye fluid can be collected. This shows the importance of such a study for fluids where biological samples are precious and hard to obtain [91].

9.2. Optical trapping in the near field

The optical manipulation methods we have discussed so far all use free space optics and as such we are constrained to free space Gaussian beam propagation. Interestingly, there has been a huge impetus in the last two decades to move to the near field in a variety of ways. Importantly the near field can circumvent the so-termed diffraction limit making it possible to create highly localised features of the optical field. In contrast to propagating fields, evanescent fields can create strong optical field gradients in excess of those that can be achieved in far field, thus yielding stronger forces, as the gradient force is proportional to ∇I. Evanescent fields may be generated by plasmonic nanostructures or dielectric waveguides and can be enhanced using cavity approaches [92–94]. Moreover, compared to the three-dimensional nature of optical tweezers working in the near field lends itself to a planar geometry so we may multiplex trap systems in a manner compatible for lab on chip or microfluidic applications. There are several drawbacks though to such systems, including ohmic heating in plasmonic traps, and difficulties in loading the trapping systems.

Interesting studies can be performed in such traps on very small biological samples. In contrast to the single-molecule studies described above, nanofilm traps have demonstrated the ***direct*** optical trapping of a single bovine serum albumin (BSA) molecule that has a hydrodynamic radius of 3.4 nm, using a double-nanohole in an Au film. The strong optical force in the trap not only stably traps the protein molecule but also unfolds it. The unfolding of the BSA is confirmed by experiments with changing optical power and with changing solution pH [95]. It is important to remark that the absence of a strong gradient field and the relatively low polarisability of a single molecule would preclude such trapping in a standard optical tweezers system given how the forces relate to these parameters (see Section 3). More broadly, nanoaperture optical tweezers are emerging as useful label-free devices for both the detection and identification of individual biological molecules and their interactions. Nanoaperture optical tweezers provide an inexpensive and scalable method to observe real-time dynamics and to quantify binding kinetics of protein–small molecule interactions without the need to use tethers or labelling. Such nanoaperture-based optical tweezers have been used to trap and isolate single DNA molecules and to study proteins such as p53, a tumour suppressor gene that is frequently mutated in human cancers to render it either inactive or in fact promote tumorigenesis. As we look forward, new trapping modes that use

nanostructures, metasurfaces and other routes to create highly localised light fields will prove more important for biomedical research. There is ample scope here for materials science to contribute to new future trap geometries creating strong localised force fields [96].

10. Multimodality: combining optical traps with other techniques

Optical tweezers have been a *tour de force* in precision measurements in biomedicine. However, they have also found rich application for the life sciences when combined with other modalities such as laser microsurgery, which we have already described in relation to cells (Section 6.4). A further area of application has been the combination of trapping with imaging modalities. This is perhaps not surprising given the response of biological systems to light-based excitation through processes such as autofluorescence, fluorescence with both endogeneous and exogenous fluorophores and inelastic (Raman) scattering to recover molecular-level information. Here we touch upon some combinations seen with tweezers and such imaging. Key technological advances in this area reside in choice of decoupling (or not) the trapping beam path with the imaging path and the mismatch of power densities required for imaging versus trapping. The presence of the trapping laser may cause deleterious photobleaching or in general just hamper faithful recording of the image.

In many studies of single molecules optical traps were combined with advanced (label-free) imaging methods. For example, optical tweezers with differential interference contrast microscopy (DIC) employed the same laser for trapping and displacement for the determination of the step size of kinesin [19]. The challenge of adding optical trapping with wide field epi-fluorescence microscopy resides in recording the fluorescence emission of a few fluorophores when we simultaneously have a relatively large optical trapping power, orders of magnitude higher in intensity. The system requires careful delineation between the trapping and fluorescence emission light. This can be achieved using special multilayer thin-film optical filters and resorting to approaches such as cycling between the trapping and excitation beams [97]. Optical tweezers can furthermore be combined with standard fluorescence and imaging as well as multiphoton microscopy [98]. The imaging laser in this latter case – generating ultrashort pulses – may also be used to perform laser microsurgery, to perforate the membrane of trapped spermatozoa. Perforation of the cell membrane at the tail results in immobilisation of the sperm [99]. Immobilisation is required for clinical *in vitro* fertilisation (IVF) when a sperm is injected directly into the oocyte in a process known as intracytoplasmic fertilisation (ICSI). Laser microsurgery circumvents the use of chemicals to immobilise sperm, which can be toxic. Importantly, laser microsurgery induced immobilisation results in successful fertilisation of oocytes by ICSI and may be a clinically useful technique.

To date, experimental configurations have also employed combinations of the single-beam optical tweezers trap and Raman spectroscopy using either the same beam or separate beams for Raman interrogation and trapping [100]. Using the same optics and microscope objective for trapping and Raman studies can add simplicity though reduces flexibility in geometry and potentially recording appropriate fields of view for the Raman image. A dual-beam counter-propagating fibre trap may immobilise a cell and be combined with an orthogonally placed microscope objective to obtain molecular Raman spectra as seen in studies of large (30 μm diameter) trapped primary human keratinocyte cells. Subsequent imaging obtained Raman spectra from local parts of the trapped cell [101].

Optical imaging itself has undergone a revolution in the last two decades both attaining super-resolution, recognised in the 2014 Nobel Prize in Chemistry, and in recording wide field and depth information from larger biological samples in a rapid fashion. Essentially, at many relevant biological size scales we are keen to perform tomography of the sample. Optical tweezers have been added to imaging systems to create novel multimodal platforms. As an example, Huser et al explored the use of holographic optical tweezers with (super-resolved) localisation microscopy. The trap allowed the bacterial cells to be turned and rotated. The team were able to explore nanoscale organisation of chromosomal DNA in the bacteria [102]. Turning to the counter-propagating trap geometry, Kreysing and colleagues developed the optical cell rotator (OCR) [103]. As with the Constable et al. [9] study optical fibres delivered the light fields. However, in this instance, one of the two trapping beams was asymmetric and used to rotate the sample. The rotation of cells occured around an axis perpendicular to the optical axis of the microscope. As with the Jess et al study, the system was decoupled from the optical detection path. The results showed data on human erythrocytes, promyelocytic leukaemia cells, and cell clusters. This forms a new method for tomographic microscopy [103].

At the larger size scale, we have seen the emergence of an imaging approach employing a sheet of light to illuminate a sample, where the fluorescent imaging path is perpendicular to the illuminated plane. This geometry termed light sheet imaging (or selective plane microscopy) offers key advantages including rapid acquisition of images and low photodamage. Optical tweezers

have been used in tandem with light sheet imaging to exert local forces and develop a predictive mechanical model of cell contact within the early Drosophila embryo. Counter-propagating dual-beam optical traps may provide new forms of sample manipulation for light sheet studies but the forces may be too weak to hold larger organisms [104]. It is not only light waves that can manipulate particles: sound waves may exert a force as well and the strength of this interaction mean it is better suited to holding larger specimens [105] including samples such as embryos for analysis in light sheet imaging [106]. Combining both optical and acoustic forces is also very worthy of consideration and can yield the 'best of both worlds' in terms of range of force and precision, to achieve new levels of control over micro-organism motion [107].

11. Conclusions

It is now over 50 years since Ashkin published his first work on the application of optical forces. This is a field that has grown in importance and retained centre stage for a plethora of biological studies that were simply not possible before the advent of optical manipulation. This review has given an insight into the biological relevance and importance of Ashkin's discoveries. Optical traps have emerged as a mainstay of biological science, operating on spatial and temporal scales of relevance.

It is a method that has crossed disciplines in a powerful and convincing way. The ingenuity lies in the method itself and its ability to discern quantifiable metrology on biological systems giving unprecedented insights. Its recent use in vivo represents a most exciting advancement where future discoveries will occur in situ: the most biologically relevant environment. In terms of single-molecule assays, advancements may depend more on the discipline of biology. For example, how to adhere proteins without affecting function, as commonly occurs with protein linkages, or how to control molecular alignment. The next few decades will bring ever more detailed science to this area. We expect to see further advances particularly on novel tailored trapping geometries and incorporating traps with other methods, not necessarily just based in optics, for the biosciences.

Disclosure statement

No potential conflict of interest was reported by the author(s).

Acknowledgements

This work was supported by the UK Engineering and Physical Sciences Research Council under Grant EP/P030017/1; The Hospital Research Foundation under Grant C-MCF-58-2019. CC thanks the University of Adelaide and University of Nottingham for the award of a PhD scholarship.

Notes on contributors

Carl Adrian Campugan is a PhD student jointly between the Faculty of Health and Medical Sciences at the University of Adelaide, Australia and the Faculty of Engineering at the University of Nottingham, UK. Carl's involvement in the subject article stems from his keen interest in the optical manipulation of biological cells. In particular, his PhD project aims to implement trapping techniques in to better understand early mammalian development.

Dr Kylie Dunning is a Hospital Research Foundation Fellow at the University of Adelaide, Australia. Kylie leads the Reproductive Success team within the Robinson Research Institute, where they use light-based technologies to better understand the biology that underpins successful development of the oocyte and early embryo. In 2020, in recognition of research excellence and community outreach, she was awarded The South Australian Tall Poppy of the Year Award, the HDA Women's Excellence in Research Award and the Robinson Research Institute Director's Award.

Kishan Dholakia is Professor at the University of St Andrews, Scotland. He works on advanced optical beam shaping for biophotonics, precision measurement and optical manipulation. He is a fellow of the Royal Society of Edinburgh, the Optical Society, SPIE and the Institute of Physics (IOP). He is recipient of the R.W. Wood Prize of the Optical Society (2016), the Institute of Physics Thomas Young Medal and Prize (2017) and the SPIE Dennis Gabor Award (2018).

Funding

This work was supported by the UK Engineering and Physical Sciences Research Council [Grant number EP/P030017/1]; The Hospital Research Foundation [Grant number C-MCF-58-2019]; CC acknowledges the support of a PhD scholarship jointly from the University of Adelaide and University of Nottingham.

ORCID

Carl A. Campugan http://orcid.org/0000-0003-4947-8251
Kylie R. Dunning http://orcid.org/0000-0002-0462-6479
Kishan Dholakia http://orcid.org/0000-0001-6534-9009

References

[1] Nichols EF, Hull GF. A preliminary communication on the pressure of heat and light radiation. Phys Rev (Series I). 1901;13(5):307–320.
[2] Nichols EF, Hull GF. The pressure due to radiation. (second paper). Phys Rev (Series I). 1903;17(1):26–50.

[3] Lebedev P. Experimental examination of light pressure. Nuovo Cimento. 1883;15(195):195.
[4] Perkins TT. Optical traps for single molecule biophysics: a primer. Laser & Photonics Review. 2009;3(1-2):203–220.
[5] Dholakia K, Čižmár T. Shaping the future of manipulation. Nat Photonics. 2011;5(6):335–342.
[6] Jones PH, Maragò OM, Volpe G. Optical tweezers: principles and applications. Cambridge: Cambridge University Press; 2015.
[7] Millen J, Stickler BA. Quantum experiments with microscale particles. Contemp Phys. 2020;61(3):1–14.
[8] Ashkin A. Acceleration and trapping of particles by radiation pressure. Phys Rev Lett. 1970;24(4):156–159.
[9] Constable A, Kim J, Mervis J, et al. Demonstration of a fiber-optical light-force trap. Opt Lett. 1993;18(21):1867–1869.
[10] Ashkin A, Dziedzic JM, Bjorkholm JE, et al. Observation of a single-beam gradient force optical trap for dielectric particles. Opt Lett. 1986;11(5):288–290.
[11] Montange RK, Bull MS, Shanblatt ER, et al. Optimizing bead size reduces errors in force measurements in optical traps. Opt Express. 2013;21(1):39–48.
[12] Novotny L, Hecht B. Principles of nano-optics. Cambridge: Cambridge university press; 2012.
[13] Roichman Y, Sun B, Stolarski A, et al. Influence of nonconservative optical forces on the dynamics of optically trapped colloidal spheres: the fountain of probability. Phys Rev Lett. 2008;101(12):128301.
[14] Greenleaf WJ, Woodside MT, Abbondanzieri EA, et al. Passive all-optical force clamp for high-resolution laser trapping. Phys Rev Lett. 2005;95(20):208102.
[15] Farré A, Marsà F, Montes-Usategui M. Optimized back-focal-plane interferometry directly measures forces of optically trapped particles. Opt Express. 2012;20(11):12270–12291.
[16] Thalhammer G, Obmascher L, Ritsch-Marte M. Direct measurement of axial optical forces. Opt Express. 2015;23(5):6112–6129.
[17] Strasser F, Moser S, Ritsch-Marte M, et al. Direct measurement of individual optical forces in ensembles of trapped particles. Optica. 2021;8(1):79–87.
[18] García LP, Pérez JD, Volpe G, et al. High-performance reconstruction of microscopic force fields from Brownian trajectories. Nat Commun. 2018;9(1):1–9.
[19] Svoboda K, Schmidt CF, Schnapp BJ, et al. Direct observation of kinesin stepping by optical trapping interferometry. Nature. 1993;365(6448):721–727.
[20] Kojima H, Muto E, Higuchi H, et al. Mechanics of single kinesin molecules measured by optical trapping nanometry. Biophys J. 1997 Oct;73(4):2012–2022.
[21] Visscher K, Schnitzer MJ, Block SM. Single kinesin molecules studied with a molecular force clamp. Nature. 1999;400(6740):184–189.
[22] Schroeder III HW, Hendricks AG, Ikeda K, et al. Force-dependent detachment of kinesin-2 biases track switching at cytoskeletal filament intersections. Biophys J. 2012;103(1):48–58.
[23] Gennerich A, Carter AP, Reck-Peterson SL, et al. Force-induced bidirectional stepping of cytoplasmic dynein. Cell. 2007;131(5):952–965.
[24] Reck-Peterson SL, Yildiz A, Carter AP, et al. Single-molecule analysis of dynein processivity and stepping behavior. Cell. 2006;126(2):335–348.
[25] Coppin CM, Pierce DW, Hsu L, et al. The load dependence of kinesin's mechanical cycle. Proc Natl Acad Sci USA. 1997;94(16):8539–8544.
[26] Hall K, Cole D, Yeh Y, et al. Kinesin force generation measured using a centrifuge microscope sperm-gliding motility assay. Biophys J. 1996;71(6):3467–3476.
[27] Fehr AN, Asbury CL, Block SM. Kinesin steps do not alternate in size. Biophys J. 2008;94(3):L20–L22.
[28] Nicholas MP, Berger F, Rao L, et al. Cytoplasmic dynein regulates its attachment to microtubules via nucleotide state-switched mechanosensing at multiple AAA domains. Proc Natl Acad Sci USA. 2015;112(20):6371–6376.
[29] Mallik R, Carter BC, Lex SA, et al. Cytoplasmic dynein functions as a gear in response to load. Nature. 2004;427(6975):649–652.
[30] Finer JT, Simmons RM, Spudich JA. Single myosin molecule mechanics: piconewton forces and nanometre steps. Nature. 1994;368(6467):113–119.
[31] Sakamoto T, Amitani I, Yokota E, et al. Direct observation of processive movement by individual myosin V molecules. Biochem Biophys Res Commun. 2000;272(2):586–590.
[32] Molloy J, Burns J, Kendrick-Jones J, et al. Movement and force produced by a single myosin head. Nature. 1995;378(6553):209–212.
[33] Wang MD, Schnitzer MJ, Yin H, et al. Force and velocity measured for single molecules of RNA polymerase. Science. 1998;282(5390):902–907.
[34] Shaevitz JW, Abbondanzieri EA, Landick R, et al. Backtracking by single RNA polymerase molecules observed at near-base-pair resolution. Nature. 2003;426(6967):684–687.
[35] Gabizon R, Lee A, Vahedian-Movahed H, et al. Pause sequences facilitate entry into long-lived paused states by reducing RNA polymerase transcription rates. Nat Commun. 2018;9(1):1–10.
[36] Abbondanzieri EA, Greenleaf WJ, Shaevitz JW, et al. Direct observation of base-pair stepping by RNA polymerase. Nature. 2005;438(7067):460–465.
[37] Smith SB, Cui Y, Bustamante C. Overstretching B-DNA: the elastic response of individual double-stranded and single-stranded DNA molecules. Science. 1996;271(5250):795–799.
[38] Wang MD, Yin H, Landick R, et al. Stretching DNA with optical tweezers. Biophys J. 1997;72(3):1335–1346.
[39] Cluzel P, Lebrun A, Heller C, et al. DNA: an extensible molecule. Science. 1996;271(5250):792–794.
[40] Schakenraad K, Biebricher AS, Sebregts M, et al. Hyperstretching DNA. Nat Commun. 2017;8(1):1–7.
[41] King GA, Gross P, Bockelmann U, et al. Revealing the competition between peeled ssDNA, melting bubbles, and S-DNA during DNA overstretching using fluorescence microscopy. Proc Natl Acad Sci USA. 2013;110(10):3859–3864.
[42] van Mameren J, Gross P, Farge G, et al. Unraveling the structure of DNA during overstretching by using multicolor, single-molecule fluorescence imaging. Proc Natl Acad Sci USA. 2009;106(43):18231–18236.

[43] Block SM, Blair DF, Berg HC. Compliance of bacterial flagella measured with optical tweezers. Nature. 1989;338(6215):514–518.
[44] Berry RM, Berg HC. Absence of a barrier to backwards rotation of the bacterial flagellar motor demonstrated with optical tweezers. Proc Natl Acad Sci USA. 1997;94(26):14433–14437.
[45] Mears PJ, Koirala S, Rao CV, et al. Escherichia coli swimming is robust against variations in flagellar number. Elife. 2014;3:e01916.
[46] Min TL, Mears PJ, Chubiz LM, et al. High-resolution, long-term characterization of bacterial motility using optical tweezers. Nat Methods. 2009;6(11): 831–835.
[47] Avsievich T, Zhu R, Popov A, et al. The advancement of blood cell research by optical tweezers. Rev Phys. 2020;5:100043.
[48] Jing P, Liu Y, Keeler EG, et al. Optical tweezers system for live stem cell organization at the single-cell level. Biomed Opt Express. 2018;9(2):771–779.
[49] Akselrod G, Timp W, Mirsaidov U, et al. Laser-guided assembly of heterotypic three-dimensional living cell microarrays. Biophys J. 2006;91(9):3465–3473.
[50] Robertson-Anderson RM. Optical tweezers microrheology: from the basics to advanced techniques and applications. ACS Macro Lett. 2018;7(8):968–975.
[51] Guck J, Ananthakrishnan R, Moon TJ, et al. Optical deformability of soft biological dielectrics. Phys Rev Lett. 2000 Jun 5;84(23):5451–5454.
[52] Guck J, Schinkinger S, Lincoln B, et al. Optical deformability as an inherent cell marker for testing malignant transformation and metastatic competence. Biophys J. 2005;88(5):3689–3698.
[53] Remmerbach TW, Wottawah F, Dietrich J, et al. Oral cancer diagnosis by mechanical phenotyping. Cancer Res. 2009 Mar 1;69(5):1728–1732.
[54] Dao M, Lim CT, Suresh S. Mechanics of the human red blood cell deformed by optical tweezers. J Mech Phys Solids. 2003;51(11-12):2259–2280.
[55] Zhu R, Avsievich T, Popov A, et al. Optical tweezers in studies of red blood cells. Cells. 2020 Feb 26;9(3).
[56] Mills J, Qie L, Dao M, et al. Nonlinear elastic and viscoelastic deformation of the human red blood cell with optical tweezers. Mol Cell Biomech. 2004;1(3):169–180.
[57] Sheikh-Hasani V, Babaei M, Azadbakht A, et al. Atorvastatin treatment softens human red blood cells: an optical tweezers study. Biomed Opt Express. 2018;9(3): 1256–1261.
[58] Agrawal R, Smart T, Nobre-Cardoso J, et al. Ultrastructural characterization of the lower motor system in a mouse model of krabbe disease. Sci Rep. 2016;6(1):1–12.
[59] De Belly H, Stubb A, Yanagida A, et al. Membrane tension gates ERK-mediated regulation of pluripotent cell fate. Cell Stem Cell. 2021 Feb 4;28(2):273–284.e6.
[60] Titushkin I, Cho M. Distinct membrane mechanical properties of human mesenchymal stem cells determined using laser optical tweezers. Biophys J. 2006;90(7):2582–2591.
[61] Tan Y, Kong C-w, Chen S, et al. Probing the mechanobiological properties of human embryonic stem cells in cardiac differentiation by optical tweezers. J Biomech. 2012;45(1):123–128.
[62] Ehrlicher A, Betz T, Stuhrmann B, et al. Guiding neuronal growth with light. Proc Natl Acad Sci USA. 2002;99(25):16024–16028.
[63] Dent EW, Gertler FB. Cytoskeletal dynamics and transport in growth cone motility and axon guidance. Neuron. 2003;40(2):209–227.
[64] Carnegie DJ, Stevenson DJ, Mazilu M, et al. Guided neuronal growth using optical line traps. Opt Express. 2008 Jul 7;16(14):10507–10517.
[65] Kress H, Park J-G, Mejean CO, et al. Cell stimulation with optically manipulated microsources. Nat Methods. 2009;6(12):905–909.
[66] Wu T, Nieminen TA, Mohanty S, et al. A photon-driven micromotor can direct nerve fibre growth. Nat Photonics. 2012;6(1):62–67.
[67] Steubing RW, Cheng S, Wright WH, et al. Laser induced cell fusion in combination with optical tweezers: the laser cell fusion trap. Cytom: J Int Soc Anal Cytol. 1991;12(6):505–510.
[68] Chen S, Cheng J, Kong C-W, et al. Laser-induced fusion of human embryonic stem cells with optical tweezers. Appl Phys Lett. 2013;103(3):033701.
[69] Blázquez-Castro A, Fernández-Piqueras J, Santos J. Genetic material manipulation and modification by optical trapping and nanosurgery-a perspective. Front Bioeng Biotechnol. 2020;8:1118.
[70] Thalhammer G, Steiger R, Bernet S, et al. Optical macrotweezers: trapping of highly motile micro-organisms. J Opt. 2011;13(4):044024.
[71] Johansen PL, Fenaroli F, Evensen L, et al. Optical micromanipulation of nanoparticles and cells inside living zebrafish. Nat Commun. 2016;7(1):1–8.
[72] Favre-Bulle IA, Stilgoe AB, Rubinsztein-Dunlop H, et al. In situ click chemistry generation of cyclooxygenase-2 inhibitors. Nat Commun. 2017;8(1):1–7.
[73] Zhong M-C, Wei X-B, Zhou J-H, et al. Trapping red blood cells in living animals using optical tweezers. Nat Commun. 2013;4(1):1–7.
[74] Čižmár T, Mazilu M, Dholakia K. In situ wavefront correction and its application to micromanipulation. Nat Photonics. 2010;4(6):388–394.
[75] Liang H, Vu KT, Krishnan P, et al. Wavelength dependence of cell cloning efficiency after optical trapping. Biophys J. 1996;70(3):1529–1533.
[76] Ashkin A, Dziedzic JM, Yamane T. Optical trapping and manipulation of single cells using infrared laser beams. Nature. 1987;330(6150):769–771.
[77] Kvam E, Tyrrell RM. Induction of oxidative DNA base damage in human skin cells by UV and near visible radiation. Carcinogenesis. 1997;18(12):2379–2384.
[78] Liebel F, Kaur S, Ruvolo E, et al. Irradiation of skin with visible light induces reactive oxygen species and matrix-degrading enzymes. J Invest Dermatol. 2012;132(7):1901–1907.
[79] Neuman KC, Chadd EH, Liou GF, et al. Characterization of photodamage to Escherichia coli in optical traps. Biophys J. 1999;77(5):2856–2863.
[80] Peterman EJ, Gittes F, Schmidt CF. Laser-induced heating in optical traps. Biophys J. 2003;84(2):1308–1316.
[81] Wetzel F, Rönicke S, Müller K, et al. Single cell viability and impact of heating by laser absorption. Eur Biophys J. 2011;40(9):1109–1114.

[82] Chan C, Whyte G, Boyde L, et al. Impact of heating on passive and active biomechanics of suspended cells. Interface Focus. 2014;4(2):20130069.
[83] Curtis JE, Koss BA, Grier DG. Dynamic holographic optical tweezers. Opt Commun. 2002;207(1-6):169–175.
[84] Dholakia K, MacDonald MP, Zemánek P, et al. Cellular and colloidal separation using optical forces. Methods Cell Biol. 2007;82:467–495.
[85] Friese ME, Nieminen TA, Heckenberg NR, et al. Optical alignment and spinning of laser-trapped microscopic particles. Nature. 1998;394(6691):348–350.
[86] Bruce GD, Rodríguez-Sevilla P, Dholakia K. Initiating revolutions for optical manipulation: the origins and applications of rotational dynamics of trapped particles. Adv Phys: X. 2021;6(1):1838322.
[87] Fernández-Nieves A, Cristobal G, Garcés-Chávez V, et al. Optically anisotropic colloids of controllable shape. Adv Mater. 2005;17(6):680–684.
[88] Bennett JS, Gibson LJ, Kelly RM, et al. Spatially-resolved rotational microrheology with an optically-trapped sphere. Sci Rep. 2013;3(1):1–5.
[89] Bishop AI, Nieminen TA, Heckenberg NR, et al. Optical microrheology using rotating laser-trapped particles. Phys Rev Lett. 2004;92(19):198104.
[90] Ma J, Bai L, Wang MD. Transcription under torsion. Science. 2013;340(6140):1580–1583.
[91] Parkin SJ, Knöner G, Nieminen TA, et al. Picoliter viscometry using optically rotated particles. Phys Rev E. 2007;76(4):041507.
[92] Juan ML, Righini M, Quidant R. Plasmon nano-optical tweezers. Nat Photonics. 2011;5(6):349–356.
[93] Kawata S, Sugiura T. Movement of micrometer-sized particles in the evanescent field of a laser beam. Opt Lett. 1992;17(11):772–774.
[94] Reece PJ, Garcés-Chávez V, Dholakia K. Near-field optical micromanipulation with cavity enhanced evanescent waves. Appl Phys Lett. 2006;88(22):221116.
[95] Pang Y, Gordon R. Optical trapping of a single protein. Nano Lett. 2012;12(1):402–406.
[96] Spesyvtseva SES, Dholakia K. Trapping in a material world. ACS Photonics. 2016;3(5):719–736.
[97] Gross P, Farge G, Peterman EJ, et al. Combining optical tweezers, single-molecule fluorescence microscopy, and microfluidics for studies of DNA–protein interactions. Meth Enzymol. 2010;475:427–453.
[98] Goksör M, Enger J, Hanstorp D. Optical manipulation in combination with multiphoton microscopy for single-cell studies. Appl Opt. 2004;43(25):4831–4837.
[99] Montag M, Rink K, Delacretaz G, et al. Laser-induced immobilization and plasma membrane permeabilization in human spermatozoa. Hum Reprod. 2000 Apr;15(4):846–852.
[100] Xie C, Dinno MA, Li Y-q. Near-infrared Raman spectroscopy of single optically trapped biological cells. Opt Lett. 2002;27(4):249–251.
[101] Jess P, Garcés-Chávez V, Smith D, et al. Dual beam fibre trap for Raman microspectroscopy of single cells. Opt Express. 2006;14(12):5779–5791.
[102] Diekmann R, Wolfson DL, Spahn C, et al. Nanoscopy of bacterial cells immobilized by holographic optical tweezers. Nat Commun. 2016;7(1):1–7.
[103] Kreysing MK, Kießling T, Fritsch A, et al. The optical cell rotator. Opt Express. 2008;16(21):16984–16992.
[104] Yang Z, Piksarv P, Ferrier DE, et al. Macro-optical trapping for sample confinement in light sheet microscopy. Biomed Opt Express. 2015;6(8):2778–2785.
[105] Dholakia K, Drinkwater BW, Ritsch-Marte M. Comparing acoustic and optical forces for biomedical research. Nat Rev Phys. 2020;2(9):480–491.
[106] Yang Z, Cole KL, Qiu Y, et al. Light sheet microscopy with acoustic sample confinement. Nat Commun. 2019;10(1):1–8.
[107] Thalhammer G, Steiger R, Meinschad M, et al. Combined acoustic and optical trapping. Biomed Opt Express. 2011;2(10):2859–2870.
[108] Capitanio M, Pavone FS. Interrogating biology with force: single molecule high-resolution measurements with optical tweezers. Biophys J. 2013;105(6):1293–1303.
[109] Kirkham GR, Britchford E, Upton T, et al. Precision assembly of complex cellular microenvironments using holographic optical tweezers. Sci Rep. 2015;5(1):1–7.
[110] Favre-Bulle I, Zhang S, Kashchuk A, et al. Optical tweezers bring micromachines to biology. Opt Photonics News. 2018;29(4):40–47.

1.6 Optical tweezers for the passive microrheology of cellular microenvironments

Following the overview provided in **Chapter 1.3 Optical Manipulation: a step change for biomedical science,** this section describes the specific use of optical tweezers for passive microrheology. To reiterate, microrheology is the study of the physical properties of materials, such as viscosity and elasticity, at the microscale. Generally, these properties can be measured at the microscale by tracking the motion of probe particles embedded within the material of interest. Microrheology techniques are categorised as either 'active', in which external forces drive the particle through the sample and strain is measured, and 'passive', where Brownian motion of the particle driven by thermal fluctuations in the surrounding medium is analysed [77, 78].

Briefly, in active microrheology with the optical tweezers a controlled oscillatory force at defined frequencies is applied to the trapped particle, and its resulting displacement is measured to characterise the sample's viscosity or elasticity. This approach allows for the direct quantification of strain-response relationships and is highly valuable in analysing materials with complex viscoelastic properties or active biological systems, or in materials where probing thermal fluctuations alone may be insufficient in resolving mechanical properties. However, active microrheology with the optical tweezers can perturb delicate systems, like the oocyte extracellular matrix and the embryo microenvironment, potentially disrupting their natural structural integrity and altering the measured viscosity. For these reasons, passive microrheology was considered a more appropriate approach.

For passive microrheology, Brownian motion of a trapped probe particle is tracked to determine the sample's viscosity. Here, several mathematical models can be applied to determine viscosity from Brownian motion. A key approach is to calculate the mean squared displacement (MSD) which measures the average distance particles travel over time and is defined as:

$$MSD(\tau) = \langle \big(x(t+\tau) - x(t)\big)^2 \rangle_t$$

(1)

In equation 1, τ represents the time lag and describes the average over all time points, $t.\ x$ describes the particle's position, with the squared value indicating the distance the particle has moved relative to its initial position, $(t = 0)$. The diffusion coefficient D, describes how quickly a particle diffuses in a fluid can then be calculated using the Stokes-Einstein equation:

$$D = \frac{k_B T}{6\pi\eta r}$$

(2)

In this equation, T is the temperature, η the medium viscosity, r the radius of the particle, and k_B is Boltzmann constant.

In contrast to traditional passive microrheology, where probe particles diffuse freely through a sample, optical tweezers confine the Brownian motion within a defined volume. This confinement allows for extended measurement periods as the particle stays within the field of view and does not diffuse away. While tracking unconfined particle motion provides an average measurement over a larger spatial region, optical trapping allows for more localised and precise characterisation of samples within a defined volume. This is beneficial when investigating micro-litre sized biological samples, such as the extracellular matrix and cytoskeleton of cells [79-81].

In addition to MSD, the position autocorrelation function can be computed to determine viscosity by describing how particle motion at one time is related to its motion at a later time. The position autocorrelation function provides insight into the sample's ability to store and dissipate energy and can be calculated as:

$$C(\tau) = \langle (x(t)x(t+\tau)) \rangle_t$$

(3)

Here, x represents the particle motion at time t. To calculate the autocorrelation C at a time lag τ, the particle's position at two different times is compared, one at time t and the other at a later time $t + \tau$. Time lag, τ , is the difference between the two times. Sample viscosity can be related to the autocorrelation function of the particle as described by Geiseler et al (2021) [82], where:

$$C(\tau) = \langle (x(t)x(t+\tau)) \rangle_t = \frac{k_B T}{k_x} \exp[-\frac{\tau k_x}{\gamma_x}]$$

(4)

Within this equation k_x describes the stiffness of the optical trap in the x dimension, which reflects the amount of force exerted by the tweezers to keep the particle trapped in place, k_B is the Boltzmann constant, T is the temperature of the sample, and τ is the time lag. The friction coefficient of the sample is given by:

$$\gamma x = 6\pi a \eta_x$$

(5)

Where a is the radius of the trapped particle and η_x is the viscosity of the sample. Crucial parameters include a high recording rate to capture fast particle motion, a high signal-to-noise ratio which enables detection of small changes in positions, and fine spatial resolution to precisely measure particle location. These features allow for accurate measurement of particle motion, and in turn allow us to calculate material viscosity.

Several studies have demonstrated the use of the optical tweezers for passive microrheology. For instance, in tracking the confined Brownian motion of a particle Hardiman et al. [79] was able to examine viscoelastic changes associated with cytoskeletal remodelling and stiffening in live HeLa cells. Similarly, Mendonca et al [80] applied optical tweezers to map local viscosity in the extracellular fluid surrounding breast cancer tumour spheroids and measure the viscoelasticity within engineered hydrogels. Their minimally perturbative approach shows a new frontier for both time-course investigations of drug transport

in cellular environments and for understanding how metastatic cells may remodel their microenvironment before migration. Within microbial systems, a similar method of passive microrheology with the optical tweezers was effective in the non-invasive measurement of sensitive viscosity changes in the microenvironment surrounding phytoplankton cells [81].

Together, these studies underscore the suitability of passive microrheology with the optical tweezers for the non-invasive characterisation of microscale environments, offering high spatial and temporal resolution. This capability is central to the present thesis, where the technique was applied to investigate the dynamic mechanical properties of the murine oocyte extracellular matrix and the murine embryo microenvironment.

While passive microrheology with the optical tweezers offers clear advantages, its performance can be constrained near sample boundaries, such as the edges of cell surfaces, where altered hydrodynamic drag and limited resolution can affect the accuracy of the measured viscosity [83]. Furthermore, the ability to resolve fast, Brownian displacements are inherently limited by the temporal and spatial resolution of the system, which are determined by the camera acquisition rate, optical precision, and signal-to-noise ratio. Edge effects, like controlled for in Guadayol et al, are particularly relevant in measurements adjacent to a cell surface. This effect is highly relevant to the embryo microenvironment chapter of this thesis, as measurements were performed at increasingly closer distances to the embryo's zona pellucida (40, 20, and 5 µm).

1.7 Impact of light exposure on embryo viability

A significant part of this thesis presents the novel use of optical tweezers to probe the microenvironment surrounding the embryo. Thus, it is important to consider the broader implications of light exposure on the developing embryo. Pre-implantation embryo development is a highly sensitive process. While embryos can develop in vitro under various conditions, there is ongoing debate about the impact of factors

beyond well-studied variables such as temperature [84], pH [85], oxygen levels [86], and culture media composition [87]. Notably, this includes the uncertain and conflicting evidence on the effect of light exposure on developing embryos in an in vitro setting as they normally develop within complete darkness. Notably, the impact of light exposure on developing embryos remains uncertain, with conflicting evidence from studies [88-91]. This is particularly relevant given that embryos develop in darkness in vivo [92, 93]. In IVF clinics, light is a powerful tool for observing and grading embryos at multiple stages of development, yet concerns have been raised regarding the intensity and spectrum of light to which embryos are exposed to during these procedures [92, 93]. Furthermore, as light-based technologies, such as label-free fluorescent imaging for embryo quality assessments increase in popularity [29-31, 94], understanding the potential risks of light exposure becomes increasingly important. These imaging modalities typically use a range of wavelengths, and it is essential to examine how discrete wavelengths might affect embryo development. Despite numerous studies exploring the effect of light on embryos, differences in experimental conditions have made direct comparisons between studies challenging. Therefore, this thesis also seeks to address this gap by utilising a standardised approach to examine the impact of discrete wavelengths of light on pre-implantation embryo development, embryo health, and post-transfer outcomes. This investigation is particularly relevant and informative as it will provide a better understanding of how light exposure may influence embryo quality and how we may avoid or mitigate any negative effects associated with particular wavelengths.

1.8 Summary and General Hypothesis

In vitro fertilisation (IVF) is a groundbreaking treatment for infertility, enabling millions of people to achieve their reproductive goals. However, despite its widespread use, IVF success rates have stagnated, with live birth rates averaging at approximately 17.5% per initiated cycle. One of the primary challenges in improving IVF outcomes lies in determining which embryo, from a cohort within a dish, has the highest potential to implant post-transfer and result in a live birth. Further, as oocyte quality is a key determinant

of IVF success, ranking oocytes – from highest to lowest developmental potential –may provide important information on the ability of the resultant embryo to lead to a live birth. However, current approaches for assessing oocyte and embryo developmental potential rely on morphological assessments which are highly subjective with an embryologist's experience dictating its predictive capacity [16, 95]. In other cell types, physical properties, of the surrounding microenvironment, such as viscosity, has been shown to correlate with cell viability. Whether this relationship exists for the oocyte and embryo has yet to be determined. To address this gap, this thesis explores the application of optical tweezers for passive microrheology to quantify the viscosity of the oocyte and embryo microenvironment. As this thesis aims to investigate these microenvironments in a previously unexplored way, murine embryos were used. While murine models have been widely used in reproductive biology due to their physiological similarities to humans, direct extrapolation should be approached with caution and requires further investigation. Using this model, **I hypothesise that microrheology with optical tweezers can detect differences in viscosity of the microenvironment surrounding oocytes and embryos. Further, I hypothesise that changes in viscosity are associated with (1) oocyte developmental competence and, (2) differences in metabolism at different stages of embryo development.** As I explore the use of light-based technologies in ART, I also investigate the impact of discrete wavelengths of light on the developing pre-implantation embryo. **I hypothesise that there will be wavelength-specific effects on the viability of pre-implantation embryos**

1.8.1 Specific hypotheses and aims

Hypothesis 1: Viscosity of the cumulus-oocyte extracellular matrix is positively correlated with oocyte developmental potential.

Aims to address this hypothesis:

1. Determine whether microrheology with optical tweezers can accurately measure viscosity.
2. Determine whether viscosity of the cumulus-oocyte matrix differs when derived from oocytes with high and low developmental potential.

Hypothesis 2: The viscosity of the microenvironment surrounding the embryo is higher at the blastocyst stage when compared to the earlier 4-cell stage of development.

Aims to address this hypothesis:

1. Determine whether microrheology with optical tweezers can measure differences in viscosity between various commercial embryo media.
2. Determine whether viscosity of the microenvironment surrounding embryos is different between pre- and post-compaction developmental stages.
3. Determine whether viscosity of the microenvironment surrounding embryos changes with increasing distance from the embryo.

Hypothesis 3: Exposure to shorter wavelengths will negatively impact embryo developmental potential compared to longer wavelengths.

Aims to address this hypothesis:

1. Determine how daily exposure to blue (470 nm), green (520 nm), yellow (590 nm), or red (620 nm) wavelengths impacts preimplantation embryo development and the viability of these embryos.
2. Determine how daily exposure to these wavelengths during preimplantation development impacts post-transfer outcomes.

1.9 References

1. Organization, W.H., *WHO fact sheet on infertility*. 2021, LWW. p. e52.
2. Organization, W.H., *Infertility prevalence estimates, 1990–2021*. 2023: World Health Organization.
3. Newman, J.E., Paul, R.C., and Chambers G.M., *Assisted reproductive technology in Australia and New Zealand 2021.* National Perinatal Epidemiology and Statistics Unit, The University of New South Wales: Sydney., 2023.
4. Jones, R.E. and K.H. Lopez, *Human reproductive biology*. 2013: Academic Press.
5. Yan, L., M. Yang, H. Guo, et al., *Single-cell RNA-Seq profiling of human preimplantation embryos and embryonic stem cells.* Nature structural & molecular biology, 2013. **20**(9): p. 1131-1139.
6. Leng, L., J. Sun, J. Huang, et al., *Single-cell transcriptome analysis of uniparental embryos reveals parent-of-origin effects on human preimplantation development.* Cell stem cell, 2019. **25**(5): p. 697-712. e696.
7. Braude, P., V. Bolton, and S. Moore, *Human gene expression first occurs between the four-and eight-cell stages of preimplantation development.* Nature, 1988. **332**(6163): p. 459-461.
8. Niakan, K.K., J. Han, R.A. Pedersen, et al., *Human pre-implantation embryo development.* Development, 2012. **139**(5): p. 829-841.
9. Marikawa, Y. and V.B. Alarcón, *Establishment of trophectoderm and inner cell mass lineages in the mouse embryo.* Molecular Reproduction and Development: Incorporating Gamete Research, 2009. **76**(11): p. 1019-1032.
10. Gardner, D.K., M. Lane, J. Stevens, et al., *Blastocyst score affects implantation and pregnancy outcome: towards a single blastocyst transfer.* Fertility and sterility, 2000. **73**(6): p. 1155-1158.
11. Mikkelsen, A.L. and S. Lindenberg, *Morphology of in-vitro matured oocytes: impact on fertility potential and embryo quality.* Human Reproduction, 2001. **16**(8): p. 1714-1718.

12. Loutradis, D., P. Drakakis, K. Kallianidis, et al., *Oocyte morphology correlates with embryo quality and pregnancy rate after intracytoplasmic sperm injection.* Fertility and sterility, 1999. **72**(2): p. 240-244.

13. Giorgetti, C., P. Terriou, P. Auquier, et al., *Implantation: Embryo score to predict implantation after in-vitro fertilization: based on 957 single embryo transfers.* Human Reproduction, 1995. **10**(9): p. 2427-2431.

14. Ziebe, S., K. Petersen, S. Lindenberg, et al., *Embryo morphology or cleavage stage: how to select the best embryos for transfer after in-vitro fertilization.* Human reproduction (Oxford, England), 1997. **12**(7): p. 1545-1549.

15. Lemseffer, Y., M.-E. Terret, C. Campillo, and E. Labrune, *Methods for assessing oocyte quality: a review of literature.* Biomedicines, 2022. **10**(9): p. 2184.

16. Wang, Q. and Q.-Y. Sun, *Evaluation of oocyte quality: morphological, cellular and molecular predictors.* Reproduction, Fertility and Development, 2006. **19**(1): p. 1-12.

17. Nasiri, N. and P. Eftekhari-Yazdi, *An overview of the available methods for morphological scoring of pre-implantation embryos in in vitro fertilization.* Cell Journal (Yakhteh), 2015. **16**(4): p. 392.

18. Xia, P., *Intracytoplasmic sperm injection: correlation of oocyte grade based on polar body, perivitelline space and cytoplasmic inclusions with fertilization rate and embryo quality.* Human reproduction (Oxford, England), 1997. **12**(8): p. 1750-1755.

19. Ebner, T., M. Moser, C. Yaman, et al., *Elective transfer of embryos selected on the basis of first polar body morphology is associated with increased rates of implantation and pregnancy.* Fertility and sterility, 1999. **72**(4): p. 599-603.

20. Ebner, T., M. Moser, M. Sommergruber, et al., *First polar body morphology and blastocyst formation rate in ICSI patients.* Human Reproduction, 2002. **17**(9): p. 2415-2418.

21. Talevi, R., R. Gualtieri, G. Tartaglione, and A. Fortunato, *Heterogeneity of the zona pellucida carbohydrate distribution in human oocytes failing to fertilize in vitro.* Human reproduction (Oxford, England), 1997. **12**(12): p. 2773-2780.

22. Gabrielsen, A., S. Lindenberg, and K. Petersen, *The impact of the zona pellucida thickness variation of human embryos on pregnancy outcome in relation to suboptimal embryo development. A prospective randomized controlled study.* Human Reproduction, 2001. **16**(10): p. 2166-2170.

23. Vanderhyden, B.C., P.J. Caron, R. Buccione, and J.J. Eppig, *Developmental pattern of the secretion of cumulus expansion-enabling factor by mouse oocytes and the role of oocytes in promoting granulosa cell differentiation.* Developmental biology, 1990. **140**(2): p. 307-317.

24. Hardarson, T., C. Hanson, A. Sjögren, and K. Lundin, *Human embryos with unevenly sized blastomeres have lower pregnancy and implantation rates: indications for aneuploidy and multinucleation.* Human Reproduction, 2001. **16**(2): p. 313-318.

25. Bendus, A.E.B., J.F. Mayer, S.K. Shipley, and W.H. Catherino, *Interobserver and intraobserver variation in day 3 embryo grading.* Fertility and sterility, 2006. **86**(6): p. 1608-1615.

26. Stensen, M.H., T. Tanbo, R. Storeng, et al., *Routine morphological scoring systems in assisted reproduction treatment fail to reflect age-related impairment of oocyte and embryo quality.* Reproductive biomedicine online, 2010. **21**(1): p. 118-125.

27. Sutter, P.D., D. Dozortsev, C. Qian, and M. Dhont, *Oocyte morphology does not correlate with fertilization rate and embryo quality after intracytoplasmic sperm injection.* Human Reproduction, 1996. **11**(3): p. 595-597.

28. Balaban, B., B. Urman, A. Sertac, et al., *Oocyte morphology does not affect fertilization rate, embryo quality and implantation rate after intracytoplasmic sperm injection.* Human reproduction (Oxford, England), 1998. **13**(12): p. 3431-3433.

29. Dwapanyin, G.O., D.J. Chow, T.C. Tan, et al., *Investigation of refractive index dynamics during in vitro embryo development using off-axis digital holographic microscopy.* Biomedical Optics Express, 2023. **14**(7): p. 3327-3342.

30. Tan, T.C., S.B. Mahbub, J.M. Campbell, et al., *Non-invasive, label-free optical analysis to detect aneuploidy within the inner cell mass of the preimplantation embryo.* Human Reproduction, 2022. **37**(1): p. 14-29.

31. Tan, T.C., H.M. Brown, J.G. Thompson, et al., *Optical imaging detects metabolic signatures associated with oocyte quality.* Biology of Reproduction, 2022. **107**(4): p. 1014-1025.

32. Dunning, K.R., K. Cashman, D.L. Russell, et al., *Beta-oxidation is essential for mouse oocyte developmental competence and early embryo development.* Biology of Reproduction, 2010. **83**(6): p. 909-918.

33. Blerkom, J.V., P. Davis, and J. Lee, *ATP content of human oocytes and developmental potential and outcome after in-vitro fertilization and embryo transfer.* Human Reproduction, 1995. **10**(2): p. 415-424.

34. Stojkovic, M., S.A. Machado, P. Stojkovic, et al., *Mitochondrial distribution and adenosine triphosphate content of bovine oocytes before and after in vitro maturation: correlation with morphological criteria and developmental capacity after in vitro fertilization and culture.* Biology of Reproduction, 2001. **64**(3): p. 904-909.

35. Radman, B.A., A. Alhameed, G. Shu, et al., *Cellular elasticity in cancer: a review of altered biomechanical features.* Journal of Materials Chemistry B, 2024.

36. Mierke, C.T., *Viscoelasticity acts as a marker for tumor extracellular matrix characteristics.* Frontiers in Cell and Developmental Biology, 2021. **9**: p. 785138.

37. Cukierman, E., R. Pankov, D.R. Stevens, and K.M. Yamada, *Taking cell-matrix adhesions to the third dimension.* Science, 2001. **294**(5547): p. 1708-1712.

38. Kshitiz, J. Park, P. Kim, et al., *Control of stem cell fate and function by engineering physical microenvironments.* Integrative biology, 2012. **4**(9): p. 1008-1018.

39. Metallo, C.M., M.A. Vodyanik, J.J. de Pablo, et al., *The response of human embryonic stem cell-derived endothelial cells to shear stress.* Biotechnology and bioengineering, 2008. **100**(4): p. 830-837.

40. Yim, E.K., S.W. Pang, and K.W. Leong, *Synthetic nanostructures inducing differentiation of human mesenchymal stem cells into neuronal lineage.* Experimental cell research, 2007. **313**(9): p. 1820-1829.

41. Dzamba, B.J. and D.W. DeSimone, *Extracellular matrix (ECM) and the sculpting of embryonic tissues.* Current topics in developmental biology, 2018. **130**: p. 245-274.

42. Elosegui-Artola, A., *The extracellular matrix viscoelasticity as a regulator of cell and tissue dynamics.* Current opinion in cell biology, 2021. **72**: p. 10-18.

43. Hoffman, B.D. and J.C. Crocker, *Cell mechanics: dissecting the physical responses of cells to force.* Annual review of biomedical engineering, 2009. **11**: p. 259-288.

44. Janmey, P.A. and C.A. McCulloch, *Cell mechanics: integrating cell responses to mechanical stimuli.* Annu. Rev. Biomed. Eng., 2007. **9**: p. 1-34.

45. Pelham Jr, R.J. and Y.-l. Wang, *Cell locomotion and focal adhesions are regulated by substrate flexibility.* Proceedings of the national academy of sciences, 1997. **94**(25): p. 13661-13665.

46. Wilems, T., S. Vardhan, S. Wu, and S. Sakiyama-Elbert, *The influence of microenvironment and extracellular matrix molecules in driving neural stem cell fate within biomaterials.* Brain research bulletin, 2019. **148**: p. 25-33.

47. Russell, D.L. and R.L. Robker, *Molecular mechanisms of ovulation: co-ordination through the cumulus complex.* Human reproduction update, 2007. **13**(3): p. 289-312.

48. Salustri, A., M. Yanagishita, C.B. Underhill, et al., *Localization and synthesis of hyaluronic acid in the cumulus cells and mural granulosa cells of the preovulatory follicle.* Developmental biology, 1992. **151**(2): p. 541-551.

49. Camaioni, A., A. Salustri, M. Yanagishita, and V.C. Hascall, *Proteoglycans and proteins in the extracellular matrix of mouse cumulus cell–oocyte complexes.* Archives of biochemistry and biophysics, 1996. **325**(2): p. 190-198.

50. Hernandez-Gonzalez, I., I. Gonzalez-Robayna, M. Shimada, et al., *Gene expression profiles of cumulus cell oocyte complexes during ovulation reveal cumulus cells express neuronal and immune-related genes: does this expand their role in the ovulation process?* Molecular endocrinology, 2006. **20**(6): p. 1300-1321.

51. Watson, L.N., D.G. Mottershead, K.R. Dunning, et al., *Heparan sulfate proteoglycans regulate responses to oocyte paracrine signals in ovarian follicle morphogenesis.* Endocrinology, 2012. **153**(9): p. 4544-4555.

52. Richards, J.S., D.L. Russell, S. Ochsner, et al., *Novel signaling pathways that control ovarian follicular development, ovulation, and luteinization.* Recent progress in hormone research, 2002. **57**(1): p. 195-220.

53. Dunning, K.R., L.N. Watson, D.J. Sharkey, et al., *Molecular filtration properties of the mouse expanded cumulus matrix: controlled supply of metabolites and extracellular signals to cumulus cells and the oocyte.* Biology of Reproduction, 2012. **87**(4): p. 89, 81-10.

54. Hong, S., P. Chiu, K. Lee, et al., *Establishment of a capillary–cumulus model to study the selection of sperm for fertilization by the cumulus oophorus.* Human Reproduction, 2004. **19**(7): p. 1562-1569.

55. Chen, H., C. Kui, and H.C. Chan, *Ca2+ mobilization in cumulus cells: Role in oocyte maturation and acrosome reaction.* Cell Calcium, 2013. **53**(1): p. 68-75.

56. Dunning, K.R., M. Lane, H.M. Brown, et al., *Altered composition of the cumulus-oocyte complex matrix during in vitro maturation of oocytes.* Human Reproduction, 2007. **22**(11): p. 2842-2850.

57. Dunning, K.R., L.N. Watson, V.J. Zhang, et al., *Activation of mouse cumulus-oocyte complex maturation in vitro through EGF-like activity of versican.* Biology of Reproduction, 2015. **92**(5): p. 116, 111-110.

58. Russell, D.L., S.A. Ochsner, M. Hsieh, et al., *Hormone-Regulated Expression and Localization of Versican in the Rodent Ovary.* Endocrinology, 2003. **144**(3): p. 1020-1031.

59. McKenzie, L., S. Pangas, S. Carson, et al., *Human cumulus granulosa cell gene expression: a predictor of fertilization and embryo selection in women undergoing IVF.* Human Reproduction, 2004. **19**(12): p. 2869-2874.

60. Cillo, F., T.A. Brevini, S. Antonini, et al., *Association between human oocyte developmental competence and expression levels of some cumulus genes.* Reproduction, 2007. **134**(5): p. 645-650.

61. Li, Y., R.-Q. Li, S.-B. Ou, et al., *Increased GDF9 and BMP15 mRNA levels in cumulus granulosa cells correlate with oocyte maturation, fertilization, and embryo quality in humans.* Reproductive biology and Endocrinology, 2014. **12**: p. 1-9.

62. Gebhardt, K.M., D.K. Feil, K.R. Dunning, et al., *Human cumulus cell gene expression as a biomarker of pregnancy outcome after single embryo transfer.* Fertility and sterility, 2011. **96**(1): p. 47-52. e42.

63. Wathlet, S., T. Adriaenssens, I. Segers, et al., *Cumulus cell gene expression predicts better cleavage-stage embryo or blastocyst development and pregnancy for ICSI patients.* Human Reproduction, 2011. **26**(5): p. 1035-1051.

64. Chen, X., R. Bonfiglio, S. Banerji, et al., *Micromechanical analysis of the hyaluronan-rich matrix surrounding the oocyte reveals a uniquely soft and elastic composition.* Biophysical Journal, 2016. **110**(12): p. 2779-2789.

65. Gardner, D.K., M. Lane, I. Calderon, and J. Leeton, *Environment of the preimplantation human embryo in vivo: metabolite analysis of oviduct and uterine fluids and metabolism of cumulus cells.* Fertility and sterility, 1996. **65**(2): p. 349-353.

66. Hannan, N., P. Paiva, K. Meehan, et al., *Analysis of fertility-related soluble mediators in human uterine fluid identifies VEGF as a key regulator of embryo implantation.* Endocrinology, 2011. **152**(12): p. 4948-4956.

67. Zhang, T., Y. Zheng, R. Han, et al., *Effects of pyruvate on early embryonic development and zygotic genome activation in pigs.* Theriogenology, 2022. **189**: p. 77-85.

68. Leese, H.J., S.A. Hugentobler, S.M. Gray, et al., *Female reproductive tract fluids: composition, mechanism of formation and potential role in the developmental origins of health and disease.* Reproduction, Fertility and Development, 2007. **20**(1): p. 1-8.

69. Thompson, J., R. Partridge, F. Houghton, et al., *Oxygen uptake and carbohydrate metabolism by in vitro derived bovine embryos.* Reproduction, 1996. **106**(2): p. 299-306.

70. Trimarchi, J.R., L. Liu, D.M. Porterfield, et al., *Oxidative phosphorylation-dependent and-independent oxygen consumption by individual preimplantation mouse embryos.* Biology of Reproduction, 2000. **62**(6): p. 1866-1874.

71. Chi, F., M.S. Sharpley, R. Nagaraj, et al., *Glycolysis-independent glucose metabolism distinguishes TE from ICM fate during mammalian embryogenesis.* Developmental cell, 2020. **53**(1): p. 9-26. e24.

72. Brown, J. and D. Whittingham, *The roles of pyruvate, lactate and glucose during preimplantation development of embryos from F1 hybrid mice in vitro.* Development, 1991. **112**(1): p. 99-105.

73. Gardner, D.K. and H.J. Leese, *Assessment of embryo viability prior to transfer by the noninvasive measurement of glucose uptake.* Journal of Experimental Zoology, 1987. **242**(1): p. 103-105.

74. Gott, A., K. Hardy, R. Winston, and H. Leese, *Non-invasive measurement of pyruvate and glucose uptake and lactate production by sigle human preimplantation embryos.* Human Reproduction, 1990. **5**(1): p. 104-108.

75. Gardner, D.K. and A.J. Harvey, *Blastocyst metabolism.* Reproduction, Fertility and Development, 2015. **27**(4): p. 638-654.

76. Reinhart, W.H., R. Gaudenz, and R. Walter, *Acidosis induced by lactate, pyruvate, or HCl increases blood viscosity.* Journal of critical care, 2002. **17**(1): p. 68-73.

77. Mao, Y., P. Nielsen, and J. Ali, *Passive and active microrheology for biomedical systems.* Frontiers in bioengineering and biotechnology, 2022. **10**: p. 916354.

78. Squires, T.M. and T.G. Mason, *Fluid mechanics of microrheology.* Annual review of fluid mechanics, 2010. **42**(1): p. 413-438.

79. Hardiman, W., M. Clark, C. Friel, et al., *Living cells as a biological analog of optical tweezers–a non-invasive microrheology approach.* Acta Biomaterialia, 2023. **166**: p. 317-325.

80. Mendonca, T., K. Lis-Slimak, A.B. Matheson, et al., *OptoRheo: Simultaneous in situ micro-mechanical sensing and imaging of live 3D biological systems.* Communications Biology, 2023. **6**(1): p. 463.

81. Guadayol, Ò., T. Mendonca, M. Segura-Noguera, et al., *Microrheology reveals microscale viscosity gradients in planktonic systems.* Proceedings of the national academy of sciences, 2021. **118**(1): p. e2011389118.

82. Gieseler, J., J.R. Gomez-Solano, A. Magazzù, et al., *Optical tweezers—from calibration to applications: a tutorial.* Advances in Optics and Photonics, 2021. **13**(1): p. 74-241.

83. Leach, J., H. Mushfique, S. Keen, et al., *Comparison of Faxén's correction for a microsphere translating or rotating near a surface.* Physical Review E—Statistical, Nonlinear, and Soft Matter Physics, 2009. **79**(2): p. 026301.

84. Walters, E.A., J.L. Brown, R. Krisher, et al., *Impact of a controlled culture temperature gradient on mouse embryo development and morphokinetics.* Reproductive biomedicine online, 2020. **40**(4): p. 494-499.

85. Swain, J.E., *Optimizing the culture environment in the IVF laboratory: impact of pH and buffer capacity on gamete and embryo quality.* Reproductive biomedicine online, 2010. **21**(1): p. 6-16.

86. Wale, P. and D. Gardner, *Time-lapse analysis of mouse embryo development in oxygen gradients.* Reproductive biomedicine online, 2010. **21**(3): p. 402-410.

87. Gardner, D. and R. Kelley, *Impact of the IVF laboratory environment on human preimplantation embryo phenotype.* Journal of Developmental Origins of Health and Disease, 2017. **8**(4): p. 418-435.

88. Bedford, J. and A. Dobrenis, *Light exposure of oocytes and pregnancy rates after their transfer in the rabbit.* Reproduction, 1989. **85**(2): p. 477-481.

89. Takenaka, M., T. Horiuchi, and R. Yanagimachi, *Effects of light on development of mammalian zygotes.* Proceedings of the national academy of sciences, 2007. **104**(36): p. 14289-14293.

90. Oh, S.J., S.P. Gong, S.T. Lee, et al., *Light intensity and wavelength during embryo manipulation are important factors for maintaining viability of preimplantation embryos in vitro.* Fertility and sterility, 2007. **88**(4): p. 1150-1157.

91. Korhonen, K., S. Sjövall, J. Viitanen, et al., *Viability of bovine embryos following exposure to the green filtered or wider bandwidth light during in vitro embryo production.* Human Reproduction, 2009. **24**(2): p. 308-314.

92. Jacques, S.L., D.R. Weaver, and S.M. Reppert, *Penetration of light into the uterus of pregnant mammals.* Photochemistry and photobiology, 1987. **45**(5): p. 637-641.

93. Del Giudice, M., *Alone in the dark? Modeling the conditions for visual experience in human fetuses.* Developmental psychobiology, 2011. **53**(2): p. 214-219.

94. Shah, J.S., M. Venturas, T.H. Sanchez, et al., *Fluorescence lifetime imaging microscopy (FLIM) detects differences in metabolic signatures between euploid and aneuploid human blastocysts.* Human Reproduction, 2022. **37**(3): p. 400-410.

95. Richani, D., K.R. Dunning, J.G. Thompson, and R.B. Gilchrist, *Metabolic co-dependence of the oocyte and cumulus cells: essential role in determining oocyte developmental competence.* Human reproduction update, 2021. **27**(1): p. 27-47.

Chapter 2
Microrheology of the cumulus-oocyte matrix using optical tweezers

2.1 Introduction and Significance

Oocyte quality is an important determinant of success in an in vitro fertilisation (IVF) cycle, yet current assessments are not predictive of clinical success. Considering the importance of oocyte quality, there is a pressing need for objective and precise methods to determine oocyte viability. Optical tweezers may be used for passive microrheology of the oocyte microenvironment. In turn, this may offer a promising, non-invasive approach for objectively determining oocyte viability. In the following study, I used optical tweezers to measure the viscosity of the cumulus-oocyte matrix derived from high- and low-viability oocytes, following in vivo or in vitro maturation, respectively. Investigation of this matrix was chosen based on the known differences in their composition between in vivo and in vitro derived oocytes and the impact of such matrices on development and function in other cell types. A significant difference in viability was first confirmed. Compared to in vivo maturation, in vitro matured oocytes had significantly lower viability, demonstrating decreased cumulus expansion and reduced developmental potential following fertilisation. Using optical tweezers, there was a positive correlation between matrix viscosity and oocyte viability. In vitro matured matrices were shown to have significantly lower viscosity than their in vivo matured counterparts. In the broader context of this thesis, this work highlights the potential of light-based measurements, in this case through optical tweezers, as novel, objective method for non-invasive identification of oocyte developmental potential. This method could supplement current clinical methods for oocyte quality assessment thus potentially enhancing IVF efficiency.

2.2 Publication Statement

This section is presented as an "Under Review" submission to the Journal of Physics: Photonics by Carl A Campugan, Megan Lim, Tiffany Cheow Yuen Tan, Erik Schartner, Yoshihiko Arita, Graham Bruce, Tania Mendonca, Amanda J Wright, Kishan Dholakia, Kylie R Dunning. *Microrheology of the Cumulus-Oocyte matrix using optical tweezers.*

2.3 Statement of Authorship

Statement of Authorship

Title of Paper	Microrheology of the Cumulus-Oocyte matrix using optical tweezers
Publication Status	☐ Published ☐ Accepted for Publication ☑ Submitted for Publication ☐ Unpublished and Unsubmitted work written in manuscript style
Publication Details	Under review. Submitted for publication 22 October 2024 to the *Journal of Physics: Photonics*

Principal Author

Name of Principal Author (Candidate)	Carl Adrian Campugan		
Contribution to the Paper	• Animal handling, development of experimental instrument • Experimental design, data acquisition, analysis, interpretation and figure generation • Wrote the first draft, edited, and revised the manuscript for submission • Accepts responsibility for all aspects of the work, ensuring that any questions regarding the accuracy or integrity of the content are thoroughly investigated and addressed.		
Overall percentage (%)	30%		
Certification:	This paper reports on original research I conducted during the period of my Higher Degree by Research candidature and is not subject to any obligations or contractual agreements with a third party that would constrain its inclusion in this thesis. I am the primary author of this paper.		
Signature	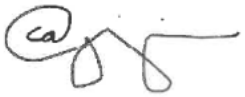	Date	30/10/24

Co-Author Contributions

By signing the Statement of Authorship, each author certifies that:

i. the candidate's stated contribution to the publication is accurate (as detailed above);

ii. permission is granted for the candidate in include the publication in the thesis; and

iii. the sum of all co-author contributions is equal to 100% less the candidate's stated contribution.

Name of Co-Author	Dr Chris Perella (joint first author)		
Contribution to the Paper	Chris' contribution in this publication were: • Experimental design, data acquisition, analysis, interpretation and figure generation • Diagnosed and resolved issues, aiding in enhancing optical tweezers functionality • Wrote the first draft, edited, and revised the manuscript for submission • Accepts responsibility for all aspects of the work, ensuring that any questions regarding the accuracy or integrity of the content are thoroughly investigated and addressed.		
Signature		Date	1/11/24

Contribution to the Paper	Graham's contributions in this publication were: • Optical tweezers logistics - built and shipped components and schematics • Provided feedback and accepted the final draft for submission • Accepts responsibility for all aspects of the work, ensuring that any questions regarding the accuracy or integrity of the content are thoroughly investigated and addressed.		
Signature	Graham D Bruce	Date	1/11/24

Name of Co-Author	Dr. Tania Mendonca		
Contribution to the Paper	Tania's contributions in this publication were: • Data interpretation • Provided feedback on the second – final draft of the submitted manuscript that led to the generation of additional figures and discussion points • Accepts responsibility for all aspects of the work, ensuring that any questions regarding the accuracy or integrity of the content are thoroughly investigated and addressed.		
Signature		Date	19/11/24

Name of Co-Author	Prof. Amanda J Wright		
Contribution to the Paper	Amanda's contributions in this publication were: • Data interpretation • Provided feedback on the second – final draft of the submitted manuscript that led to the generation of additional figures and discussion points • Accepts responsibility for all aspects of the work, ensuring that any questions regarding the accuracy or integrity of the content are thoroughly investigated and addressed.		
Signature		Date	30/10/24

Name of Co-Author	Prof. Kishan Dholakia		
Contribution to the Paper	Kishan's contributions to this publication were: • Served as the primary contributor for the acquisition, funding and development of the optical tweezers • Diagnosed and resolved issues, aiding in enhancing optical tweezers functionality • Aided in framing the experiment • Provided seminal feedback on framing the experimental design and data analysis and interpretation • Wrote and edited the working drafts, and approved the final manuscript for submission • Accepts responsibility for all aspects of the work, ensuring that any questions regarding the accuracy or integrity of the content are thoroughly investigated and addressed.		
Signature	K Dholakia	Date	19/11/2024

Name of Co-Author	Associate Professor Kylie R. Dunning		
Contribution to the Paper	Kylie's contributions to this publication were: • Conceived the idea and primary supervisor of this work • Secured funding for the study • Provided seminal feedback on framing the experimental design, data analysis, figure generation, and data interpretation • Wrote and edited the working drafts, and approved the final manuscript for submission • Accepts responsibility for all aspects of the work, ensuring that any questions regarding the accuracy or integrity of the content are thoroughly investigated and addressed.		
Signature		Date	19/11/2024

2.4 Microrheology of the Cumulus-Oocyte Matrix using Optical Tweezers

Microrheology of the Cumulus-Oocyte Matrix using Optical Tweezers

C. A. Campugan[1,4,†], C. Perrella[2,†], M. Lim[1], C. Y. Tan[1], E. P. Schartner[2], Y. Arita[3], G. D. Bruce[3], T. Mendonca[4], A. J. Wright[4], K. Dholakia[2,3,‡,*], K. R. Dunning[1,‡,]**

[1] Centre of Light for Life & The Robinson Research Institute, School of Biomedicine, University of Adelaide, Adelaide, SA, Australia.
[2] Centre of Light for Life & Institute for Photonics and Advanced Sensing & School of Biological Sciences, University of Adelaide, Adelaide, SA, Australia.
[3] SUPA, School of Physics & Astronomy, University of St Andrews, North Haugh, St Andrews KY16 9SS, UK.
[4] Optics and Photonics Research Group, Faculty of Engineering, University of Nottingham, Nottingham, NG7 2RD, UK.
†, ‡ These authors contributed equally to this work.

E-mail: *kd1@st-andrews.ac.uk, **kylie.dunning@adelaide.edu.au

17 November 2024

Abstract. Optical tweezers has emerged as a powerful, versatile approach for a range of studies in cellular and molecular biology. A particular highlight has been its use for microrheology measurements in miniscule sample volumes. In this study, we demonstrate the first ever application of optical tweezers to investigate the viscosity of the extracellular matrix surrounding mammalian oocytes and determine whether this is associated with oocyte developmental potential. By analysing the motion of a trapped particle, we can quantify the mechanical properties of this matrix, thus overcoming limitations of traditional passive microrheology techniques that rely on free diffusion. We utilise two maturation methods - in vivo and in vitro - to generate oocytes with differing developmental potential. Our findings indicate that oocytes matured in vivo exhibit higher viability post-fertilisation compared to their in vitro counterparts, and we establish a positive correlation between extracellular matrix viscosity and oocyte developmental potential. This work demonstrates that optical tweezers are a novel, non-invasive tool for assessing oocyte quality, contributing to valuable insights to the field of reproductive biology.

Keywords: microrheology, optical tweezers, viscosity, extracellular matrix, cumulus oocyte complex, oocyte quality

1. Introduction

The mechanical effects of light upon matter have been used to manipulate particles since 1970, with the first demonstration of the counter-propagating dual-beam optical trap geometry [1]. Subsequently, Ashkin demonstrated optical tweezers in 1986, which confined a particle in three dimensions using a single laser beam [2]. Optical tweezers have established themselves as the method of choice for manipulating micro- to nano-sized particles [3], enabling researchers to readily track particles with nanometer precision. For small displacements from equilibrium position, a trapped particle acts as a Hookean spring. In knowing the position of a particle, optical tweezers can be used as a force transducer, able to detect forces in the pico- to femto-Newton scales [4, 5, 6, 7]. This has made optical tweezers of particular relevance to the field of single molecule biophysics. They have found use in characterizing the dynamics of molecular motors such as kinesin [4], as well as force and velocity measurements of RNA polymerase [5]. At a larger scale, optical tweezers have proved useful in studying interactions between cells such as the binding of malaria to red blood cells [8] and other cell-cell interactions [9, 10]. By analyzing the motion of a trapped bead across a broad frequency range, optical tweezers offer a powerful method for microrheology, enabling the quantification of mechanical properties in materials with volumes ranging from femto- to microliters [11, 12, 13, 14].

Contemporary passive microrheology techniques involve tracking the free diffusion of probe particles within a medium [15, 16]. While these methods are useful in monitoring how samples change mechanically over time, they have limitations in their capacity to measure only equilibrium systems that exhibit linear response characteristics [17, 18]. Furthermore, using free diffusion of a particle may limit the duration of tracking we can record thus limiting the low frequency information we can acquire. Finally, as a freely diffusing particle is not localized, in contrast to a trapped particle, the measurement region is large. The application of optical tweezers for passive microrheology addresses these limitations by confining a single particle to a localized region within the sample of interest. This setup is advantageous for the collection of particle thermal motion over extended periods. Such a measurement can thus represent a broad range of frequencies, a capability crucial for the precise characterization of nonlinear viscoelastic properties in various heterogenous materials [19]. Interestingly, the viscoelastic properties of cells and their surrounding extracellular matrix are associated with viability and function [20, 21]. For example, an increase in extracellular matrix stiffness is positively correlated with cancer cell malignancy [22]. In the current study we aim to determine whether extracellular matrix viscosity is associated with the viability of mammalian oocytes.

The growth and maturation of oocytes is critical for fertilization and subsequent embryo development [23, 24]. The final stage of oocyte maturation involves the production of extracellular matrix by the cells that surround the oocyte. Interestingly, the expression of several genes responsible for the production of this matrix are positively associated with live birth outcomes in clinical IVF [25, 26]. Further, disrupting the production of these matrix components in mouse models is associated with reduced or failed ovulation and poor oocyte quality [27, 28, 25]. Considering the importance of this matrix, its viscosity may act as a surrogate measure of oocyte quality.

In this paper, we employ microrheology with optical tweezers for the first time to measure the viscosity of the extracellular matrix that surrounds the oocyte. To generate oocytes with varying developmental potential, we utilize two methods of maturation: In vivo and in vitro oocyte maturation. Oocyte maturation in vivo occurs within ovarian follicles in the body, while in vitro maturation occurs in a laboratory setting using culture media. We confirm that oocytes matured in vivo have a higher developmental potential, post-fertilization, than those matured in vitro. Excitingly, we demonstrate that extracellular matrix viscosity positively correlates with oocyte developmental potential. The small sample volume required for these measurements, together with its non-invasive approach, shows that optical tweezers may offer an original approach for assessing oocyte developmental potential.

The paper is structured in the following way: The optical tweezers used for these measurements is presented in Sec. 2 along with results verifying their measurement precision and accuracy. Section 3 describes the preparation of oocytes and examines their developmental potential post-fertilization. The microrheology of the extracellular matrix using optical tweezers is presented in Sec. 4. Finally the results and their significance are discussed in Sec. 5, and our conclusion presented in Sec. 6.

2. Optical Tweezers Setup and Calibration

A schematic of the optical tweezers system is shown in Fig. 1a. The trapping laser operates at 1064 nm (Coherent Mephisto). The laser was set to be linearly polarised using a polarising beam splitter (PBS), with fine tuning of the laser power achieved using a half-wave plate and second PBS. The beam was expanded with a telescope to over-fill the back aperture of the

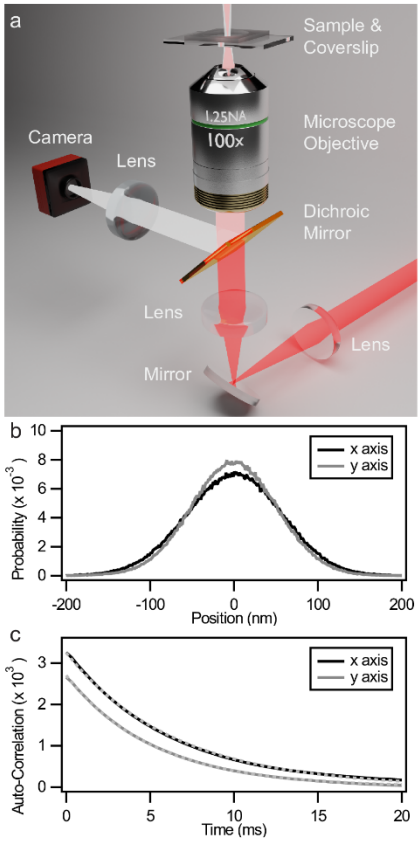

Figure 1. (a) Diagram showing the trapping beam being focused by a microscope objective into the sample creating the optical trap. b) Histogram of the bead's position distribution in the optical trap. c) Auto-correlation of the particle position with fits to Eqn. 1 (dashed lines). Particle position distribution and auto-correlation amplitudes differ between the x and y dimensions due to slight differences in trap stiffnesses in each dimension.

microscope objective by more than 100 %. A second telescope in the path made the back aperture conjugate with a steering mirror to position the beam as desired within the sample volume. A 100× magnification oil immersion microscope objective was used to generate a highly focused light beam for three-dimensional trapping (Nikon CFI E Plan Achromat, NA = 1.25). This resulted in a laser spot size at the focal point of approximately $\lambda / (2\,\mathrm{NA}) = 0.4\,\mu$m. The optical power of the trapping laser in the sample was approximately 0.4 mW. This optical power density was two-fold lower than that which would produce heating within the sample and influence viscosity measurements above the measurement precision [29].

Samples for the optical tweezers were held on a three-axis translation stage to control both the lateral and axial bead position when trapped. The stage was temperature controlled with a nominal set temperature of 37 °C at a stability of 20 mK over 10 minutes as per cell culture conditions to ensure the samples retained their biological viability [30]. The samples were mounted on a Type 1 cover-slip (150 μm thick) with a 13 mm diameter, 120 μm deep, adhesive well which contained the 16 μL of sample. A second cover-slip was mounted on top of the well to prevent evaporation. Silica beads with a $1.05 \pm 0.16\,\mu$m diameter (Polysciences 24326-15) were used to probe the viscosity of the sample medium. The silica bead diameter, along with its tight three-dimensional confinement within the trap, result in a measurement volume of approximately a few femto-liters. For validation of the system, the silica bead solution was diluted to a concentration of 1:10,000, corresponding to 1×10^7 particles/ml, using heavy water (D_2O). This medium was chosen for its low absorption at 1064 nm so we could reduce heating from the trapping beam.

To image the trapped silica bead, a white light LED illuminated the sample from above through a long working distance 20× magnification microscope objective (Mitutoyo M Plan Apo NIR) with NA = 0.4. The sample was subsequently imaged through the 100× magnification microscope objective that created the optical trap. The imaging path incorporated a dichroic filter which separated the white light from the 1064 nm trapping light. An imaging lens focused the white light onto a camera (Basler ACA1440-220um). The image magnification was determined using a 1951 USAF resolution test target and contact reticle giving an image magnification of 49×, or 69.5 nm/pixel scaling. The motion of a trapped bead was recorded in a 36×36 pixels region of interest to reduce data transfer requirements, allowing the camera to record at approximately 3,000 fps.

Once a bead was trapped, it was moved 20 μm above the surface of the cover slip to avoid this boundary wall significantly affecting viscosity measurements [31]. A typical measurement of the bead spanned 36 s, or 110,000 frames. To locate the centre of the bead, each frame was fitted with a two-dimensional Gaussian function with the x and y centre locations being free fitting parameters, whilst the background offset, width of the bead, and shadow depth were held constant to speed up the fitting routine. The returned parameters tracked the x and y centre position of the bead over the 36 s recording. A typical data set of x

and y positions is shown in Fig. 1b.

To determine the viscosity of the sample and the trap stiffness of the optical tweezers, auto-correlation analysis of the particle position was utilised. The relationship between the particle's auto-correlation function (as in Fig. 1c) and these physical parameters is given by [32]:

$$c_\tau = \langle x\,(t)\,x\,(t+\tau)\rangle = \frac{k_B T}{\kappa_x}\exp\left[-\frac{\tau\kappa_x}{\gamma_x}\right] \quad (1)$$

where k_B is the Boltzmann constant, T is the temperature of the sample, and κ_x is the stiffness of the optical tweezers potential in the x dimension, and τ is the delay time. The friction coefficient of the sample given by:

$$\gamma_x = 6\pi a\eta_x \quad (2)$$

and a is the radius of the trapped particle, and η_x is the viscosity of the sample. This analysis is performed on both the x and y dimensions with the retrieved viscosity being the average of η_x and η_y. This analysis assumes the fluids that are being measured are Newtonian in their behaviour. This was verified in all of our measurements by calculating the complex shear modulus and its Fourier frequency dependence in which we found the elastic (storage) modulus to be negligible, and the viscous (loss) modulus to increase linearly with Fourier frequency, both of which are indicators of a Newtonian fluid [33, 14].

The performance of the optical tweezers system, temperature controlled stage, and data analysis was verified using two liquid media with well-documented viscosities: heavy water (D_2O) and glycerol. Heavy water was initially tested as it has a well known temperature dependent viscosity [34]. To account for any variability, the viscosity of each sample was measured at 4 different locations (separated by 1-2 mm) with a different bead trapped at each location. This procedure was undertaken as the biological samples to be tested may exhibit a non-uniform, e.g. spatially varying, viscosity. Thus an average viscosity was derived from these multiple samples. At each location, three sets of 110,000 frames were recorded to ensure enough measurements were taken to obtain reliable statistics. In total, 12 individual viscosity measurement were made and averaged together to form the average viscosity measurement for the set temperature. This measurement procedure was repeated for temperatures from room temperature (22 °C) to 39 °C. The measured viscosities were compared to literature [34] showing good agreement, see Fig. 2a.

A wider range of viscosities was tested using varying concentrations of glycerol dissolved in water. Mass fractions of glycerol from 0 % (only water) up to 45 % were used producing sample viscosities from 0.9 mPa.s up to near 3 mPa.s. The same experimental procedure as described for D_2O was followed, leading to measured viscosities presented in Fig. 2b. The measured values were compared to literature [35], again showing good agreement.

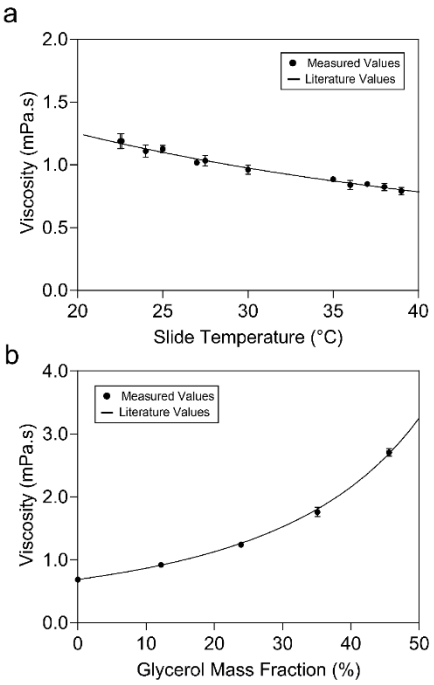

Figure 2. (a) Viscosity measurements of D_2O at increasing sample temperature showing good agreement with literature [34]. (b) Viscosity measurements of glycerol with varying glycerol mass fraction dissolved in H_2O, also showing good agreement with literature [35].

3. Maturation of and assessment of developmental potential

Oocytes were isolated from prepubertal female (21–23 days old) CBA x C57BL/6 first filial (F1) generation (CBAF1) mice provided by the Laboratory Animal Services (University of Adelaide, SA, Australia). All experiments were approved by the University of Adelaide Animal Ethics Committee (M-2023-004) and conducted in accordance with the Australian Code of Practice for the Care and Use of Animals for Scientific Purposes.

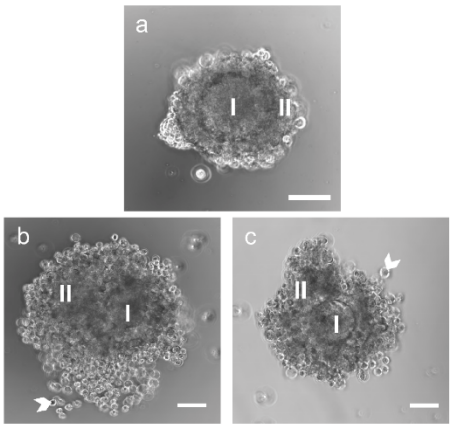

Figure 3. (a) Representative image of an immature cumulus oocyte complex. (b) and (c) show representative images of in vivo and in vitro matured cumulus oocyte complexes, respectively. I and II in all images denote the oocyte and surrounding cumulus cells, respectively. Notches indicate cumulus cells located away from the main mass of cells indicating extracellular matrix existence beyond the visible cumulus mass. Scale bar 50 μm in length.

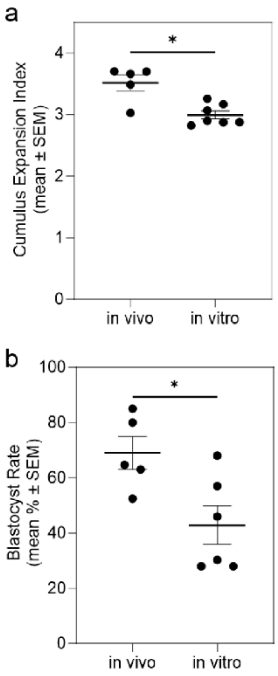

Figure 4. (a) Cumulus expansion of in vivo and in vitro matured cumulus oocyte complexes. (b) Developmental potential, or quality, of in vivo and in vitro matured oocytes (assessed by the ability of fertilized oocytes to reach the blastocyst stage of preimplantation embryo development). Blastocyst rate calculated from the number of 2-cell embryos at 24 hours post fertilization. Data are presented as mean ± standard error of the mean (SEM). Data in (a) is from 5 - 7 experimental replicates representative of 590 (in vivo) or 788 (in vitro) cumulus oocyte complexes. Data in (b) is from 5 - 6 experimental replicates, representative of 264 (in vivo) or 262 (in vitro) blastocyst-stage embryos. Data were analyzed using an unpaired t-test. * $P < 0.05$

For in vivo matured oocytes, female mice were injected with 5 IU of equine chorionic gonadotropin (eCG; Folligon, Braeside, VIC, Australia). Forty six hours later, mice received an injection of 5 IU of human chorionic gonadotrophin (hCG; ILEX; North Carolina, United States). At 16 hours post hCG injection, mice were culled and their ovaries and associated oviducts dissected and placed into HEPES buffered alpha MEM medium supplemented 5 % (v/v) fetal calf serum (FCS) at 37 °C. In vivo matured oocytes and their associated cumulus cells – collectively known as cumulus oocyte complexes (COCs) – were isolated by puncturing the ampulla region of the oviduct. These COCs comprise of a central oocyte surrounded by cumulus cells (Fig. 3). During the process of oocyte maturation, the cumulus cells undergo volumetric expansion (Fig. 3: (a) immature, unexpanded COC *vs.* (b,c) mature, expanded COCs) due to the production and release of vast amounts of extracellular matrix from the cumulus cells [36].

For in vitro matured COCs, female mice received a 5 IU injection of eCG. Forty six hours post eCG, mice were culled by cervical dislocation and ovaries dissected and placed into in HEPES buffered alpha MEM medium supplemented 5 % (v/v) fetal calf serum (FCS) at 37 °C. Immature, unexpanded COCs were released from ovaries by gently puncturing large antral follicles. Immature, unexpanded COCs (Fig. 3a) were then placed into culture drops (10 COCs per 500 μL) of pre-equilibrated bicarbonate buffered alpha MEM medium containing 5 % (v/v) FCS, 50 mIU/mL follicle stimulating hormone (Los Angeles Biomedical Research Institute, LA, USA), and 3 ng/mL recombinant epidermal growth factor (R and D Systems, MN, USA) overlaid with paraffin oil (Merck Group, Darmstadt, Germany). The in vitro maturation process was carried out at 37 °C in a humidified incubator with 6 % CO_2 and 94 % air for 16 hours.

To evaluate the impact of these maturation

conditions on oocyte developmental potential, we quantified the degree of cumulus expansion (as described in [37]) following in vivo or in vitro maturation. Cumulus expansion is scored on a scale of 0 to 4. Briefly, a score of 0 indicates no expansion of the cumulus cell layers and that some or all of these cells have detached from the oocyte; a score of 1 indicates no expansion but cumulus cells remain attached to the oocyte; 2 indicates expansion of the outer layer of cells; 3 indicates expansion of all layers except those immediately surrounding the oocyte; and 4 indicates expansion of all cumulus cell layers. Visually, the degree of cumulus expansion appeared greater when COCs were matured in vivo (Fig. 3b) compared to those matured in vitro (Fig. 3c). This observation was confirmed following scoring of cumulus expansion: in vitro matured COCs had significantly lower levels of cumulus expansion compared to in vivo matured COCs (Fig. 4a). Developmental potential was also assessed by performing IVF on both in vivo and in vitro matured oocytes and scoring whether the resultant embryos were able to develop to the blastocyst-stage of preimplantation development [38]. This confirmed that in vitro matured oocytes were of poorer quality, with significantly fewer reaching the blastocyst-stage when compared to embryos derived from in vivo matured oocytes (Fig. 4b; approximately 35 % fewer embryos).

4. Optical tweezers measurements of cumulus matrix viscosity

Prior to measuring the COC extracellular matrix, we first assessed the viscosity of hyaluronan. Hyaluronan was chosen as it is the predominant structural component of the COC extracellular matrix [39]. Hyaluronan of different molecular weights (15-30 kDa and 130-300 kDa; Contipro Inc., Czech Republic) were dissolved in phosphate buffered saline supplemented with polyvinyl alcohol (0.3 mg/ml). Concentrations of 1.25, 2.5, 5, and 10 mg/ml were tested and compared to the diluent (0 mg/ml). The silica bead solution used in Sec. 2 was combined to each sample in a 3:10,000 ratio, corresponding to 3×10^7 particles/ml. Viscosities for both molecular weights at different concentrations are presented in Fig. 5. Analysing particle movement, we found that viscosity increases linearly with increasing hyaluronan concentration. This finding is evident in both the relatively low and high molecular weight hyaluronan samples, 15-30 kDa and 130-300 kDa, respectively. While previous work has found hyaluronan to be a non-Newtonian fluid [40, 41], at the concentrations of hyaluronan used here the samples displayed negligible viscous (loss) modulus and thus Newtonian fluid dynamics dominated.

We next assessed the viscosity of the COC extracellular matrix derived from in vivo and in vitro matured oocytes. Cumulus oocyte matrix samples were prepared as follows: 20 COCs were dissociated in 50 μL of Research Wash medium (ART Lab Solutions, South Australia, Australia) supplemented with hyaluronidase (Sigma; 10 IU/mL) and 4 mg/ml bovine serum albumin. Hyaluronidase is an enzyme that was employed here to dissociate the extracellular matrix from the cumulus cells and oocyte of the cumulus oocyte complexes. Samples were vortexed for 1 minute then centrifuged at $20,238 \times g$ for 1 minute to pellet the cell fraction. The supernatant containing the COC derived extracellular matrix was aspirated and used for microrheology measurements. For these experiments a control was included (*Blank culture medium*: Research Wash medium supplemented with 10 IU/mL hyaluronidase and 4 mg/ml bovine serum albumin).

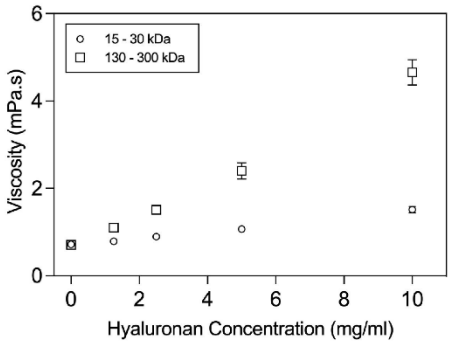

Figure 5. Viscosity of increasing concentrations of hyaluronan with two molecular weight ranges (15-30 kDa and 130-300 kDa). Error bars represent the standard deviation of the results. Data were collected from 15 repetitions, each consisting of 100,000 frames. At lower concentrations, the standard deviation is small and thus not visible on the plot.

Similar to the hyaluronan samples, the silica bead solution used in Sec. 2 was combined with the supernatant in a 3:10,000 dilution, corresponding to 3×10^7 particles/ml. Four independent experimental replicates were performed, each on a different day. For each experimental replicate, three samples were measured: (1) supernatant from in vivo matured COCs, (2) supernatant from in vitro matured COCs and (3) a blank control. Coverslips were pre-coated with Sigmacote to prevent beads adhering.

The viscosity of the COC extracellular matrix is presented in Fig. 6. The dashed horizontal line in Fig. 6 shows the measured viscosity of H_2O at 37 °C [42]. The viscosity of H_2O is presented as it forms the base solvent for the blank culture media.

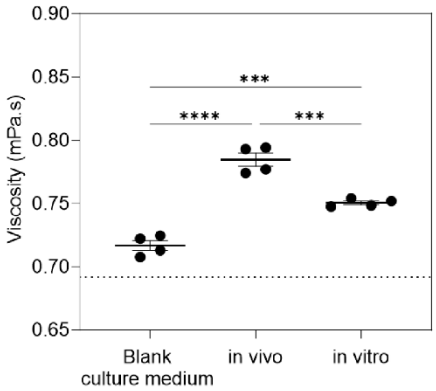

Figure 6. Viscosity of the extracellular matrix derived from cumulus oocyte complexes matured in vivo or in vitro. Data are presented as mean ± standard error in the mean. Data were analysed using a One-way ANOVA with Tukey post-hoc test. *** $P < 0.001$, **** $P < 0.0001$. The dashed line shows viscosity obtained for H_2O (the base solvent for the culture media).

When compared to blank culture medium, both in vivo and in vitro derived COC matrices had significantly higher viscosities. Interestingly, the viscosity of in vivo derived extracellular matrix was significantly higher (***P< 0.001) than those isolated from in vitro matured COCs. Given that in vivo matured COCs result in a approximately 35% higher in blastocyst development (Fig. 4b), our results indicate a positive correlation between COC matrix viscosity and oocyte developmental potential.

5. Discussion

Microrheology with optical tweezers is an accurate approach to assess the mechanical properties of biological samples in very small volumes. To the best of our knowledge, we have demonstrated the first use of optical tweezers for microrheological measurement of the COC extracellular matrix. Importantly, we have shown that the viscosity of this matrix correlates with oocyte developmental potential.

Passive microrheology with optical tweezers offers a number of advantages over contemporary 'passive' particle tracking techniques in enabling the precise localisation of a particle within a region of interest and maintining this position over extended periods of time. The trapped particle may also be precisely positioned relative to any surface, avoiding perturbations to the viscosity measurements as a consequence of hydrodynamic interactions [31]. This approach is ideal for measuring across a broad range of frequencies. This allows for accurate characterization of nonlinear viscoelastic properties in various heterogenous materials. Furthermore, the ability to hold a particle in focus and measure its Brownian motion for arbitrary time periods allows viscosity measurements to be made over long periods of time and with high precision which may be a challenge for 'passive' particle tracking [43, 44].

To verify the ability of optical tweezers to measure viscosity within a biological sample, we first examined two homogeneous samples of hyaluronan with different molecular weights (15-30 kDa and 130-300 kDa). Hyaluronan was selected as it is the predominant constituent of the COC matrix [36]. Our results agree with previous findings, affirming a positive correlation between viscosity and molecular weight. This can be attributed to differences in chain lengths [45]. When measuring the extracellular matrix derived from in vivo and in vitro matured COCs, we found that viscosity positively correlated with oocyte quality. The lower viscosity of the in vitro derived extracellular matrix is most likely attributed to the absence of crucial proteins (e.g. versican and ADAMTS1) involved in matrix assembly that are normally abundant following in vivo maturation [46]. As the number of cumulus cells and the rate of hyaluronan production per cell are comparable between in vitro and in vivo matured COCs [47, 48], these factors are unlikely contributors to the differences in viscosity reported here. The contribution of particular proteins to COC matrix viscosity and their association with oocyte quality would be of interest to investigate in future studies.

6. Conclusion

The current clinical approach for assessing oocyte quality relies on visual inspection and examination of morphology by an embryologist [49]. This subjective approach is not an accurate predictor of IVF success [30, 49]. Here, we have demonstrated the potential of microrheology with optical tweezers to assess oocyte developmental potential in an objective manner.

In the current study, the COC matrix was separated from the oocyte and cumulus cells prior to viscosity measurement through the activity of the enzyme hyaluronidase. This approach aligns with current clinical practice where the cumulus cells and associated matrix are removed from the oocyte and discarded, prior to the injection of a sperm into the oocyte to facilitate fertilization [50]. Our study employs this discarded material and as such is non-

invasive: It does not effect the viability of the oocyte. This makes our experimental design of relevance for future studies using human samples and making a clinical impact in this field.

Acknowledgments

We thank C. Ricciadelli and Z. Parker for providing the Hyaluronan samples. K.R.D is supported by a Future Making Fellowship from the University of Adelaide. K.D is supported by funding from the UK Engineering and Physical Sciences Research Council (EP/P030017/1) and the Australian Research Council (FL210100099 and DP220102303). We thank the Optofab node of the Australian National Fabrication Facility (ANFF) which utilize Commonwealth and South Australia State Government funding. The authors thank Evan Johnson and the rest of the Optofab team for their technical support. We thank A. Trowbridge for his assistance to generate Fig. 1a.

References

[1] A. Ashkin. Acceleration and trapping of particles by radiation pressure. *Physical Review Letters*, 24(4):156, 1970.

[2] A. Ashkin, J. M. Dziedzic, J. E. Bjorkholm, and S. Chu. Observation of a single-beam gradient force optical trap for dielectric particles. *Optics Letters*, 11(5):288, 1986.

[3] C. A. Campugan, K. R. Dunning, and K. Dholakia. Optical manipulation: a step change for biomedical science. *Contemporary Physics*, 61(4):277–294, 2020.

[4] J. T. Finer, R. M. Simmons, and J. A. Spudich. Single myosin molecule mechanics: piconewton forces and nanometre steps. *Nature*, 368(6467):113–119, 1994.

[5] M. D. Wang, M. J. Schnitzer, H. Yin, R. Landick, J. Gelles, and S. M. Block. Force and Velocity Measured for Single Molecules of RNA Polymerase. *Science*, 282(5390):902–907, 1998.

[6] W. M. Lee, P. J. Reece, R. F. Marchington, Nikolaus K. Metzger, and K. Dholakia. Construction and calibration of an optical trap on a fluorescence optical microscope. *Nat. Protoc.*, 2(12):3226–3238, 2007.

[7] G. Volpe, O. M. Maragò, H. Rubinsztein-Dunlop, G. Pesce, A. B. Stilgoe, G. Volpe, G. Tkachenko, V. G. Truong, S. N. Chormaic, and F. Kalantarifard. Roadmap for optical tweezers. *JPhys Photonics*, 5(2):1–136, 2023.

[8] A. J. Crick, M. Theron, T. Tiffert, V. L. Lew, P. Cicuta, and J. C. Rayner. Quantitation of malaria parasite-erythrocyte cell-cell interactions using optical tweezers. *Biophysical Journal*, 107(4):846–853, 2014.

[9] M. S. Yousafzai, G. Coceano, S. Bonin, J. Niemela, G. Scoles, and D. Cojoc. Investigating the effect of cell substrate on cancer cell stiffness by optical tweezers. *Journal of Biomechanics*, 60:266–269, 2017.

[10] X. Gou, H. C. Han, S. Hu, A. Y. H. Leung, and D. Sun. Applying combined optical tweezers and fluorescence microscopy technologies to manipulate cell adhesions for cell-to-cell interaction study. *IEEE Trans Biomed Eng.*, 60(8):2308–2315, 2013.

[11] T. Mendonca, K. Lis-Slimak, A. B. Matheson, M. G. Smith, A. B. Anane-Adjei, J. C. Ashworth, R. Cavanagh, L. Paterson, P. A. Dalgarno, C. Alexander, M. Tassieri, C. L .R Merry, and A. J. Wright. Optorheo: Simultaneous in situ micro-mechanical sensing and imaging of live 3d biological systems. *Communications Biology*, 6(1):463, 2023.

[12] Ò. Guadayol, T. Mendonca, M. Segura-Noguera, A. J. Wright, M. Tassieri, and S. Humphries. Microrheology reveals microscale viscosity gradients in planktonic systems. *Proc. Natl. Acad. Sci. U S A*, 118(1):1–5, 2021.

[13] F. Watts, L. E Tan, C. G. Wilson, J. M. Girkin, M. Tassieri, and A. J. Wright. Investigating the micro-rheology of the vitreous humor using an optically trapped local probe. *J. Opt.*, 16(1):1–7, 2013.

[14] M. Tassieri. Microrheology with optical tweezers: peaks & troughs. *Curr. Opin. Colloid Interface Sci.*, 43:39–51, 2019.

[15] T.M. Squires and T. G. Mason. Fluid mechanics of microrheology. *Annu. Rev. Fluid Mechan*, 42:413–438, 2010.

[16] L. L. Josephson, E. M. Furst, and W. J. Galush. Particle tracking microrheology of protein solutions. *Journal of Rheology*, 60(4):531–540, 2016.

[17] Z. Xing, A. Caciagli, T. Cao, I. Stoev, M. Zupkauskas, T. O'Neill, T. Wenzel, R. Lamboll, D. Liu, and E. Eiser. Microrheology of dna hydrogels. *Proc. Natl. Acad. Sci. U S A*, 115(32):8137–8142, 2018.

[18] J. A. McGlynn, N. Wu, and K. M. Schultz. Multiple particle tracking microrheological characterization: Fundamentals, emerging techniques and applications. *Journal*

of Applied Physics, 127(20), 2020.

[19] Y. Mao, P. Nielsen, and J. Ali. Passive and active microrheology for biomedical systems. *Front. bioeng. biotechnol.*, 10:1–32, 2022.

[20] B. D. Hoffman and J. C. Crocker. Cell mechanics: dissecting the physical responses of cells to force. *Annual Review of Biomedical Engineering*, 11:259–288, 2009.

[21] P. A. Janmey and C. A. McCulloch. Cell mechanics: integrating cell responses to mechanical stimuli. *Annual Review of Biomedical Engineering*, 9:1–34, 2007.

[22] M. J. Paszek, N. Zahir, K. R. Johnson, J. N. Lakins, G. I. Rozenberg, A. Gefen, C. A. Reinhart-King, S. S. Margulies, M. Dembo, D. Boettiger, D. A Hammer, and V. M. Weaver. Tensional homeostasis and the malignant phenotype. *Cancer Cell*, 8(3):241–254, 2005.

[23] R. L. Krisher. The effect of oocyte quality on development. *J. Anim. Sci.*, 82(suppl_13):14–23, 2004.

[24] S. Beall, C. Brenner, and J. Segars. Oocyte maturation failure: a syndrome of bad eggs. *Fertility and Sterility*, 94(7):2507–2513, 2010.

[25] K. M. Gebhardt, D. K. Feil, K. R. Dunning, M. Lane, and D. L. Russell. Human cumulus cell gene expression as a biomarker of pregnancy outcome after single embryo transfer. *Fertility and Sterility*, 96(1):47–52, 2011.

[26] J. Bouckenheimer, P. Fauque, C.H. Lecellier, C. Bruno, T. Commes, J.M. Lemaître, J. De Vos, and S. Assou. Differential long non-coding rna expression profiles in human oocytes and cumulus cells. *Sci. Rep.*, 8(1):2202, 2018.

[27] E. Nagyova, A. Camaioni, S. Scsukova, A. Mlynarcikova, R. Prochazka, L. Nemcova, and A. Salustri. Activation of cumulus cell smad2/3 and epidermal growth factor receptor pathways are involved in porcine oocyte–cumulus cell expansion and steroidogenesis. *Mol. Reprod. Dev.*, 78(6):391–402, 2011.

[28] Q. Shen, M. Chen, X. Zhao, Y. Liu, X. Ren, and L. Zhang. Versican expression level in cumulus cells is associated with human oocyte developmental competence. *Sys. Biol. Reprod. Med.*, 66(3):176–184, 2020.

[29] E. J. G. Peterman, F. Gittes, and C. F. Schmidt. Laser-induced heating in optical traps. *Biophysical Journal*, 84(2):1308–1316, February 2003.

[30] T. C. Y. Tan and K. R. Dunning. Non-invasive assessment of oocyte developmental competence. *Reprod. Fertil. Dev.*, 35(2):39–50, 2022.

[31] J. Leach, H. Mushfique, S. Keen, R. Di Leonardo, G. Ruocco, J. M. Cooper, and M. J. Padgett. Comparison of faxén's correction for a microsphere translating or rotating near a surface. *Phys.Rev. E.*, 79(2):1–4, 2009.

[32] I. Castillo, L. Pérez García, M. Gironella-Torrent, X. Viader-Godoy, F. Ritort, G. Pesce, A. V. Arzola, K. Volke-Sepúlveda, and G. Volpe. Optical tweezers — from calibration to applications: a tutorial. *Advances in Optics and Photonics*, 13(1):74, 2021.

[33] F. Gittes, B. Schnurr, P. D. Olmsted, F. C. MacKintosh, and C. F. Schmidt. Microscopic Viscoelasticity: Shear Moduli of Soft Materials Determined from Thermal Fluctuations. *Physical Review Letters*, 79(17):3286–3289, October 1997.

[34] M. J. Assael, S. A. Monogenidou, M. L. Huber, R. A. Perkins, and J. V. Sengers. New international formulation for the viscosity of heavy water. *Journal of Physical and Chemical Reference Data*, 50(3):1–21, 2021.

[35] J. A. Trejo González, M. P. Longinotti, and H. R. Corti. The viscosity of glycerol - water mixtures including the supercooled region. *Journal of Chemical & Engineering Data*, 56(4):1397–1406, 2011.

[36] D. L. Russell and A. Salustri. Extracellular matrix of the cumulus-oocyte complex. *Sem. Reprod. Med.*, 24(04):217–227, 2006.

[37] B. C. Vanderhyden, P. J. Caron, R. Buccione, and J. J. Eppig. Developmental pattern of the secretion of cumulus expansion-enabling factor by mouse oocytes and the role of oocytes in promoting granulosa cell differentiation. *Developmental Biology*, 140(2):307–317, 1990.

[38] T. C. Y. Tan, H. M. Brown, J. G. Thompson, S. Mustafa, and K. R. Dunning. Optical imaging detects metabolic signatures associated with oocyte quality. *Biol. Reprod.*, 107(4):1014–1025, 2022.

[39] D. McClean and I. W. Rowlands. Role of hyaluronidase in fertilization. *Nature*, 150(3813):627–628, 1942.

[40] Sabato Fusco, Assunta Borzacchiello, Lisa Miccio, Giuseppe Pesce, Giulia Rusciano, Antonio Sasso, and Paolo A Netti. High frequency viscoelastic behaviour of low molecular weight hyaluronic acid water solutions. *Biorheology*, 44:403, 2007.

[41] Giuseppe Pesce, Giulia Rusciano, and Antonio Sasso. Blinking Optical Tweezers for microrheology measurements of weak elasticity complex fluids. *Optics Express*, 18(3):2116, February 2010.

[42] Joseph Kestin, Mordechai Sokolov, and William A. Wakeham. Viscosity of liquid water in the range −8°c to 150°c. *Journal of Physical and Chemical Reference Data*, 7(3):941–948, July 1978.

[43] D. Ernst and J. Köhler. Measuring a diffusion coefficient by single-particle tracking: statistical analysis of experimental mean squared displacement curves. *Physical Chemistry Chemical Physics*, 15(3):845–849, 2012.

[44] X. Michalet and A. J. Berglund. Optimal diffusion coefficient estimation in single-particle tracking. *Physical Review E*, 85(6):1–14, 2012.

[45] A. Dodero, R. Williams, S. Gagliardi, S. Vicini, M. Alloisio, and M. Castellano. A micro-rheological and rheological study of biopolymers solutions: Hyaluronic acid. *Carbohydrate Polymers*, 203:349–355, 2019.

[46] K. R. Dunning, M. Lane, H. M. Brown, C. Yeo, R. L. Robker, and D. L. Russell. Altered composition of the cumulus-oocyte complex matrix during in vitro maturation of oocytes. *Hum. Reprod.*, 22(11):2842–2850, 2007.

[47] A. Salustri, S. Ulisse, M. Yanagishita, and V.C. Hascall. Hyaluronic acid synthesis by mural granulosa cells and cumulus cells in vitro is selectively stimulated by a factor produced by oocytes and by transforming growth factor-beta. *Journal of Biological Chemistry*, 265(32):19517–19523, 1990.

[48] K. R. Dunning, M. R. Anastasi, V. J. Zhang, D. L. Russell, and R. L. Robker. Regulation of fatty acid oxidation in mouse cumulus-oocyte complexes during maturation and modulation by ppar agonists. *PloS One*, 9(2):1–11, 2014.

[49] L. Rienzi, G. Vajta, and F. Ubaldi. Predictive value of oocyte morphology in human ivf: a systematic review of the literature. *Hum. Reprod. Update.*, 17(1):34–45, 2011.

[50] S. Mizuno, Y. Ishikawa, H. Matsumoto, M. Sato, M. Ida, A. Fukuda, and Y. Morimoto. The timing of cumulus cell removal for intracytoplasmic sperm injection influences the capability of embryonic development. *Reprod. Med. Biol.*, 18(1):111–117, 2019.

Chapter 3
Microrheology of the embryo microenvironment using optical tweezers

3.1 Abstract

The mechanical response of cells to their microenvironment, particularly the elastic and viscous properties, plays an important role in cellular function and viability. In vitro, the viscosity of the embryo microenvironment may vary depending on the composition of the surrounding media and the production of biological compounds by the embryo during pre-implantation development. However, objective characterisation of this microenvironment at the microscale has not yet been achieved. In this Chapter, I used optical tweezers for passive microrheology to measure the viscosity of both commercially available embryo media and the microenvironment surrounding pre-implantation embryos in vitro. There were significant differences in viscosity between murine and human embryo culture and transfer media. A viscous microenvironment was also detected around both 4-cell and blastocyst-stage murine embryos, with viscosity decreasing progressively with increasing distance (measured radially outwards) from the edge of the embryo. This was mapped in two dimensions. This microenvironment was heterogeneous, demonstrating variability in viscosity at similar radii from the centre of the embryo. The average measurement of viscosity remained the same even after washing. While proximity to the zona pellucida (the protein coat surrounding embryos) influenced the viscosity measurements, my findings support the use of optical tweezers as a promising tool for measuring the viscosity of the embryo microenvironment. However, further optimisation is needed to refine experimental parameters.

3.2 Introduction

Microrheology examines the mechanical properties of materials at a given position and in a microscale volume. Microrheology techniques utilise small probe particles, of micron-sized dimensions, embedded within a sample to quantify viscoelasticity – the property of a material to exhibit both viscous and elastic behaviour when deformed – at a micron to sub-micron scale [96]. This is crucial for the study of complex materials limited in volume, such as biological materials. Microrheology techniques can be classified as active or passive. In active microrheology, particle motion is driven by external forces, such as forces

from optical tweezers [97-100]. In contrast, for passive microrheology, particle motion is driven by the thermal fluctuations in the surrounding medium [78]. For passive microrheology, tracking the Brownian motion (refer to **Chapter 1.6**) of a probe particle enables the measurement of the viscoelastic properties of the surrounding medium. In contrast to traditional methods that track free particle motion, the use of optical tweezers in passive microrheology enables the confinement of the probe particle within a defined volume in three dimensions, using a tightly focused laser beam [101]. While trapped, the particle is still capable of Brownian motion, and its displacement over time from the trapped position can in turn be used to determine the mechanical properties of the medium [80, 81, 102-104]. The use of optical tweezers for passive microrheology is highly beneficial, as the confinement of the particle allows tracking to occur over an extended period thus enabling an accurate measurement of the mechanical properties of a sample [81, 105, 106].

The mechanical properties of cells and their surrounding extracellular matrix have been associated with cell function and viability [107, 108], influencing processes such as cell spreading, growth, proliferation, and differentiation [41, 42, 45]. As an example, in cancer cells, an increase in extracellular matrix stiffness was positively correlated with migration [109]. In **Chapter 2**, I reported a positive correlation between the viscosity of the extracellular matrix around oocytes and their developmental potential. Using optical tweezers, I was able to detect significant differences in matrix viscosity between good and poor quality oocytes. These results demonstrated the effectiveness of the optical tweezers for sensitive measurements of the extracellular matrix that surrounds an oocyte. In this Chapter I used optical tweezers to measure the viscosity of the extracellular microenvironment surrounding pre-implantation embryos.

The embryo microenvironment plays an important role during pre-implantation development. Extracellular factors present within the fluids of the female reproductive tract, such as nutrients, growth factors, hormones, metabolites, and cytokines, dramatically impact embryo development [65, 66, 110]. The in vitro culture environment is far less complex but attempts to replicate the metabolic substrates available in vivo by incorporating components such as glucose and pyruvate [111-114]. During the preimplantation

stages of development, the metabolism of the embryo undergoes dynamic changes that are crucial for successful development. At earlier stages of development (from the 1- to the 8-cell stage) the embryo is dependant on oxidative phosphorylation, primarily relying on pyruvate and lactate as energy substrates [65, 67, 68]. Post-compaction (morula-stage), the metabolic demands of the embryo dramatically increase due to rapid cell proliferation and the requirement to generate a fluid-filled blastocoel cavity during the blastocyst-stage [68-71]. This increased metabolic demand is met by the embryo shifting its metabolism from oxidative phosphorylation to glycolysis [115]. By the blastocyst stage, glucose becomes the predominant substrate for energy production with high amounts of glucose (50-90%) converted to lactate and secreted into the surrounding microenvironment [73, 75, 116]. Interestingly, at the blastocyst-stage a higher rate of glucose uptake is linked to high developmental potential [73]. Thus, the concentration of secreted lactate may be a surrogate measure of embryo developmental potential at this stage. Interestingly, in whole blood, high concentrations of lactate increases viscosity [76]. In summary, (1) glucose metabolism dominates during the later stages of embryo development and is associated with developmental potential, (2) most of this glucose is converted to lactate and secreted, and (3) elevated lactate concentration increases the viscosity of blood. Based on these three points, I hypothesised that the embryo microenvironment exhibits a higher viscosity at the blastocyst stage when compared to the earlier 4-cell stage of development.

In this chapter, I used optical tweezers for passive microrheology to measure the viscosity of the embryo microenvironment during in vitro culture. I found a significantly higher viscosity surrounding the blastocyst-stage embryo when compared to 4-cell stage embryos. Interestingly, the viscosity of the microenvironment of both of these developmental stages decreased with increasing radial distance from the embryo. Furthermore, I discovered that this microenvironment was heterogenous, with viscosity around the embryo varying at similar radii. Overall, my results demonstrate the ability of the optical tweezers to measure viscosity at discrete locations around the embryo, providing a novel method for characterising the embryo microenvironment. This study is an important first step towards determining

whether the viscosity of the microenvironment surrounding blastocyst-stage embryos is a surrogate measure of lactate production and in turn, embryo developmental potential.

3.3 Methods

3.3.1 Optical tweezers setup

The optical trap was generated by a 1064-nm DPSS laser (Opus, Laser Quantum) with a maximum output power of 5 W, directed into an inverted microscope (Olympus IX-73) equipped with a high NA water-immersion objective lens (LUMFLN60XW 60x,1.1, NA 1.2, WD; Olympus) (Figure 1a). A 530 nm, green LED (Thorlabs LED-C13) was used for sample illumination, and images were captured using a Hamamatsu sCMOS (ORCA Flash 4.0) camera. The objective lens was used to image a small field of view (14 μm × 14 μm), enabling high-rate imaging of 300,000 frames at ~300 frames per second. Videos of the time-dependent Brownian motion of the trapped particle were recorded using Micro-Manager (version 1.4)[117]. To ensure that the trapping laser overfills the back aperture of the objective, and thus can trap in three dimensions, a beam expander system consisting of two achromatic doublet lenses was used. Indirect damage caused by laser heating on the sample was minimised by using a 1064 nm laser, which is weakly absorbed by water, and using a low trap power at the sample plane of <10 mW. A H301-K frame with a central slide insert (1xGS-M, Okolab) was used to house samples during optical trapping. This chamber facilitated the maintenance of temperature of 37°C and CO_2 concentration at 6% within a humidified environment, ensuring the biological integrity of the embryos were preserved during measurements. The local chamber temperature was monitored to ensure thermal stability. This optical tweezers system is illustrated in Figure 1a.

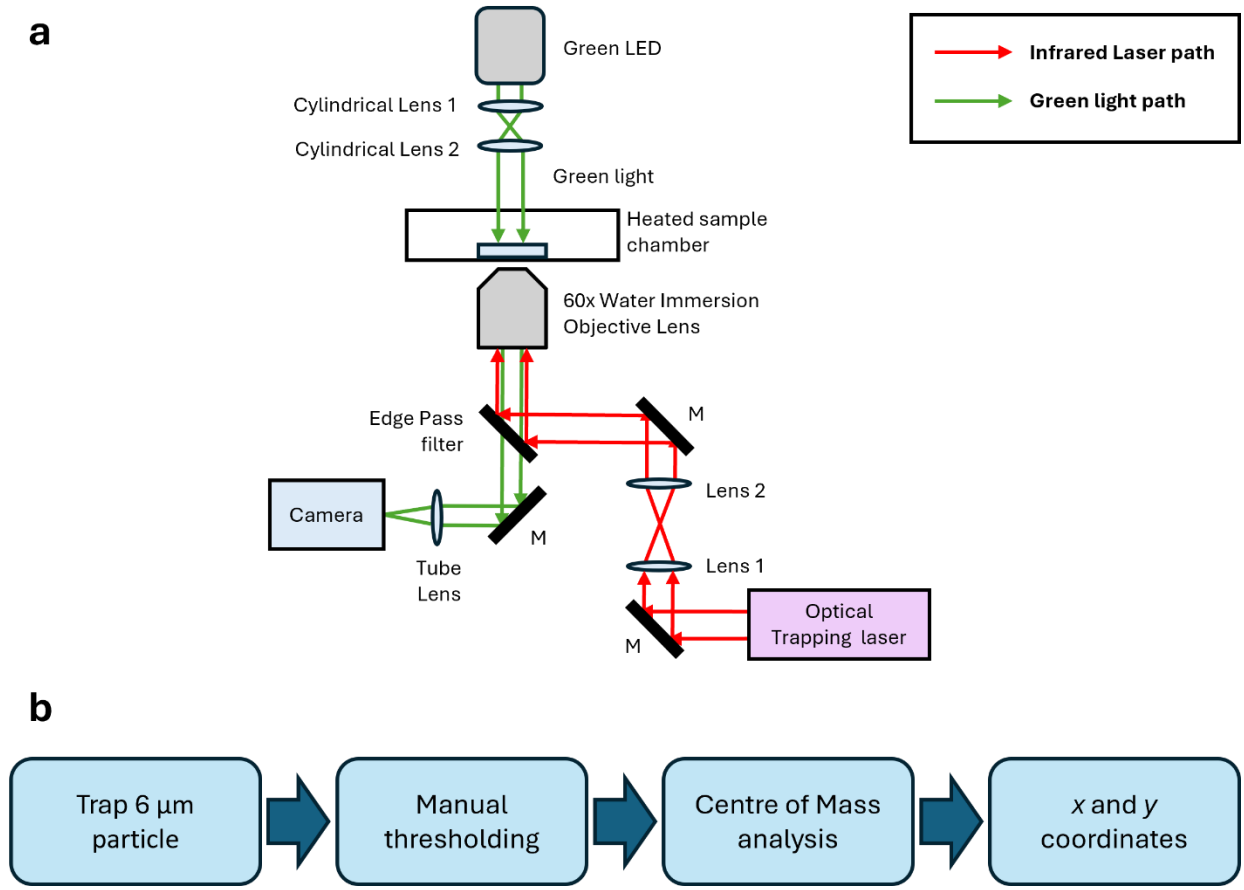

Figure 1. Schematic diagram of the optical tweezers system and image processing flow chart. (a) A 60x water immersion microscope objective collects transmitted light (green) and directs the trapping laser (red; 1064 nm) to the sample. Lenses 1 and 2 function as a beam expander, allowing over-filling of the back aperture of the 60x objective. Dimensions are not to scale. (b) Visual representation of the workflow for the image processing method to extract *x* and *y* coordinates from the captured raw images.

Using Micro-Manager (Version 1.4)[117] a real-time particle script was used to track particle motion. Prior to video acquisition, manual thresholding was applied to the region of interest to separate the foreground (centre of the trapped particle) from the background. This thresholding process resulted in the particle's centre being the only region of high intensity within the field of view, while the intensity of the surrounding background was zero. This approach was standardised across all measurements to prevent inconsistencies in particle tracking. A centre-of-mass analysis was performed on the resulting videos to extract the *x* and *y* coordinates of the trapped particle. Figure 1b illustrates a flowchart of this method.

A comprehensive description of the principles underlying the microrheology analysis of particle motion is described in Tassieri et al (2012) and Yao et al (2009) [101, 118]. Briefly, microrheology analysis on the particle trajectory involved extracting the normalized position autocorrelation function (NPAF) of the particle in the *x* and *y* directions, which was calculated in the following equation:

$$NPAF = 1 - \exp\left(-\frac{\kappa_\chi \tau}{6\pi\eta r}\right) \quad (1)$$

In this equation τ represents lag-time, *r* is particle radius, and η is the zero-shear viscosity of the fluid. For a Newtonian fluid (i.e. water), η is constant and frequency-independent. For a non-Newtonian fluid (e.g. blood), η is frequency-dependent but becomes stable at lower frequencies, referred to as the low-frequency plateau, where fluid behaviour becomes predictable. In this context κ_χ represents the trap stiffness in the *x* direction, which is defined as:

$$\kappa_\chi = k_B T < x^2 > \quad (2)$$

where $< x^2 >$ is the mean squared displacement of the particle motion in the *x*-axis, *T* is the absolute temperature, and k_B is Boltzmann constant. The NPAF formula in equation 1 is mathematically related to the position autocorrelation function in **Chapter 1.6 (**equation 3) where particle positions at different lag times were compared to quantify viscosity. In the NPAF equation, the trap stiffness and system parameters are incorporated allowing for a direct relationship between viscosity and the rate of

exponential decay. For viscosity measurements, only particle motion along the *x*-axis was quantified due to observed discrepancies between the *x*- and *y*-axis particle motion. This was attributed to misalignment of the two cylindrical lenses in the LED illumination path (used as part of a separate light sheet system, not utilised in this work). This resulted in uneven illumination along the *y*-axis, affecting particle tracking in that direction. Despite adjustments to the angle and position of the first cylindrical lens (cylindrical lens 1), the tracking issue along the *y*-axis persisted. Therefore, viscosity in this study was derived solely from measurements along the x-axis. Calibration studies along this axis showed that measured viscosity values for water matched those from the literature.

3.3.2 Viscosity of commercial embryo media

Prior to embryo measurements, I first quantified the viscosity of commercially available media for embryo culture and embryo transfer. To do this, the samples were mounted in an 8-well glass bottom slide (IBIDI, 80827). Each well housed a single 20 µL drop of either: murine embryo culture media – Research Cleave (ART Lab Solutions, South Australia, Australia); human embryo culture media: G1-PLUS™ (Vitrolife, 10128), G2-PLUS™ (Vitrolife, 10132), and SAGE 1-STEP™ (Origio, 67010010A); or human embryo transfer media: EmbryoGlue® (Vitrolife 10085), and UTM™ (Origio, 10520010A). Each drop was placed in the centre of each well and overlaid with 175 µL paraffin viscous oil (Merck Millipore, 107160). The use of oil minimises osmolarity changes caused by evaporation of the medium, which can negatively impact embryo development [119]. To ensure temperature stability within the drop, 8-well slides were incubated for 4 hours in a 37°C humidified incubator with 5% O_2, 6% CO_2 and a balance of N_2. For optical trapping, slides were transferred from the incubator to a heated chamber stage on the inverted microscope. Prior to measurement, a stock solution of 6 µm diameter polystyrene particles (Polysciences 07312-5) was prepared in each of the commercial media at a concentration of 7.05 x 10^3 particles/ml. From this stock, 1 µL was added to the 20 µL drop of medium resulting in a final concentration of 3.36 x 10^2 particles/ml. This concentration allowed sufficient time to locate and optically trap a single particle

before all particles settled to the bottom of the slide. Further, this particle concentration also avoided an over-abundance of free moving, non-trapped particles which may interfere with viscosity measurements.

3.3.3 Animal Ethics

The use of animals for the research presented in this chapter was approved by the Animal Ethics Committee of the University of Adelaide (M-2023-004) and was conducted in accordance with the Australian Code of Conduct for Animal Care and Use for Scientific Purposes. Female mice (CBA × C57BL/6 first filial (F1) generation; CBAF1, 21-23 days old) and male mice (CBAF1, 6-8 weeks old) were acquired from Laboratory Animal Services (LAS) at the University of Adelaide, South Australia, Australia. All mice were maintained in a controlled light-dark cycle (12 h light: 12 h dark cycle). Mice were fed with rodent chow and water *ad libitum*. The use of biological material derived from mice was approved by the Animal Ethics Committees at both The University of Adelaide and The University of Nottingham.

3.3.4 Collection, vitrification, and warming of embryos

Female mice were administered with an intraperitoneal (I.P.) injection of 5 IU equine chorionic gonadotrophin (eCG; Folligon, Braeside, VIC, Australia), followed by 5 IU of human chorionic gonadotrophin I.P. (hCG; Pregnyl, Kilsyth, VIC, Australia) 46 h later. Female mice were then mated with male mice of proven fertility. At 23 h post-hCG, females were culled via cervical dislocation, and oviducts dissected. Presumptive zygotes were harvested by puncturing the ampulla with a 29-gauge insulin needle. Presumptive zygotes were denuded using hyaluronidase (50 U/mL) diluted 1:4 in pre-warmed Research Wash medium (ART Lab Solutions, South Australia, Australia) supplemented with 4mg/ml Bovine Serum Albumin (BSA; MP Biomedicals, 02180620) for 2 min and then washed in a separate pre-warmed Research Wash medium and screened for polar body extrusions to confirm successful fertilisation.

As microrheology measurements were to be conducted at The University of Nottingham, UK, embryos were generated and vitrified (cryopreserved) in Adelaide and transported to the UK while I undertook my

12 months of required study at The University of Nottingham. Embryo vitrification was performed on zygotes with polar body extrusions, using the methodology described in Yagoub et al (2022) [120].

The composition of each of the media required fro vitrification and warming of embryos is as follows: Handling media (HM) consisting of Research Wash supplemented with 5 mg/ml BSA, while sucrose media (SM) was prepared by dissolving 1 M sucrose in HM. The equilibration solution (ES) included 10% (v/v) ethylene glycol and 10% (v/v) dimethyl sulfoxide (DMSO) diluted in HM. The vitrification solution (VS) was formulated with 16.6% (v/v) ethylene glycol, 16.6% (v/v) DMSO, and 6.7% (v/v) of HM in SM.

Zygotes were vitrified using the Cryologic vitrification method. Briefly, embryos were first placed in HM for washing, followed by transfer into ES for 3-minute, and then a 30-second exposure in VS, before being loaded into a Fibreplug (CryoLogic, Pty. Ltd, VIC, Australia) straw and plunged into the vapor phase of liquid nitrogen for vitrification. The vitrified straws were subsequently stored in liquid nitrogen. The total duration of the vitrification process was 3 minutes and 30 seconds, with all media maintained at 37°C prior to loading.

Before embryo warming, an 8-well glass bottom slide was prepared with 20 µL drops of Research Cleave supplemented with 4 mg/ml Bovine Serum Albumin in each well. Each drop was overlaid with 175 µL of paraffin oil. A separate slide containing 3 x 20 µL drops of Research Cleave was prepared for washing. All slides were pre-equilibrated prior to use for 4 h at 37°C in a humidified incubator of 5% O_2, 6% CO_2 with a balance of N_2. The embryo warming process involved four distinct solutions denoted as Warming Solution 1 (WS1), WS2, WS3, and WS4. This procedure followed the methodology established by Yagoub et al (2022) [120]. In summary, the warming solutions contained decreasing sucrose concentrations of 0.3 M, 0.25 M, 0.15 M, and 0 M, respectively, all diluted in handling media (HM). For warming, Fibreplugs with vitrified embryos were taken out of liquid nitrogen and quickly placed into WS1 for 30 seconds. The embryos were then collected and successively transferred into WS2, WS3, and WS4, with a 5 minutes incubation time in each solution. The entire warming process lasted 15 minutes and 30

seconds, ensuring that all media were maintained at 37°C throughout. After warming in WS4, embryos were aggregated and transferred into the pre-warmed 3 x 20 µL drops of Research Cleave media for washing. Embryos were washed sequentially in each drop to remove residual cryopreservatives which may negatively impact embryo development [121]. Following washing, embryos were transferred and cultured at a density of 10 embryos per 20 µL in the pre-equilibrated Research Cleave drops.

3.3.5 In vitro embryo culture of warmed embryos

All embryo culture procedures took place within a Research Cleave medium supplemented with 4 mg/ml BSA, overlaid with 175 µL of paraffin oil, located in an 8-well slide. Slides containing embryos were incubated at 37°C in a humidified incubator of 5% O_2, 6% CO_2 with a balance of N_2. Prior to morphological assessment at 24 and 40 h post-warming, separate 8-well slides containing fresh 20 µL drops of Research Cleave medium were prepared and allowed to pre-equilibrate overnight in a humidified incubator of 5% O_2, 6% CO_2 with a balance of N_2, operating at 37°C.

At 24 h post-warming, embryos were subjected to on-time morphological assessment to separate 2 cell-stage embryos from developmentally arrested or degenerated embryos. Two cell embryos were identified based on the presence of two similarly sized blastomeres (cells). All two cell embryos were aggregated and transferred into the pre-warmed slide containing 20 µL drops of Research Cleave media, at a density of 10 embryos per drop, for continued incubation following assessment in the incubator. At 40 h post-warming, on-time morphological assessment was performed for 4 cell-stage embryos. Four cell embryos were identified based on the presence of four similarly sized blastomeres. A cohort of ten 4 cell-stage embryos were maintained in their respective culture drops for viscosity measurement, while all the remaining 4 cell embryos was separated from developmentally arrested or degenerated embryos. Aggregated 4 cell embryos were transferred into the pre-warmed slide containing 20 µL drops of Research Cleave media, at a density of 10 embryos per drop, for continued incubation following assessment in the incubator. Following 90 h post-warming, the slides containing embryos were removed from the incubator and embryos were assessed as to whether they had reached the blastocyst-stage.

Similar to 4 cell-stage embryos, ten blastocyst-stage embryos were maintained in their respective culture drops for viscosity measurements.

3.3.6 Viscosity measurements of the microenvironment surrounding the pre-implantation embryo

To avoid disrupting the embryo microenvironment before viscosity measurements, 4 cell- or blastocyst-stage embryos were left undisturbed in their respective culture drops following on-time morphological assessment as defined in Tan et al (2022) [31]. On the same slide, an empty drop of Research Cleave medium with no embryos acted as a negative control ("Blank control").

Prior to viscosity measurements with the optical tweezers, 4 cell- and blastocyst-stage embryos were examined with a benchtop microscope to determine their general location. Slides containing embryos were then transferred onto the heated stage of the optical trapping system. Prior to measurement, a stock solution of 6 µm diameter polystyrene particles (Polysciences 07312-5) was prepared in Research Cleave media at a concentration of 7.05 x 10^3 particles/ml. From this stock, 1 µL was carefully added to the top of the 20 µL drops of media containing embryos. This resulted in a final concentration of 3.36 x 10^2 particles/ml. A single polystyrene particle was trapped and precisely positioned at distances 40, 20, or 5 µm, measured from the outer edge of the zona pellucida to the edge of the trapped particle. Viscosity measurements at 40, 20, and 5 µm constituted a single set of measurements for a single embryo and subsequent sets of measurements were performed on other embryos with the same polystyrene particle, again from furthest to closest (Figure 2a). Additional measurements were taken 100 µm from the edge of the embryo to the edge of the particle to obtain a reference viscosity of the embryo-containing media, under the same temperature conditions, in order to determine whether the observed viscosity changes in the microenvironment are attributed to the presence of embryos in the culture drop (Figure 2a). All viscosity measurements were performed in one of four radial directions relative to the embryo (north, east, west, or south), with the *x*-axis motion of the particle either parallel or perpendicular to the surface of the embryo (Figure 2b). The direction of measurement was selected based on the location of adjacent embryos may have influenced viscosity

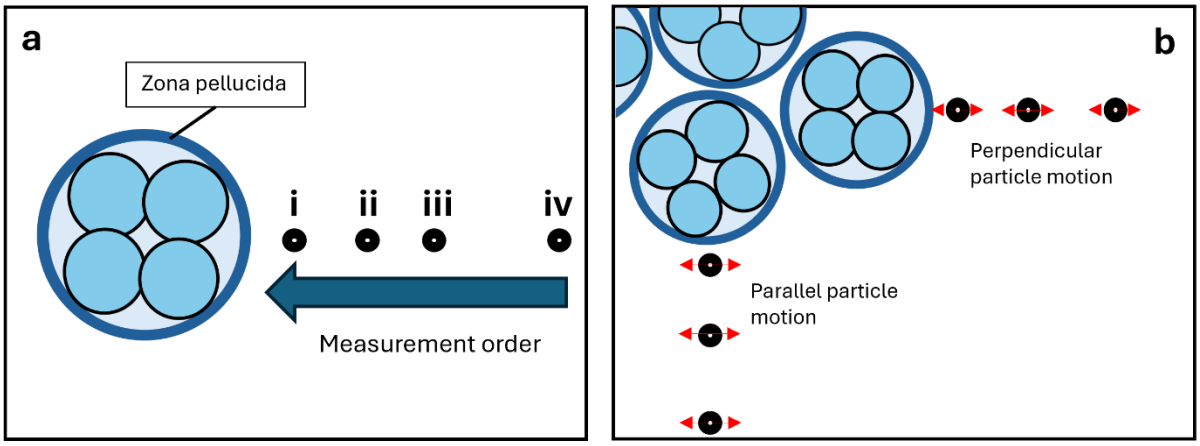

Figure 2. Schematic diagram illustrating the process for measuring viscosity around the pre-implantation embryo. (a) A single 6 µm diameter trapped particle was used to measure viscosity at distances of 5, 20, 40, or 100 µm from the outer edge of the zona pellucida surrounding the embryo (i, ii, iii, and iv, respectively). Measurements were taken in sequential order based on distance, from furthest to closest: iv, iii, ii, then i. (b) For adjacent embryos, the same trapped particle was used, following the same sequence. *Red arrows* represent the *x*-axis motion of the particle relative to the surface of the embryo, either parallel or perpendicular. Measurements of viscosity were acquired in specific directions relative to the embryo (north, east, west, or south) to minimise the potential impact of adjacent embryos on the measurements. Distance and dimensions are not to scale.

measurements. Finally, measurements were taken from furthest to closest to avoid disturbing the embryo's microenvironment before each measurement.

Separate to these measurements, I also isolated a single 4 cell- and blastocyst-stage embryo and measured the viscosity of the microenvironment at arbitrary distances and directions from the embryo to determine whether the microenvironment is uniform in viscosity. Field of view images were captured for each measurement point, and all images were overlaid to create a composite image showing all the measured locations around the embryo.

Particle motion data were subjected to inclusion and exclusion criteria by analysing the field of view images, centre-of-mass scatter plots, and *x*- and *y*-axis trajectory plots captured during measurement. Examples of included and excluded data can be viewed in Supplementary Figure 1. Briefly, data were excluded if they portrayed asymmetrical scatter plots (Supplementary Figure 1f) and transient fluctuations in the trajectory plots (Supplementary Figure 1g,h) – both indicative of external or environmental interference on trapped particle motion. For viscosity measurements, only particle motion along the *x*-axis was included as described in **Section 2.1**.

3.3.7 Viscosity measurements of the blastocyst-stage embryo following washing

To investigate whether the microenvironment around embryos is stable and resistive to external mechanical forces, I measured the viscosity of blastocyst stage embryos before and after repeated washing. Ten blastocyst-stage embryos were selected for washing, which first involved embryos placed into pre-warmed Research Cleave medium for 10 minutes. Using a micropipette, all blastocysts were washed five times by repeatedly withdrawing and expelling media into the same 20 µL Research Cleave drop. After washing, embryos were mounted in a fresh pre-warmed single 20 µL Research Cleave drop overlaid with paraffin oil on an 8-well slide. Viscosity measurements of washed blastocyst-stage embryos were performed at 5 µm from the edge of the embryo in the north, east, west, or south direction as described in **Section 3.3.6**.

3.3.8 Faxén's correction

To account for surface boundary effects which may arise due to the proximity of my viscosity measurements to the embryo zona pellucida, I used Faxén's corrections on the 'Blank control" measurements to establish benchmark values at each distance where surface boundary effects were negligible (as no embryos were present). Absolute viscosity from the 4-cell and blastocyst-stage embryos were compared to this benchmark to establish viscosity deviations which could be indicative of surface boundary effects imposed by the zona pellucida. Faxén's equations, expressed as a power series in the ratio of particle radius $'a'$ to the distance from edge of the embryo's zona pellucida to the centre of the particle $'s'$, were utilised to correct the Stokes drag on a particle moving near a surface, like previously described in the microrheology of planktonic systems [81]. Two correction equations were applied depending on the direction of particle motion: parallel or perpendicular to the surface. Faxén's correction for particle motion parallel to the surface is given by:

$$\gamma^{||} = \frac{\gamma}{1 - \left(\frac{9}{16}\right)\left(\frac{a}{s}\right) + \left(\frac{1}{8}\right)\left(\frac{a}{s}\right)^3} \tag{3}$$

where $\gamma^{||}$ is the corrected hydrodynamic drag coefficient for a particle moving parallel to the embryo zona pelluicida, and γ represents $\gamma = 6\pi\eta r$, which is the hydrodynamic drag coefficient for a sphere in the absence of nearby surfaces. Faxén's correction for particle motion perpendicular to the surface is given by:

$$\gamma^{\perp} = \frac{\gamma}{1 - \left(\frac{9}{8}\right)\left(\frac{a}{s}\right) + \left(\frac{1}{2}\right)\left(\frac{a}{s}\right)^3} \tag{4}$$

where $\gamma^{\perp}$ represents the corrected hydrodynamic drag coefficient of a particle moving perpendicular to the embryo zona pellucida. In applying Faxén's correction, I assume a rigid planar surface for ease of calculation. I note that the embryo zona is actually non-rigid and convex which may cause deviation in the calculated values.

3.3.9 Statistical Analysis

Statistical analyses were completed using GraphPad Prism Version 10 for Windows (GraphPad Holdings LLC, CA, USA). All data were subjected to normality testing (D'Agostino-Pearson omnibus, Anderson-Darling, Shapiro-Wilk, and Kolmogorov-Smirnov normality test) to assess for normal distribution, and appropriate statistical tests (Ordinary One-way ANOVA, Kruskal Wallis with a Dunn's post hoc, two-way ANOVA, and a Mann-Whitney test) were carried out as described in the figure legends. A Grubbs' test was also performed on all collected data to identify significant outliers. Statistical significance was defined as a $P< 0.05$.

3.4 Results

3.4.1 Commercial embryo culture and transfer media vary significantly in viscosity

I first verified the ability of optical tweezers to measure viscosity of media in the absence of embryos. I measured the viscosity of murine embryo culture medium (Research Cleave) as well as human embryo culture (G1-PLUS™, G2-PLUS™, SAGE 1-STEP,) and human embryo transfer media (EmbryoGlue®, and UTM™). All of the media had viscosities consistently higher than water (Figure 3; *dashed line*). For embryo culture media, both human G1-PLUS™ (1.11 ± 0.07 mPa.s) and G2-PLUS™ (1.16 ± 0.03 mPa.s) were significantly more viscous than human SAGE 1-STEP™ (0.93 ± 0.05 mPa.s) and murine Research Cleave (0.87± 0.03 mPa.s) (Figure 3; $P<0.0001$). Notably, the viscosities of SAGE 1-STEP™ and Research Cleave were not significantly different from each other ($P>0.05$). These findings suggest that continuous 1-step culture media (SAGE 1-STEP™ and Research Cleave) were significantly less viscous when compared to two-step culture media (G1-PLUS™ and G2-PLUS™). For embryo transfer media, EmbryoGlue® (2.52 ± 0.09 mPa.s) was significantly more viscous when compared to UTM™ (0.87 ± 0.08 mPa.s) (Figure 3, $P<0.0001$). Interestingly, EmbryoGlue® had a dramatically and significally higher viscosity when compared to all other media, while UTM™ showed similar viscosity to that of SAGE 1-STEP™ and Research Cleave. These results highlight distinct brand-specific and developmental-stage specific viscosity profiles of various embryo culture and embryo transfer media.

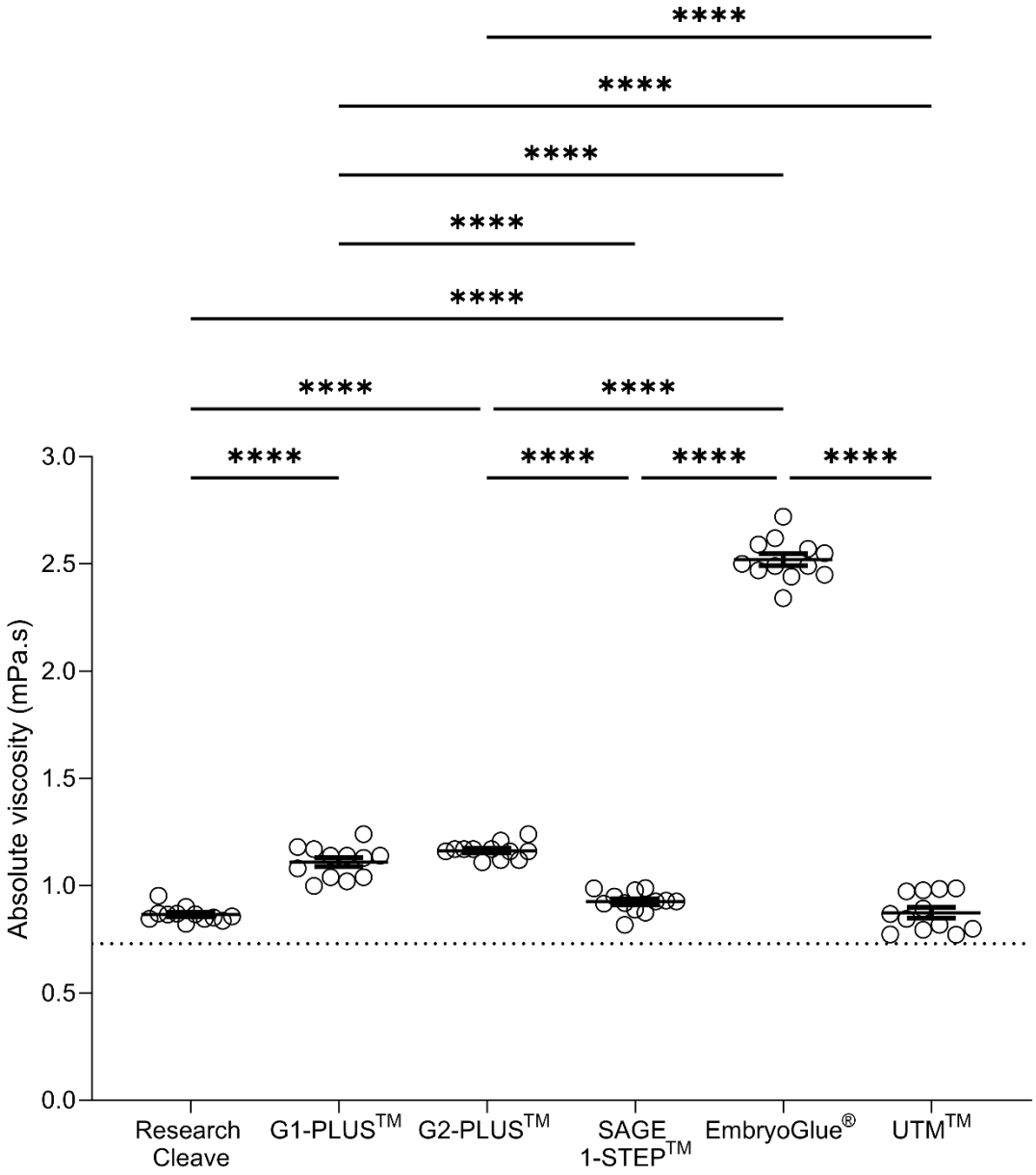

Figure 3. The viscosity of embryo culture and transfer media varies significantly between brands. Optical tweezers were used to measure the viscosity of water (dotted line), media for murine embryo culture (Research Cleave), human embryo culture (G1-PLUS™, G2-PLUS™, and SAGE 1-STEP™) and human embryo transfer (EmbryoGlue®, and UTM™). All measurements were performed at 37°C. Data are presented as mean ± SEM. *n* = 12 measurements per group, from 3 independent experimental replicates. Data were analysed using an Ordinary One-way ANOVA with a Tukey's post hoc test. ****$P < 0.0001$

3.4.2 Viscosity of the microenvironment surrounding embryos at early and late stages of preimplantation development

During pre-implantation, embryos shift metabolically to adapt to changes in physiology. Early stages (e.g., 4-cell) rely on oxidative phosphorylation [65, 67, 68], while at later stages (e.g. blastocyst) use glycolysis to meet higher energy needs [71]. At the blastocyst-stage, glucose uptake rises, with 50–90% of this converted to lactate and secreted [73, 75, 116]. Notably, higher glucose uptake is linked to higher developmental potential. Thus, the concentration of secreted lactate may be a surrogate measure of embryo developmental potential at the blastocyst-stage. Interestingly, in whole blood elevated levels of lactate increases viscosity [76]. In this Chapter, I investigated whether microrheology with optical tweezers could detect a difference in the viscosity in the microenvironment surrounding early (4-cell stage) and late (blastocyst stage) embryos. These developmental stages were chosen based on the aforementioned difference in their rate of glycolysis and secretion of lactate. This is a precursor to investigating whether such an approach can detect differences in viscosity associated with embryo developmental potential (lactate production/secretion).

I measured the viscosity of the embryo microenvironment surrounding 4 cell- and blastocyst-stage embryos at distances of 5, 20, and 40 µm from the edge of the embryo to the edge of the trapped particle. For comparison, a negative control was also included (Research Cleave culture media with no embryos; *blank control*).

For the 4-cell stage, I found that the viscosity of the microenvironment at 5 µm from the edge of embryos (0.94 ± 0.16 mPa.s) was significantly higher than the blank control (0.81 ± 0.04 mPa.s; Figure 4a, $P<0.0001$). Further, the viscosity at 5 µm away from 4-cell stage embryos was significantly higher when compared to measurements performed at 20 (0.85 ± 0.04 mPa.s, $P<0.05$), 40 (0.84 ± 0.04 mPa.s, $P<0.01$), and 100 µm (0.78 ± 0.04 mPa.s, $P<0.0001$) (Figure 4a). No difference was found when comparing viscosity measured at distances beyond 5 µm (Figure 4a; *20* vs. *40* vs. *100* µm; $P>0.05$).

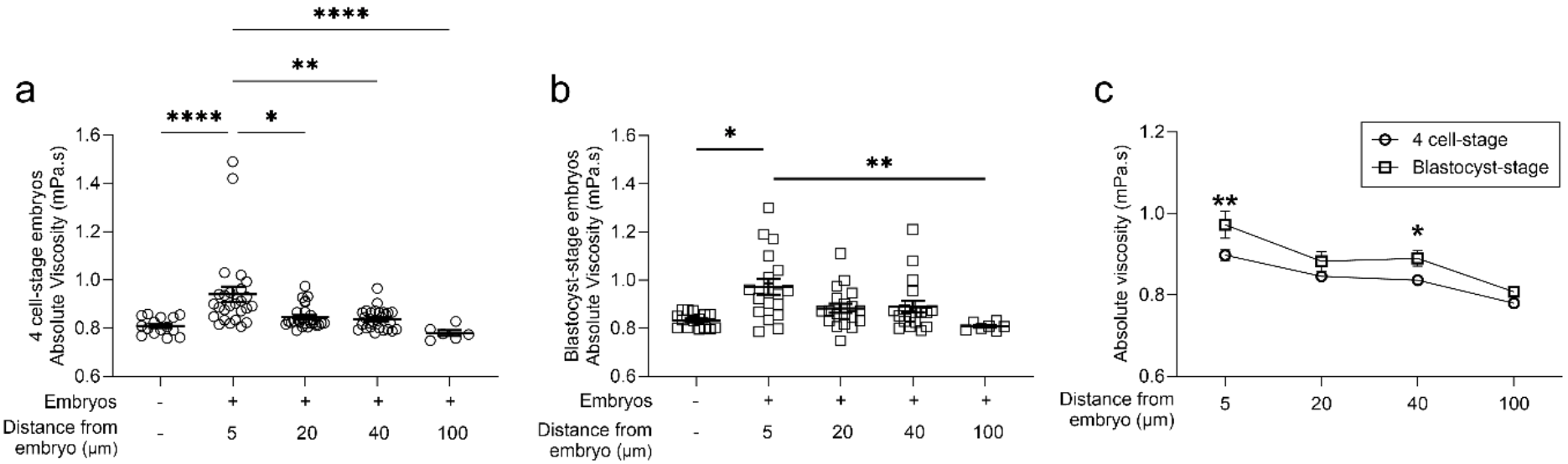

Figure 4. The viscosity of the microenvironment surrounding blastocyst-stage embryos is significantly higher than that surrounding embryos at the 4-cell stage. Viscosity was measured at distances of 5, 20, 40, and 100 µm from the outer edge of the zona pellucida to the edge of the trapped particle. This was performed for both the (a) 4 cell- and (b) blastocyst-stages of development. (c) Mean viscosity was compared between both embryo stages. Data are presented as mean ± SEM. *n* = 6 – 27 embryo measurements per group, from 6 independent experimental replicates. Data were analysed either using a Kruskal Wallis test with a Dunn's multiple post hoc test (a,b) or a two-way ANOVA test (c). Asterisks indicate statistical significance between measured distances (a, b) or within a measured distance (c). *P < 0.05, **P < 0.01, ****P < 0.0001

I next measured the viscosity of the microenvironment surrounding blastocyst-stage embryos. Similar to 4-cell stage embryos, the microenvironment 5 µm from the edge of the blastocyst was significantly higher (0.97 ± 0.14 mPa.s) when compared to the blank control (0.83 ± 0.03 mPa.s)(Figure 4b, P<0.05). Further, viscosity of the microenvironment measured at 5 µm (0.97 ± 0.14 mPa.s) was significantly higher than that measured at 100 µm from blastocyst-stage embryos (0.81 ± 0.02 mPa·s)(Figure 4b, *P*<0.001). In contrast, there were no differences in viscosity between the 5, 20, and 40 µm distances from the blastocyst-stage embryo.

I also directly compared the viscosity of the microenvironment surrounding of 4 cell and blastocyst-stage embryos (Figure 4c). Interestingly, I found that viscosity for both developmental stages was highest at 5 µm from the embryo, and that viscosity decreased with increasing distance (Figure 4c). Excitingly, at 5 and 40 µm from the embryo I found viscosity to be significantly higher at the blastocyst-stage (5 µm: 0.97 ± 0.14 mPa.s; 40 µm: 0.89 ± 0.11 mPa.s) when compared to the 4-cell stage embryo (5 µm: 0.94 ± 0.16 mPa.s; 40 µm: 0.84 ± 0.04 mPa.s) (Figure 4c, *P*<0.01). This suggests a stage-specific variation in viscosity in the microenvironment surrounding embryos.

3.4.3 Heterogeneous viscosity in the embryo microenvironment

As I had demonstrated the presence of a viscous microenvironment surrounding preimplantation embryos, I next measured the microenvironment around a single 4-cell and blastocyst-stage embryo (Figure 5). I took measurements at arbitrary distances and directions from the edge of each embryo. This approach allowed me to investigate whether the viscosity of the microenvironment is uniform around embryos at these developmental stages. For the 4 cell-stage, I found that viscosity was not uniform and highly variable even at identical radii; for example: at 5 µm from the edge of the 4-cell stage embryo I measured viscosities of 1.24 mPa.s and 1.03 mPa.s (Figure 5a). Similarly, the viscosity of the microenvironment surrounding the blastocyst-stage embryo was variable at similar radii from the edge of the embryo; for example: 1.87 mPa.s at 7 µm *vs.* 0.97 mPa.s at 8 µm and 0.92 mPa.s at 9 µm (Figure 5b). While viscosity generally decreased with increasing distance from the edge of the embryo

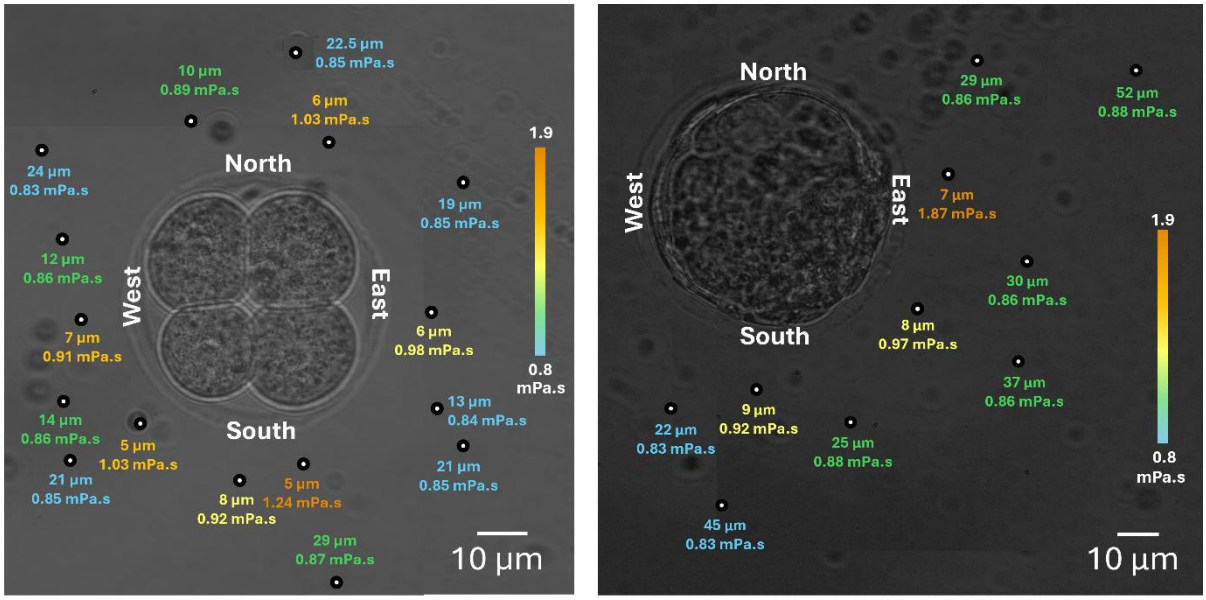

Figure 5. Viscosity of the pre-implantation embryo microenvironment is heterogeneous. Viscosity around a single (a) 4 cell- and (b) blastocyst-stage embryo varied at arbitrary distances and directions from the pre-implantation embryo. Data are presented as the viscosity measurements from a single experimental replicate for a single embryo. The vertical colour scale is used to indicate relatively high and low viscosities within each sample, with high viscosity represented by orange and low viscosity represented by blue.

for both developmental stages, I observed sporadic areas of elevated viscosity that deviated from the measured viscosity seen at similar distances within the same embryo. For example, at 0.87 mPa.s at 29 µm (south of the embryo) *vs.* 0.83 mPa.s at 24 µm (north-west of the embryo) from the edge of the 4 cell-stage embryo (Figure 5a), and 0.88 mPa.s at 52 µm (north-east of the embryo) *vs.* 0.83 mPa.s at 45 µm (south of the embryo) from the edge of the blastocyst-stage embryo (Figure 5b). Overall, my results suggest that the viscosity of the microenvironment surrounding the embryo is heterogeneous.

3.4.4 Viscosity of the microenvironment surrounding blastocyst-stage embryos is retained after washing

To further investigate the viscosity of the microenvironment surrounding the embryo, I next sought to determine the stability of this viscous property over time. This assessment is critical in determining whether the observed viscosity reflects a stable, embryo-derived microenvironment or a transient biochemical change in the media influenced by environmental conditions, such as the deterioration of components in the culture media over time. To investigate this, I measured the viscosity at 5 µm from blastocyst-stage embryos before and after washing (Figure 6). I found no statistical difference in mean viscosity of the microenvironment between unwashed and washed blastocysts (*Unwashed*: 0.97 ± 0.14 mPa.s, *Washed*: 0.92 ± 0.08 mPa.s; $P>0.05$) (Figure 6). However, I did observe a reduction in the spread of data (min-max) post-washing (*Unwashed*: 0.79 – 1.38 mPa.s: 0.59 mPa.s *vs. Washed*: 0.78 – 1.07 mPa.s: 0.29 mPa.s) (Figure 6). Further investigation the viscosity of microenvironment surrounding blastocyst-stage embryos is warranted.

3.4.5 Ruling out blastomere-specific effects on viscosity measurements around the 4 cell-stage embryo

To investigate the potential influence of cells on the microrheology measurements, I examined whether the presence of an adjacent blastomere (individual cell within the 4-cell stage embryo) directly beneath the zona pellucida affected viscosity measurements. Since I used optical tweezers to assess the viscosity at various distances and locations around the embryo, I aimed to determine whether the proximity of a blastomere to the measurement site introduced variability in the recording of viscosity.

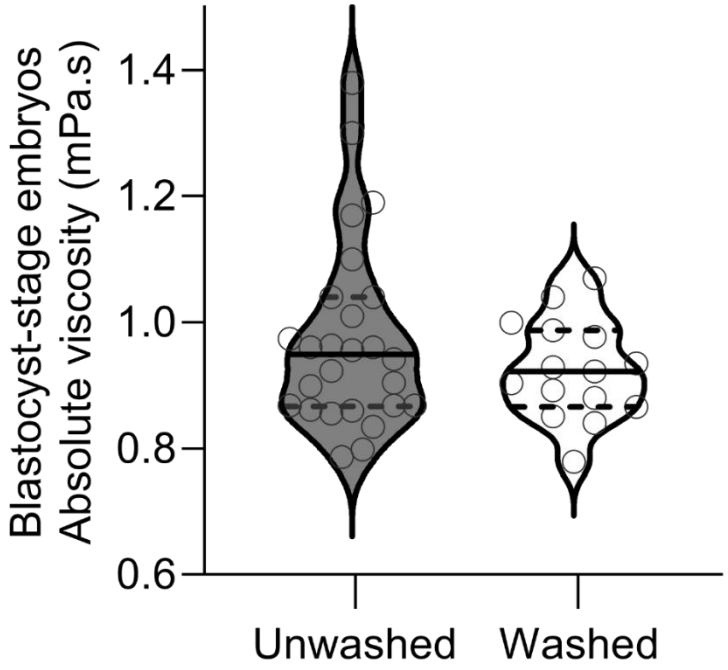

Figure 6. Washing the blastocyst-stage embryo did not impact the mean viscosity of the microenvironment surrounding these embryo. The microenvironment 5 µm away from the embryo was measured in both unwashed and washed blastocyst-stage embryos. Data is presented as a violin plot; median (solid line) ± interquartile range (dashed lines). *n* = 15 – 26 embryo measurements per group, from 6 independent experimental replicates. Data was analysed using a Mann-Whitney test.

I categorised the 4-cell viscosity measurements based on the presence (+) or absence (-) of a blastomere under the zona pellucida, while also considering its proximity to the zona edge (Figure 7a). I observed no significant difference between viscosity measurements with (+) or without (-) an underlying blastomere at all distances (Figure 7b; $P>0.05$) (Table 1). This finding indicates that the presence of an adjacent blastomere does not significantly influence the measured viscosity of the microenvironment. This analysis was necessary for distinguishing blastomere-specific effects from broader surface interactions with the zona pellucida, which was further explored in **Section 3.4.6**. Therefore, any changes in viscosity observed in **Section 3.4.6** are most likely attributed to the zona pellucida rather than the blastomere itself.

3.4.6 The impact of the zona pellucida on viscosity measurements

Based on the analysis reported in **Section 3.4.5**, I ruled out the impact of the blastomere on viscosity measurements. I next investigated whether the zona pellucida influenced viscosity measurements. To determine whether there was an impact on particle motion, and thus viscosity, I categorised viscosity data based on particle motion relative to the zona pellucida. Perpendicular measurements corresponded to translational particle motion either toward or away from the zona pellucida, while parallel measurements corresponded to linear particle motion along the surface of the embryo (Figure 8). To account for potential hydrodynamic effects between the particle and the zona pellucida, I applied Faxén's corrections to the blank control medium to establish benchmark viscosity values (red line) at each distance. These values were then overlaid with the individual viscosity measurements (blue dots) and their respective mean ± SEM (grey box plot) (Figure 8).

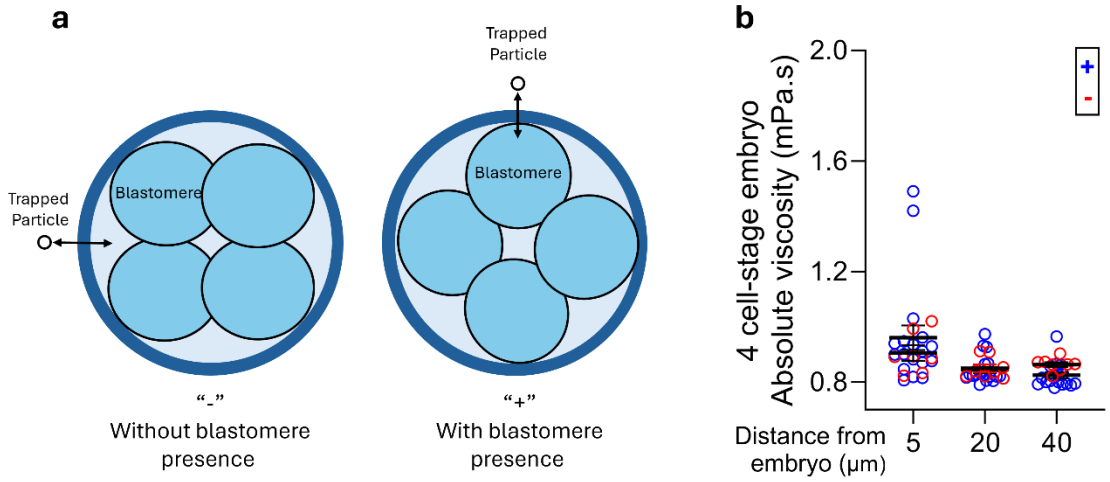

Figure 7. Viscosity measurements of the microenvironment surrounding 4 cell-stage embryos were not impacted by the presence of an underlying blastomere. (a) Viscosity measurements were categorised based on whether a blastomere was absent (-) or present (+) adjacent to the measurement site. (b) Categorical results of viscosity measured at distances 5, 20, and 40 and µm away from the edge of the zona pellucida surrounding 4 cell-stage embryos. Data are presented as mean ± SEM. *n* = 9 – 18 embryo measurements per group, from 6 independent experimental replicates. Data were analysed using a Kruskal Wallis test with a Dunn's multiple post hoc test.

Distance (μm)	With blastomere (+) (mean ± SEM)	Without blastomere (-) (mean ± SEM)
5	0.96 ± 0.04 mPa.s	0.91 ± 0.03 mPa.s
20	0.84 ± 0.01 mPa.s	0.85 ± 0.01 mPa.s
40	0.83 ± 0.01 mPa.s	0.86 ± 0.01 mPa.s

Table 1. Viscosity measurements at varying distances from the embryo surface with or without an underlying blastomere. Viscosity was measured at 5, 20, and 40 μm from the embryo surface, with and without the presence of an underlying blastomere. Data are presented as mean ± SEM. From 6 independent experimental replicates, *n* = 9 – 18 embryos measured per group. Data were analysed using a Kruskal Wallis test with a Dunn's multiple post hoc test.

For the 4 cell-stage embryo, the mean viscosity of all parallel measurements were lower than the calculated benchmark at 5 (1.01 mPa.s vs 0.95 mPa.s), 20 (0.97 mPa.s vs 0.83 mPa.s), and 40 µm (0.84 mPa.s vs 0.83 mPa.s) from the embryo (Figure 8b). Similarly, the mean viscosity of all perpendicular measurements were lower than benchmark at 5 (1.34 mPa.s vs 0.92 mPa.s), 20 (0.95 mPa.s vs 0.85 mPa.s), and 40 µm (0.87 mPa.s vs 0.84 mPa.s) from the embryo (Figure 8c). Notably, for parallel measurements, the mean viscosity at 40 µm was consistent with benchmark, showing a difference of less than 15%. This suggests a decrease in hydrodynamic interactions between the particle and the embryo. Contrastingly, perpendicular measurements did not converge to the benchmark at 40 µm, indicating that the decrease in hydrodynamic interaction was less pronounced in this orientation.

For blastocyst-stage embryos, mean parallel viscosity of my measurements were once more lower than the established benchmark viscosity at 5 (1.04 mPa.s vs 0.94 mPa.s), 20 (0.90 mPa.s vs 0.89 mPa.s), and 40 µm (0.86 mPa.s vs 0.88 mPa.s) from the embryo (Figure 8d). Perpendicular measurements were also impacted by proximity to the zona pellucida, as mean viscosity was lower than the benchmark at 5 (1.37 mPa.s vs 1.03 mPa.s), 20 (0.97 mPa.s vs 0.87 mPa.s), and 40 µm (0.90 mPa.s vs 0.91 mPa.s) from the embryo (Figure 8e). Interestingly, mean parallel measurements converged at 20 and 40 µm, ± 15% difference, with the benchmark viscosity suggesting a lack of hydrodynamic interactions at this distance. Moreover, the mean of perpendicular measurements at 40 µm was consistent with the benchmark value, showing a difference of less than 15%.

In both cell stages, the greatest difference between the calculated benchmark viscosity values and my viscosity values was observed in the perpendicular measurements. However, I observed that the difference between mean viscosity and benchmark viscosity in both parallel and perpendicular decreased with increasing distance. This further confirms that hydrodynamic interactions between the trapped particle and zona pellucida of the the embryo was interfering with the viscosity measured by the particle.

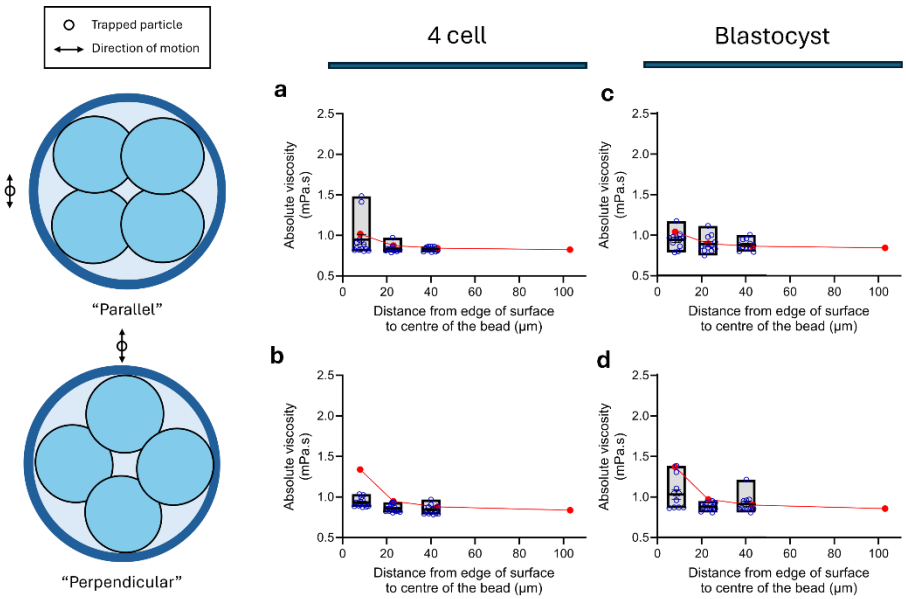

Figure 8. Viscosity of the microenvironment surrounding pre-implantation embryos was negatively impacted by the particle proximity to the zona pellucida of embryos. (a) Viscosity measurements were categorised based on particle motion, either parallel (a, c) or perpendicular (b, d) to the zona pellucida. Microenvironment viscosity measured for 4 cell- (a, b) and blastocyst-stage (c, d) are shown. The red line denotes the expected viscosity at all measured distances using values from Faxén's correction of blank Research Cleave media. Data are presented as mean ± SEM with minimum and maximum values included. *n* = 15 – 27 measurements per group; from 6 independent experimental replicates.

Parallel				
	4 cell		Blastocyst	
Distance (μm)	Faxén's corrected viscosity (mean)	Measured viscosity (mean)	Faxén's corrected viscosity (mean)	Measured viscosity (mean)
5	1.01 mPa.s	0.95 mPa.s	1.34 mPa.s	0.92 mPa.s
20	0.97 mPa.s	0.83 mPa.s	0.95 mPa.s	0.85 mPa.s
40	0.84 mPa.s	0.83 mPa.s	0.87 mPa.s	0.84 mPa.s
Perpendicular				
	4 cell		Blastocyst	
Distance (μm)	Faxén's corrected viscosity (mean)	Measured viscosity (mean)	Faxén's corrected viscosity (mean)	Measured viscosity (mean)
5	1.04 mPa.s	0.94 mPa.s	1.37 mPa.s	1.03 mPa.s
20	0.90 mPa.s	0.89 mPa.s	0.97 mPa.s	0.87 mPa.s
40	0.86 mPa.s	0.88 mPa.s	0.90 mPa.s	0.91 mPa.s

Table 2. Viscosity of the microenvironment surrounding pre-implantation embryos was negatively impacted by the particle proximity to the zona pellucida of embryos. Faxén's corrected viscosity was compared to mean viscosities measured in parallel and perpendicular orientiations for both 4 cell and blastocyst embryos, at distances 5, 20, and 40 μm from the embryo surface. Data are presented as mean from 6 independent experimental replicates, n = 15 – 27 measurements per group.

3.5 Discussion

Optical tweezers has proven to be a reliable tool for microrheological measurements in cell microenvironments [79, 80, 122, 123]. The use of optical tweezers enables a probe particle to be confined within a defined volume, enabling precise, long-term measurements that capture the intricate mechanical properties of biological materials. In this Chapter, I used optical tweezers to quantify the viscosity of various commercially available media used for embryo culture and embryo transfer. Further, I also measured the viscosity of the microenvironment surrounding preimplantation embryos. My findings demonstrated brand-specific differences in viscosity in media used for embryo culture and embryo transfer. Excitingly, I found a non-uniform, viscous microenvironment surrounding the preimplantation embryo and that this viscosity decreases as a function of radial distance. Further, this viscous microenvironment is stable and resistant to external mechanical forces (washing).

Using optical tweezers, I identified viscosity differences between commercially available embryo culture and transfer media. This finding suggests that the composition may alter the viscosity of each media, and that optical tweezers can detect these variations. While water is a primary component, the variation in viscosity of media used for embryo culture may be due to differences in the concentration of macromolecules, ions, and/or antibiotics that support pre-implantation embryo development [124-127]. Specifically, embryo culture media, G1-PLUS™ and G2-PLUS™, are sequential two-step formulations designed to provide specific nutrients to support embryos at different developmental stages. In contrast, SAGE 1-STEP™ and Research Cleave are media designed for single-step continuous culture that ensures stable nutrient availability throughout the duration of pre-implantation embryo culture. Consequently, an increase in viscosity, such as that observed for the G-series media when compared to SAGE 1-STEP™, likely stems from a higher concentration of glucose, lactate, pyruvate, and non-essential amino acids (e.g. alanine and glycine) [124, 126]. Additionally, G2-PLUS™ media is also rich in essential amino acids that function as energy sources, pH buffers, and components for protein and antioxidant synthesis, making it suited for the stages of genomic activation and compaction in human

embryos [125, 128-132]. On the other hand, embryo transfer media are specifically formulated to improve implantation success by incorporating components such as hyaluronan and human serum albumin to promote the implantation of embryos in the endometrium to establish a pregnancy [133, 134]. Previous studies have shown that a higher concentration of hyaluronan is associated with positive implantation outcomes [135, 136], as it promotes embryo attachment after transfer by improving the miscibility between transferred embryos and the uterine fluid, which is estimated to have a high viscosity of 1 Pa.s [137, 138]. The high viscosity of EmbryoGlue® may be attributed to the inclusion of hyaluronan at a concentration of 0.5mg/ml [139]. The ability to detect differences between culture and transfer media confirms the precision of optical tweezers in providing accurate and sensitive microscale viscosity measurements [137].

Excitingly, using optical tweezers, I measured a viscous microenvironment surrounding the pre-implantation embryo, and observed viscosity decreasing with increasing radial distance from the embryo. Furthermore, the viscosity of this microenvironment was significantly higher in the blastocyst-stage embryo compared to the 4-cell stage. This supports my hypothesis, which was based on the knowledge that blastocyst-stage embryos shift their metabolism to glycolysis and increase secretion of lactate into the surrounding microenvironment. As higher concentrations of lactate increase whole blood viscosity, the secretion of lactate at this later stage of embryo development was hypothesised to result in an increase in the viscosity of the immediate microenvironment – my results support this. However, we note that the viscosity of the microenvironment surrounding the 4-cell embryo was also significantly higher in comparison to the base (blank) culture media. Whilst lactate is unlikely to contribute at this early developmental stage, other compounds secreted by the embryo such as growth factors TGF-α and TGF-β1 [140-143], chloride and bicarbonate [144, 145] may contribute to increased microenvironment viscosity. Further investigation is needed to clarify whether lactate is the sole contributor or is part of a wider range of compounds that contribute to increased microenvironment viscosity at the blastocyst stage.

Interestingly, measurements of viscosity at arbitrary distances and directions from the embryo revealed that viscosity was heterogeneous. Specifically, I observed sporadic areas of high viscosity that were substantially different from the average viscosities of measurements performed at similar distances from the embryo. Though this observation was highly intriguing, this measurement was performed on a single 4 cell and blastocyst embryo and thus repeated measurements on multiple embryos is required.

It is important to highlight that all measured 4-cell- and blastocyst-stage embryos displayed minimal visual signs of degeneration during the measurement period. This was confirmed through visual inspection of embryos before, during, and after measurement, where 4-cell embryos were assessed for uniform blastomere size and blastocyst embryos were checked for the preservation of their structure and cavity. Of the embryos measured, only one demonstrated visual signs of damage, with blastocyst cavity collapse occurring after four hours of measurement. Damage prior to four hours may have been minimised by the use of a stage-top chamber, which maintained temperature, CO_2 levels, and humidity, reducing pH fluctuations in the media that lead to oxidative stress on the embryo [146, 147]. The use of a near-infrared (NIR) 1064 nm laser for optical trapping will have also minimised cellular damage and maintained biological integrity during measurement. This aligns with previous studies that highlight the relative safety of NIR lasers, particularly at 1064 nm, due to their lower absorption by water [148] compared to shorter wavelengths which induce phototoxic effects and generate reactive oxygen species that are harmful to cellular health [149, 150]. Additionally, the laser was not directly aimed at the embryos, further minimising any potential cellular damage. However, despite the advantages of NIR laser for optical trapping near biological cells, careful management of both laser power and exposure duration is nonetheless important. Several publications have shown that excessive NIR exposure can lead to one-photon excitation of water molecules in the surrounding media which may cause localised heating [151-154] that may be detrimental to embryo health. This might provide explanation to the observed blastocyst cavity collapse following measurement for four hours, with collapse being an indication of physiological stress possibly induced by heating of the media as laser exposure was highly localised on the particle [155, 156]. While turning off

the laser between measurements may provide an immediate solution to this observation, further studies measuring local temperature changes in the media are needed to clarify the impact of NIR exposure on the media. Additionally, further research should explore how NIR exposure might affect other molecular aspects of the embryo. Such studies would provide valuable insights into the safe operational parameters for NIR light-based technologies, such as optical tweezers, in reproductive research.

As the viscosity measurements were performed near the embryo, I investigated whether the Brownian motion of the probe particle was affected by surface boundary effects, specifically from the zona pellucida that surrounds the cells of the embryo. To determine this I applied Faxén's correction to the measurements from the blank culture media, generating a benchmark viscosity value that accounts for the apparent increase in viscosity due to hydrodynamic interaction between the trapped particle and the zona pellucida [83]. My results showed that close proximity to a surface, in this case the zona pellucida, may have affected the motion in the probe which would appear in the calculations as an apparent increase in the viscosity measured by the trapped particle. Specifically, I observed that the measured viscosity was lower than benchmark suggesting that the fluid immediately surrounding the embryo was less viscous than expected. Whether this is simply due to the presence of the zona pellucida, or the composition of the microenvironment requires further investigation. Nonetheless, I observed increasing alignment between the mean and the benchmark viscosity as measurements were taken further from the embryo. This was a consistent outcome for parallel measurements, with a <15% difference being recorded between the benchmark viscosity and the measured viscosity at 40 µm from the 4-cell, and 20 µm and 40 µm from the blastocyst. The agreement between benchmark and actual measurement at these distances suggests negligible influence of the embryo's zona pellucida on trapped particle motion. Interestingly, the impact of proximity of the zona pellucida was more pronounced along the perpendicular axis in all embryos, which aligns with Faxén's law. This fluctuating proximity may have intensified the influence of the zona on the trapped particle motion. Intriguingly, the mean of the perpendicular measurements taken at 40 µm from the blastocyst embryo aligned with the benchmark values, while

those for the the 4-cell embryo did not. This outcome raises an interesting question on the potential limitations in Faxén's correction, which assumes a rigid planar surface, which is not the case for the embryo. While the zona is consistently curved or non-planar throughout development, the discrepancy could stem from the dynamic changes in the zona pellucida which undergoes softening during development, a process that facilitates implantation [157, 158]. The increased impact of zona proximity on the 4 cell embryo's viscosity measurements may therefore reflect the greater rigidity of the zona at this early stage, amplifying particle-zona interactions. Considering the limitations introduced by the assumptions underlying Faxén's correction, caution is warranted in interpreting these corrected results, as the current model may not fully capture the complex dynamics that exist between the trapped particle and the embryo zona pellucida. More refined models accounting for these specific properties are essential to accurately quantify these effects enabling the accurate characterisation of the physical properties of the embryo microenvironment. For example, a control measurement using a Giant Unilamellar Vesicle, previously employed to isolate the mechanical effects of cell boundaries in viscoelastic measurements [159], could be used to model the size and rigidity of the embryo and its zona pellucida.

Future research should focus on the hydrodynamic effects imposed by the embryo on viscosity measurements. As this study trapped 6 μm diameter particles to measure viscosity, future studies could use a higher NA lens (NA > 1.2) to trap smaller particles, such as those with a diameter of less than 1 μm, to explore the impact of the zona pellucida on viscosity. Additionally, as this study focused solely on viscosity, future research could also look to assess the elastic properties of the embryo microenvironment to explore new correlations or determine if the observed trends persist. The integration of techniques such as mass spectrometry or a lactate assay kit – together with viscosity measurements – would enable the detailed quantification of the lactate secreted by developing embryos. Performing lactate measurements through the proposed methods, in conjunction with assessments of developmental competence, implantation success, and natal outcomes, would aid in establishing the connection

between my viscosity measurements and these key biological outcomes. Further studies should also investigate the potential effects of near-infrared (NIR) laser exposure on embryo health, particularly regarding DNA damage and reactive oxygen species generation. Establishing safe operational parameters for NIR light-based technologies, such as optical tweezers, will be crucial for their application in reproductive research. Collectively, these studies may deepen current understanding of the changes in viscosity of the microenvironment surrounding embryos. Furthermore, these may demonstrate how optical tweezers can reliably assess these changes in a non-invasive manner within a microlitre volume.

3.6 Conclusion

The embryo microenvironment is highly dynamic and important for pre-implantation development. In vivo, the composition of this environment is tailored to meet the changing energy demands of the embryo. As embryos shift from oxidative phosphorylation to glycolysis for energy production, lactate production and secretion by the embryo also increases. While high concentrations of lactate within whole blood increases viscosity, whether lactate secretion by the embryo increases viscosity in the surrounding microenvironment is yet to be established. In this chapter, I used optical tweezers for the microrheological measurements of the microenvironment surrounding the embryos at varying developmental stages.

This study shows the first quantitative detection of a viscous microenvironment surrounding pre-implantation embryos at both the 4-cell and blastocyst-stages. Importantly, I found that the microenvironment surrounding the blastocyst-stage embryo was significantly higher in viscosity when compared to 4 cell-stage embryos. Intriguingly, for both stages of development, I observed a decreasing viscosity gradient with increasing radial distance from the embryo suggesting that the primary driver of this viscosity was secreted by the embryo. Although Faxén's correction highlights the importance of considering surface proximity effects, it assumes a rigid and planar surface, which may be inappropriate for the curved and non-rigid zona pellucida. Future studies should address this, whilst also investigating whether lactate is responsible for the increased viscosity. Integrating lactate quantification methods with

assessments of developmental competence, implantation success, and natal outcomes, would be highly insightful in linking the viscosity of the embryo microenvironment to these important biological outcomes.

Overall, my findings highlight the potential of the optical tweezers as a precise tool for measuring viscosity at specific locations around the embryo, offering a novel approach to characterising its microenvironment. This study represents an important first step towards exploring whether the viscosity surrounding blastocyst-stage embryos can serve as a surrogate marker for lactate production, and ultimately, for assessing embryo developmental potential.

3.7 References

1. Campugan, C.A., K.R. Dunning, and K. Dholakia, *Optical manipulation: a step change for biomedical science.* Contemporary Physics, 2020. **61**(4): p. 277-294.
2. Bausch, A.R., W. Möller, and E. Sackmann, *Measurement of local viscoelasticity and forces in living cells by magnetic tweezers.* Biophysical Journal, 1999. **76**(1): p. 573-579.
3. Norregaard, K., R. Metzler, C.M. Ritter, et al., *Manipulation and motion of organelles and single molecules in living cells.* Chemical reviews, 2017. **117**(5): p. 4342-4375.
4. Brau, R., J. Ferrer, H. Lee, et al., *Passive and active microrheology with optical tweezers.* Journal of Optics A: Pure and Applied Optics, 2007. **9**(8): p. 1-11.
5. Waigh, T.A., *Advances in the microrheology of complex fluids.* Reports on Progress in Physics, 2016. **79**(7): p. 1-64.
6. Squires, T.M. and T.G. Mason, *Fluid mechanics of microrheology.* Annual review of fluid mechanics, 2010. **42**(1): p. 413-438.
7. Yao, A., M. Tassieri, M. Padgett, and J. Cooper, *Microrheology with optical tweezers.* Lab on a Chip, 2009. **9**(17): p. 2568-2575.
8. Guadayol, Ò., T. Mendonca, M. Segura-Noguera, et al., *Microrheology reveals microscale viscosity gradients in planktonic systems.* Proceedings of the National Academy of Sciences, 2021. **118**(1): p. e2011389118.
9. Mendonca, T., K. Lis-Slimak, A.B. Matheson, et al., *OptoRheo: Simultaneous in situ micro-mechanical sensing and imaging of live 3D biological systems.* Communications Biology, 2023. **6**(1): p. 463.
10. Avsievich, T., R. Zhu, A. Popov, et al., *The advancement of blood cell research by optical tweezers.* Reviews in Physics, 2020. **5**: p. 1-23.
11. Meyer, A., A. Marshall, B.G. Bush, and E.M. Furst, *Laser tweezer microrheology of a colloidal suspension.* Journal of rheology, 2006. **50**(1): p. 77-92.

12. Pesce, G., A. Sasso, and S. Fusco, *Viscosity measurements on micron-size scale using optical tweezers.* Review of scientific instruments, 2005. **76**(11).

13. Català-Castro, F., E. Schäffer, and M. Krieg, *Exploring cell and tissue mechanics with optical tweezers.* Journal of cell science, 2022. **135**(15): p. jcs259355.

14. Vos, B.E., T.M. Muenker, and T. Betz, *Characterizing intracellular mechanics via optical tweezers-based microrheology.* Current Opinion in Cell Biology, 2024. **88**: p. 102374.

15. Hoffman, B.D. and J.C. Crocker, *Cell mechanics: dissecting the physical responses of cells to force.* Annual review of biomedical engineering, 2009. **11**(1): p. 259-288.

16. Janmey, P.A. and C.A. McCulloch, *Cell mechanics: integrating cell responses to mechanical stimuli.* Annu. Rev. Biomed. Eng., 2007. **9**(1): p. 1-34.

17. Pelham Jr, R.J. and Y.-l. Wang, *Cell locomotion and focal adhesions are regulated by substrate flexibility.* Proceedings of the National Academy of Sciences, 1997. **94**(25): p. 13661-13665.

18. Elosegui-Artola, A., *The extracellular matrix viscoelasticity as a regulator of cell and tissue dynamics.* Current Opinion in Cell Biology, 2021. **72**: p. 10-18.

19. Dzamba, B.J. and D.W. DeSimone, *Extracellular matrix (ECM) and the sculpting of embryonic tissues.* Current Topics in Developmental Biology, 2018. **130**: p. 245-274.

20. Paszek, M.J., N. Zahir, K.R. Johnson, et al., *Tensional homeostasis and the malignant phenotype.* Cancer cell, 2005. **8**(3): p. 241-254.

21. Gardner, D.K., M. Lane, I. Calderon, and J. Leeton, *Environment of the preimplantation human embryo in vivo: metabolite analysis of oviduct and uterine fluids and metabolism of cumulus cells.* Fertility and sterility, 1996. **65**(2): p. 349-353.

22. Thouas, G.A., F. Dominguez, M.P. Green, et al., *Soluble ligands and their receptors in human embryo development and implantation.* Endocrine reviews, 2015. **36**(1): p. 92-130.

23. Hannan, N., P. Paiva, K. Meehan, et al., *Analysis of fertility-related soluble mediators in human uterine fluid identifies VEGF as a key regulator of embryo implantation.* Endocrinology, 2011. **152**(12): p. 4948-4956.

24. Choi, J.-W., S.-W. Kim, H.-S. Kim, et al., *Effects of melatonin, GM-CSF, IGF-1, and LIF in culture media on embryonic development: potential benefits of individualization.* International Journal of Molecular Sciences, 2024. **25**(2): p. 751.

25. Shankar, K., R. Pivik, S.L. Johnson, et al., *Environmental forces that shape early development: What we know and still need to know.* Current developments in nutrition, 2018. **2**(8): p. nzx002.

26. Richter, K.S., *The importance of growth factors for preimplantation embryo development and in-vitro culture.* Current Opinion in Obstetrics and Gynecology, 2008. **20**(3): p. 292-304.

27. D'souza, F., S. Uppangala, G. Asampille, et al., *Spent embryo culture medium metabolites are related to the in vitro attachment ability of blastocysts.* Scientific reports, 2018. **8**(1): p. 17025.

28. Zhang, T., Y. Zheng, R. Han, et al., *Effects of pyruvate on early embryonic development and zygotic genome activation in pigs.* Theriogenology, 2022. **189**: p. 77-85.

29. Leese, H.J., S.A. Hugentobler, S.M. Gray, et al., *Female reproductive tract fluids: composition, mechanism of formation and potential role in the developmental origins of health and disease.* Reproduction, Fertility and Development, 2007. **20**(1): p. 1-8.

30. Thompson, J., R. Partridge, F. Houghton, et al., *Oxygen uptake and carbohydrate metabolism by in vitro derived bovine embryos.* Reproduction, 1996. **106**(2): p. 299-306.

31. Trimarchi, J.R., L. Liu, D.M. Porterfield, et al., *Oxidative phosphorylation-dependent and-independent oxygen consumption by individual preimplantation mouse embryos.* Biology of reproduction, 2000. **62**(6): p. 1866-1874.

32. Chi, F., M.S. Sharpley, R. Nagaraj, et al., *Glycolysis-independent glucose metabolism distinguishes TE from ICM fate during mammalian embryogenesis.* Developmental cell, 2020. **53**(1): p. 9-26. e24.

33. Thompson, J., C. McNaughton, B. Gasparrini, et al., *Effect of inhibitors and uncouplers of oxidative phosphorylation during compaction and blastulation of bovine embryos cultured in vitro.* Journal of reproduction and fertility, 2000. **118**(1): p. 47-56.

34. Gardner, D.K. and H.J. Leese, *Assessment of embryo viability prior to transfer by the noninvasive measurement of glucose uptake.* Journal of Experimental Zoology, 1987. **242**(1): p. 103-105.

35. Gardner, D.K. and A.J. Harvey, *Blastocyst metabolism.* Reproduction, Fertility and Development, 2015. **27**(4): p. 638-654.

36. Clough, J. and D. Whittingham, *Metabolism of [14C] glucose by postimplantation mouse embryos in vitro.* Development, 1983. **74**(1): p. 133-142.

37. Reinhart, W.H., R. Gaudenz, and R. Walter, *Acidosis induced by lactate, pyruvate, or HCl increases blood viscosity.* Journal of critical care, 2002. **17**(1): p. 68-73.

38. Edelstein, A., N. Amodaj, K. Hoover, et al., *Computer control of microscopes using μManager.* Current protocols in molecular biology, 2010. **92**(1): p. 14.20. 11-14.20. 17.

39. Tassieri, M., R. Evans, R.L. Warren, et al., *Microrheology with optical tweezers: data analysis.* New Journal of Physics, 2012. **14**(11): p. 115032.

40. Wale, P.L. and D.K. Gardner, *The effects of chemical and physical factors on mammalian embryo culture and their importance for the practice of assisted human reproduction.* Human reproduction update, 2016. **22**(1): p. 2-22.

41. Yagoub, S.H., M. Lim, T.C. Tan, et al., *Vitrification within a nanoliter volume: oocyte and embryo cryopreservation within a 3D photopolymerized device.* Journal of Assisted Reproduction and Genetics, 2022. **39**(9): p. 1997-2014.

42. Movahed, E., R. Shabani, S. Hosseini, et al., *Interfering effects of in vitro fertilization and vitrification on expression of Gtl2 and Dlk1 in mouse blastocysts.* International Journal of Fertility & Sterility, 2020. **14**(2): p. 110.

43. Tan, T.C., H.M. Brown, J.G. Thompson, et al., *Optical imaging detects metabolic signatures associated with oocyte quality.* Biology of reproduction, 2022. **107**(4): p. 1014-1025.

44. Guadayol, Ò., T. Mendonca, M. Segura-Noguera, et al., *Microrheology reveals microscale viscosity gradients in planktonic systems.* Proceedings of the National Academy of Sciences, 2021. **118**(1): p. 1-5.

45. Watts, F., L.E. Tan, C.G. Wilson, et al., *Investigating the micro-rheology of the vitreous humor using an optically trapped local probe.* Journal of Optics, 2013. **16**(1): p. 015301.

46. Hardiman, W., M. Clark, C. Friel, et al., *Living cells as a biological analog of optical tweezers–a non-invasive microrheology approach.* Acta Biomaterialia, 2023. **166**: p. 317-325.

47. Morbeck, D.E., R.L. Krisher, J.R. Herrick, et al., *Composition of commercial media used for human embryo culture.* Fertility and sterility, 2014. **102**(3): p. 759-766. e759.

48. Tarahomi, M., F. Vaz, J.v. Straalen, et al., *The composition of human preimplantation embryo culture media and their stability during storage and culture.* Human Reproduction, 2019. **34**(8): p. 1450-1461.

49. Morbeck, D.E., N.A. Baumann, and D. Oglesbee, *Composition of single-step media used for human embryo culture.* Fertility and sterility, 2017. **107**(4): p. 1055-1060. e1051.

50. Biggers, J., L. McGinnis, and J. Lawitts, *One-step versus two-step culture of mouse preimplantation embryos: is there a difference?* Human Reproduction, 2005. **20**(12): p. 3376-3384.

51. Molè, M.A., A. Weberling, and M. Zernicka-Goetz, *Comparative analysis of human and mouse development: From zygote to pre-gastrulation.* Current Topics in Developmental Biology, 2020. **136**: p. 113-138.

52. Partridge, R. and H. Leese, *Consumption of amino acids by bovine preimplantation embryos.* Reproduction, Fertility and Development, 1996. **8**(6): p. 945-950.

53. Takahashi, Y. and N. First, *In vitro development of bovine one-cell embryos: influence of glucose, lactate, pyruvate, amino acids and vitamins.* Theriogenology, 1992. **37**(5): p. 963-978.

54. Baltz, J.M., *Osmoregulation and cell volume regulation in the preimplantation embryo.* 2001.

55. Menezo, Y.J., E. Silvestris, B. Dale, and K. Elder, *Oxidative stress and alterations in DNA methylation: two sides of the same coin in reproduction.* Reproductive Biomedicine Online, 2016. **33**(6): p. 668-683.

56. Gardner, D.K., *Changes in requirements and utilization of nutrients during mammalian preimplantation embryo development and their significance in embryo culture.* Theriogenology, 1998. **49**(1): p. 83-102.

57. Gruber, I. and M. Klein, *Embryo culture media for human IVF: which possibilities exist?* Journal of the Turkish German Gynecological Association, 2011. **12**(2): p. 110.

58. Urman, B., K. Yakin, B. Ata, et al., *Effect of hyaluronan-enriched transfer medium on implantation and pregnancy rates after day 3 and day 5 embryo transfers: a prospective randomized study.* Fertility and sterility, 2008. **90**(3): p. 604-612.

59. Karadbhajne, P. and A. More, *Effect of hyaluronic acid-enriched media in embryo implantation.* Cureus, 2022. **14**(7).

60. Reed, M.L. and A.-H. Said, *Estimation of embryo transfer media viscosity and consideration of its effect on media and uterine fluid interactions.* Reproductive Biomedicine Online, 2019. **39**(6): p. 931-939.

61. Ding, D., W. Shi, and Y. Shi, *Numerical simulation of embryo transfer: how the viscosity of transferred medium affects the transport of embryos.* Theoretical Biology and Medical Modelling, 2018. **15**: p. 1-10.

62. Nishihara, T. and Y. Morimoto, *Evaluation of transfer media containing different concentrations of hyaluronan for human in vitro fertilization.* Reproductive medicine and biology, 2017. **16**(4): p. 349-353.

63. Paria, B. and S. Dey, *Preimplantation embryo development in vitro: cooperative interactions among embryos and role of growth factors.* Proceedings of the National Academy of Sciences, 1990. **87**(12): p. 4756-4760.

64. Rappolee, D.A., C.A. Brenner, R. Schultz, et al., *Developmental expression of PDGF, TGF-α, and TGF-β genes in preimplantation mouse embryos.* Science, 1988. **241**(4874): p. 1823-1825.

65. Kallapur, S., I. Ormsby, and T. Doetschman, *Strain dependency of TGFβ1 function during embryogenesis.* Molecular reproduction and development, 1999. **52**(4): p. 341-349.

66. Dardik, A. and R.M. Schultz, *Blastocoel expansion in the preimplantation mouse embryo: stimulatory effect of TGF-a and EGF.* Development, 1991. **113**(3): p. 919-930.

67. Zhao, Y., P.J. Chauvet, S.L. Alper, and J.M. Baltz, *Expression and Function of Bicarbonate/Chloride Exchangers in the Preimplantation Mouse Embryo (∗).* Journal of Biological Chemistry, 1995. **270**(41): p. 24428-24434.

68. Zhao, Y. and J. Baltz, *Bicarbonate/chloride exchange and intracellular pH throughout preimplantation mouse embryo development.* American Journal of Physiology-Cell Physiology, 1996. **271**(5): p. C1512-C1520.

69. Swain, J.E. and T.B. Pool, *New pH-buffering system for media utilized during gamete and embryo manipulations for assisted reproduction.* Reproductive Biomedicine Online, 2009. **18**(6): p. 799-810.

70. Carney, E. and B. Bavister, *Regulation of hamster embryo development in vitro by carbon dioxide.* Biology of reproduction, 1987. **36**(5): p. 1155-1163.

71. Ashkin, A., J.M. Dziedzic, and T. Yamane, *Optical trapping and manipulation of single cells using infrared laser beams.* Nature, 1987. **330**(6150): p. 769-771.

72. Kvam, E. and R.M. Tyrrell, *Induction of oxidative DNA base damage in human skin cells by UV and near visible radiation.* Carcinogenesis, 1997. **18**(12): p. 2379-2384.

73. Liebel, F., S. Kaur, E. Ruvolo, et al., *Irradiation of skin with visible light induces reactive oxygen species and matrix-degrading enzymes.* Journal of Investigative Dermatology, 2012. **132**(7): p. 1901-1907.

74. Schneckenburger, H., A. Hendinger, R. Sailer, et al., *Cell viability in optical tweezers: high power red laser diode versus Nd: YAG laser.* Journal of biomedical optics, 2000. **5**(1): p. 40-44.

75. Sakatani, M., *Effects of heat stress on bovine preimplantation embryos produced in vitro.* Journal of Reproduction and Development, 2017. **63**(4): p. 347-352.

76. Patil, U., *Overview of lasers.* Indian Journal of Plastic Surgery, 2008. **41**(S 01): p. 101-113.

77. Wetzel, F., S. Rönicke, K. Müller, et al., *Single cell viability and impact of heating by laser absorption.* European Biophysics Journal, 2011. **40**: p. 1109-1114.

78. Marcos, J., S. Perez-Albala, A. Mifsud, et al., *Collapse of blastocysts is strongly related to lower implantation success: a time-lapse study.* Human Reproduction, 2015. **30**(11): p. 2501-2508.

79. Sciorio, R., K. Thong, and S.J. Pickering, *Spontaneous blastocyst collapse as an embryo marker of low pregnancy outcome: a time-lapse study.* JBRA Assisted Reproduction, 2020. **24**(1): p. 34.

80. Leach, J., H. Mushfique, S. Keen, et al., *Comparison of Faxén's correction for a microsphere translating or rotating near a surface.* Physical Review E—Statistical, Nonlinear, and Soft Matter Physics, 2009. **79**(2): p. 026301.

81. Murayama, Y., J. Mizuno, H. Kamakura, et al., *Mouse zona pellucida dynamically changes its elasticity during oocyte maturation, fertilization and early embryo development.* Human cell, 2006. **19**: p. 119-125.

82. Azarkh, D., Y. Cao, J. Floehr, and U. Schnakenberg, *Viscoelastic properties of zona pellucida of oocytes characterized by transient electrical impedance spectroscopy.* Biosensors, 2023. **13**(4): p. 442.

83. Limozin, L., A. Roth, and E. Sackmann, *Microviscoelastic moduli of biomimetic cell envelopes.* Physical review letters, 2005. **95**(17): p. 178101.

3.8 Supplementary Figure

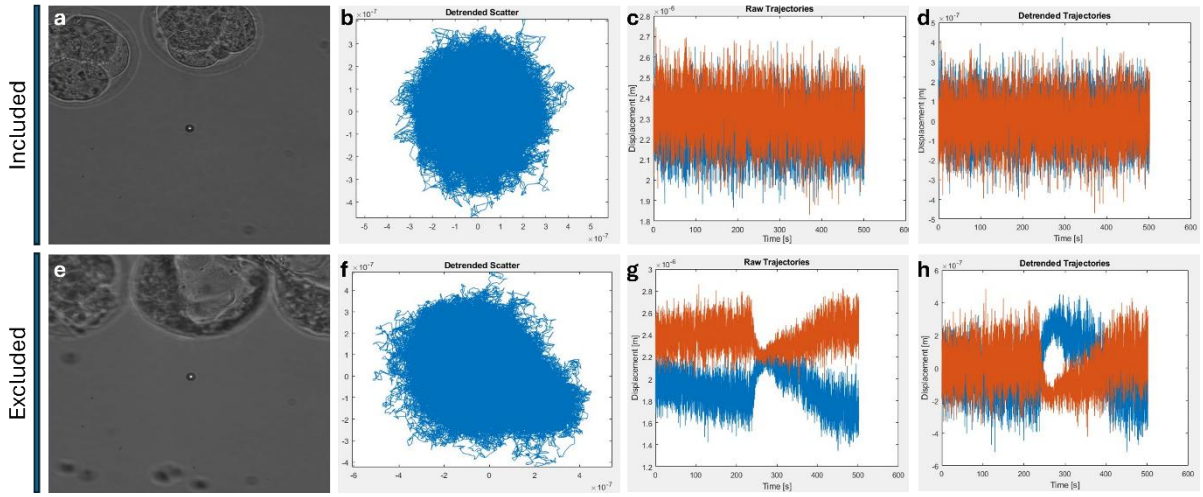

Supplementary Figure 1. Inclusion and exclusion criteria for viscosity analysis. Examples of a single (a, e) field-of-view frame, (b, f) scatter plot, and (c, g) raw and (d, h) detrended trajectory plots of the embryo microenvironment measurements that were included (top row) or excluded (bottom row) from analysis. Included data for analysis had symmetrical scatter in both the x and y direction (b) as is also depicted in their resulting (c) raw and (d) detrended trajectory plots. In contrast, data showing (f) asymmetrical scatter in both the *x* and *y* direction that showed irregular (g) raw and (h) detrended trajectory plots were excluded.

Chapter 4
The effect of discrete wavelengths of visible light on the developing murine embryo

4.1 Introduction and Significance

Light-based technologies are emerging as important tools in the field of assisted reproductive technologies (ART), yet the impact of light exposure on the live oocyte and pre-implantation embryo remains inadequately understood. In previous chapters, this thesis explores the use of the light, through optical tweezers, as a means to measure the viscosity of the environment surrounding oocytes and embryos. My results demonstrate that this technique can quantitatively measure the viscosity of the microenvironment surrounding the oocyte (Chapter 2) and embryo (Chapter 3) and that viscosity was associated with viability and developmental stage, respectively. In the case of the oocyte, measurements of viscosity were performed on isolated extracellular matrix. In contrast, measurements of viscosity for the embryo were performed adjacent to these developing cells. In this chapter, I seek to investigate the impact of light exposure on developing embryos. Though optical tweezers use near-infra-red light, visible wavelengths are typically used for imaging. This includes the various imaging modalities described in **Chapter 1.1** which have become increasingly prevalent in this field. I aim to determine how discrete wavelengths, typically used in these systems, impact various aspects of embryo health. While temperature. pH, oxygen, and culture media composition are well-established factors that influence in vitro embryo culture, whether light exposure has a similar impact remains unclear. Although several studies have reported negative effects of broad-spectrum light exposure on embryo development, the varying experimental conditions between these studies prevent direct comparison thus leaving the impact of light exposure unclear. Taking these into account, I investigated the influence of four discrete wavelengths of light within the visible range – which are commonly used in clinical imaging modalities – on embryo development. I specifically assessed the impact of exposure on blastocyst formation, DNA integrity, cellular lineage allocation, lipid metabolism, pregnancy rate, and natal outcomes. My results demonstrate varying levels of wavelength-specific impact on our parameters assessed. This indicates that previous assessments for light-induced damage are inadequate for investigating the effect of light

on the developing embryo. This chapter contributes to the broader narrative of this thesis in how optical imaging in reproductive biology and ART, should be applied with caution.

4.2 Publication Statement

This section is presented as a "Published" submission to the Journal of Assisted Reproduction and Genetics by Carl A Campugan, Megan Lim, Darren J Chow, Tiffany Cheow Yuen Tan, Tong Li, Avishkar Saini, Anthony Ornth, Phillip Reineck, Erik P Schartner, Jeremy G Thompson, Kishan Dholakia, Kylie R Dunning. *The effect of discrete wavelengths of visible light on the developing murine embryo.*

4.3 Statement of Authorship

Statement of Authorship

Title of Paper	The effect of discrete wavelengths of visible light on the developing murine embryo Published on the *Journal of Assisted Reproduction and Genetics*, June 23, 2022
Publication Status	☑ Published ☐ Accepted for Publication ☐ Submitted for Publication ☐ Unpublished and Unsubmitted w ork w ritten in manuscript style
Publication Details	Campugan, C.A., Lim, M., Chow, D.J., Tan, T.C., Li, T., Saini, A.A., Orth, A., Reineck, P., Schartner, E.P., Thompson, J.G., Dholakia, K. and Dunning, K.R. 2022. The effect of discrete wavelengths of visible light on the developing murine embryo. *Journal of Assisted Reproduction and Genetics*, *39*(8), pp.1825-1837.

Principal Author

Name of Principal Author (Candidate)	Carl Adrian Campugan		
Contribution to the Paper	• Animal handling, data acquisition, interpretation • Experimental design, data acquisition, analysis, interpretation and figure generation • Wrote the first draft, edited, and revised the manuscript for submission • Accepts responsibility for all aspects of the work, ensuring that any questions regarding the accuracy or integrity of the content are thoroughly investigated and addressed		
Overall percentage (%)	50%		
Certification:	This paper reports on original research I conducted during the period of my Higher Degree by Research candidature and is not subject to any obligations or contractual agreements with a third party that would constrain its inclusion in this thesis. I am the primary author of this paper.		
Signature		Date	30/10/24

Co-Author Contributions

By signing the Statement of Authorship, each author certifies that:

i. the candidate's stated contribution to the publication is accurate (as detailed above);

ii. permission is granted for the candidate in include the publication in the thesis; and

iii. the sum of all co-author contributions is equal to 100% less the candidate's stated contribution.

Name of Co-Author	Dr. Megan Lim
Contribution to the Paper	Megan's contribution in this publication were: • Animal handling, data acquisition, interpretation • Edited the first draft, revised, and approved the manuscript for submission • Accepts responsibility for all aspects of the work, ensuring that any questions regarding the accuracy or integrity of the content are thoroughly investigated and addressed.

Signature		Date	4/11/24

Name of Co-Author	Dr. Darren Chow		
Contribution to the Paper	Darren's contributions in this publication were: • Animal handling, data acquisition, interpretation • Edited the first draft, revised, and approved the manuscript for submission • Accepts responsibility for all aspects of the work, ensuring that any questions regarding the accuracy or integrity of the content are thoroughly investigated and addressed.		
Signature		Date	19/11/24

Name of Co-Author	Dr. Tiffany Cheow Yuen Tan		
Contribution to the Paper	Tiffany's contributions to this publication were: • Animal handling, data acquisition • Edited and revised the manuscript for submission • Accepts responsibility for all aspects of the work, ensuring that any questions regarding the accuracy or integrity of the content are thoroughly investigated and addressed.		
Signature		Date	4/11/24

Name of Co-Author	Ms. Tong Li		
Contribution to the Paper	Tong's contributions to this publication were: • Animal handling, Data acquisition • Provided feedback and accepted the final draft for submission • Accepts responsibility for all aspects of the work, ensuring that any questions regarding the accuracy or integrity of the content are thoroughly investigated and addressed.		
Signature		Date	8/11/24

Name of Co-Author	Mr. Avishkar Saini
Contribution to the Paper	Avishkar's contributions to this publication were: • Performed initial LED exposure experiments • Provided feedback and accepted the final draft for submission • Accepts responsibility for all aspects of the work, ensuring that any questions regarding the accuracy or integrity of the content are thoroughly investigated and

	addressed		
Signature	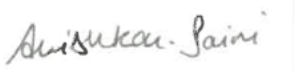	Date	31/10/24

Name of Co-Author	Dr. Anthony Orth		
Contribution to the Paper	Anthony's contributions to this publication were: • Developed the LED sources used for initial exposure experiments • Provided feedback and accepted the final draft for submission • Accepts responsibility for all aspects of the work, ensuring that any questions regarding the accuracy or integrity of the content are thoroughly investigated and addressed		
Signature		Date	4/11/24

Name of Co-Author	Dr. Philipp Reineck		
Contribution to the Paper	Philipp's contributions to this publication were: • Developed the LED sources used for initial exposure experiments • Provided feedback and accepted the final draft for submission • Accepts responsibility for all aspects of the work, ensuring that any questions regarding the accuracy or integrity of the content are thoroughly investigated and addressed		
Signature		Date	30/10/24

Name of Co-Author	Dr. Erik Schartner		
Contribution to the Paper	Erik's contributions to this publication were: • Developed the LED sources and sample mounting stage used for experiments found within this publication • Provided feedback and accepted the final draft for submission • Accepts responsibility for all aspects of the work, ensuring that any questions regarding the accuracy or integrity of the content are thoroughly investigated and addressed.		
Signature		Date	21/11/24

Name of Co-Author	Prof. Jeremy G Thompson		
Contribution to the Paper	Jeremy's contributions to this publication were: • Conceived the idea • Experimental design • Provided feedback and accepted the final draft for submission • Accepts responsibility for all aspects of the work, ensuring that any questions regarding the accuracy or integrity of the content are thoroughly investigated and		

	addressed.		
Signature	J. Thomas	Date	20/11/24

Name of Co-Author	Prof. Kishan Dholakia		
Contribution to the Paper	Kishan's contributions to this publication were: • Provided seminal feedback on framing the experimental design • Wrote, edited, critically revised, and approved the final version of the manuscript for submission • Accepts responsibility for all aspects of the work, ensuring that any questions regarding the accuracy or integrity of the content are thoroughly investigated and addressed.		
Signature	K Dholakia	Date	19/11/2024

Name of Co-Author	Associate Professor Kylie R. Dunning		
Contribution to the Paper	Kylie's contributions to this publication were: • Primary supervisor of this work • Secured funding for the study • Provided seminal feedback on framing the experimental design, data analysis, figure generation, and data interpretation • Wrote and edited the working drafts, and approved the final manuscript for submission • Accepts responsibility for all aspects of the work, ensuring that any questions regarding the accuracy or integrity of the content are thoroughly investigated and addressed.		
Signature		Date	19/11/2024

4.4 The effect of discrete wavelengths of visible light on the developing murine embryo

Journal of Assisted Reproduction and Genetics (2022) 39:1825–1837
https://doi.org/10.1007/s10815-022-02555-4

EMBRYO BIOLOGY

The effect of discrete wavelengths of visible light on the developing murine embryo

Carl A. Campugan[1,2,3] · Megan Lim[1,2,3] · Darren J. X. Chow[1,2,3] · Tiffany C. Y. Tan[1,2,3] · Tong Li[1] · Avishkar A. Saini[1,2,3] · Antony Orth[4] · Philipp Reineck[5] · Erik P. Schartner[2,3,6] · Jeremy G. Thompson[1,2,3,7] · Kishan Dholakia[8,9,10] · Kylie R. Dunning[1,2,3]

Received: 18 August 2021 / Accepted: 15 June 2022 / Published online: 23 June 2022

Abstract

Purpose A current focus of the IVF field is non-invasive imaging of the embryo to quantify developmental potential. Such approaches use varying wavelengths to gain maximum biological information. The impact of irradiating the developing embryo with discrete wavelengths of light is not fully understood. Here, we assess the impact of a range of wavelengths on the developing embryo.

Methods Murine preimplantation embryos were exposed daily to wavelengths within the blue, green, yellow, and red spectral bands and compared to an unexposed control group. Development to blastocyst, DNA damage, and cell number/allocation to blastocyst cell lineages were assessed. For the longer wavelengths (yellow and red), pregnancy/fetal outcomes and the abundance of intracellular lipid were investigated.

Results Significantly fewer embryos developed to the blastocyst stage when exposed to the yellow wavelength. Elevated DNA damage was observed within embryos exposed to blue, green, or red wavelengths. There was no effect on blastocyst cell number/lineage allocation for all wavelengths except red, where there was a significant decrease in total cell number. Pregnancy rate was significantly reduced when embryos were irradiated with the red wavelength. Weight at weaning was significantly higher when embryos were exposed to yellow or red wavelengths. Lipid abundance was significantly elevated following exposure to the yellow wavelength.

Conclusion Our results demonstrate that the impact of light is wavelength-specific, with longer wavelengths also impacting the embryo. We also show that effects are energy-dependent. This data shows that damage is multifaceted and developmental rate alone may not fully reflect the impact of light exposure.

Keywords Photodamage · Phototoxicity · Microscopy · Preimplantation embryo · Blastocyst

✉ Kylie R. Dunning
kylie.dunning@adelaide.edu.au

[1] School of Biomedicine, Robinson Research Institute, The University of Adelaide, Adelaide, SA 5005, Australia

[2] Australian Research Council Centre of Excellence for Nanoscale BioPhotonics, The University of Adelaide, Adelaide, SA 5005, Australia

[3] Institute for Photonics and Advanced Sensing, The University of Adelaide, Adelaide, South Australia, Australia

[4] National Research Council of Canada, Ottawa, Ontario, Canada

[5] Australian Research Council Centre of Excellence for Nanoscale BioPhotonics, School of Science, Royal Melbourne Institute of Technology, Melbourne, VIC 3000, Australia

[6] School of Physical Sciences, The University of Adelaide, Adelaide, SA 5005, Australia

[7] Fertilis Pty Ltd, Adelaide, South Australia 5005, Australia

[8] School of Physics and Astronomy, University of St Andrews, North Haugh, Scotland KY16 9SS, UK

[9] School of Biological Sciences, The University of Adelaide, Adelaide, SA 5005, Australia

[10] Department of Physics, College of Science, Yonsei University, Seoul 03722, South Korea

Introduction

Preimplantation embryo development is a highly sensitive period. During in vitro fertilization (IVF), preimplantation development is external from the oviduct, where its environment plays a critical role in development. Though mammalian embryos are capable of developing under varying culture conditions, sub-optimal conditions exert stressors that disrupt specific and global gene expression patterns [1, 2]. Oxygen level [3], temperature [4], pH [5], and culture media composition [6] have emerged as important culture factors which may determine the in vitro development of embryos. However, there is contention amongst other factors which may impact in vitro development including plastic-ware [7] and light exposure [8]. Though some studies suggest that embryos are exposed to some external light in vivo, this is far less than that present in vitro where light exposure is inevitable [9, 10].

In IVF clinics, light is used to observe embryos. In some cases, embryos are graded daily exposing embryos to light more frequently. A number of previous studies have investigated the impact of light on the developing embryo [11–18]. Light has several parameters that will affect embryos. These include wavelength, the average power applied, and the peak power of the light (if used in pulsed mode, e.g., multiphoton imaging)—all of which have to be considered with regard to the illuminated region and duration of illumination. Consideration of all these parameters contributes to the overall energy dose delivered to the embryo. The issue is further complicated in the previous literature as several papers use the measure of lux [11, 14, 15]. Lux is defined as one lumen per square meter (lm/m^2), whereas irradiance is denoted in watts per square meter (W/m^2) and is more commonly used for rigorous comparison. There is no direct conversion factor between lux and irradiance. This factor varies for each wavelength, and thus conversion is not straightforward unless one knows the spectral decomposition of the illumination source. As such, results employing lux as a measure are not as useful as those using irradiance [19]. Turning to irradiance itself, it is not just the power per unit area that matters but also (i) ensuring that this is applied uniformly across the whole embryo, (ii) the overall energy dose supplied which thus needs the period of irradiance to be considered, and (iii) knowledge of the spectral bandwidth of the light source. A key aspect of this present paper is to enable rigorous comparison of the effect between optical wavelengths by accounting for all the above-mentioned aspects.

Several previous studies have used broadband (often termed "white") light and explored how that might affect the embryo [2, 8, 11–13, 16, 20]. In this context, broadband means the light source has a wide spectral bandwidth (> 50 nm). Takenaka et al. [16] compared "cool" versus "warm" fluorescent light, where the difference in source lies in the relative strengths of wavelength peaks around a wavelength of 430 nm (higher in "cool" light) versus those at 620 nm (higher in "warm" light). Umaoka et al. [20] exposed embryos to broadband fluorescence (from 340 to 760 nm) while Ottosen et al. [8] explored light exposure from a broadband source covering 400–700 nm. Bognar et al. [11] showed that exposure to broadband white light (400 to 700 nm, major peaks around 430 nm, 550 nm, and 620 nm) decreases implantation potential. This study took a step towards revealing wavelength selectivity by showing that restriction, largely to the red wavelength region (~620 nm), improved the implantation potential [11]. All these studies used lux to characterize the incident light. The use of filters restricted the optical emission but not to a level that this could be termed narrowband ($\leq$ 10 nm). Overall, these studies indicated that there was an effect from light and that shorter wavelengths seemed more detrimental. While these studies broadly show that light may have an impact on embryo development, the precise influence on embryos in modern imaging methods requires a detailed study of narrowband light sources.

As label-free optical imaging to determine embryo developmental potential increase in popularity [21, 22], it is imperative that the impact of different wavelengths of light on the preimplantation embryo is carefully characterized. Mapping the stress tolerance embryos show for each wavelength may be advantageous in identifying how damage can be mitigated in clinical manipulation and modern imaging techniques. Our work aims to show the effect of wavelength during embryo development. In particular, the current study has direct relevance for the use of established and emerging optical microscopies such as confocal, multiphoton, hyperspectral, and fluorescence lifetime imaging which all often use narrow band illumination (wavelengths varying $\pm$ 10 nm around a given center wavelength). Here, we investigate the impact of four wavelengths with equivalent energy doses (blue (470 nm), green (520 nm), yellow (590 nm), and red (620 nm)) on the developing preimplantation embryo in vitro. We assess whether daily exposure during preimplantation development affects (1) development to the blastocyst stage; (2) levels of DNA damage, and (3) the number of cells within resultant blastocysts and their allocation to the inner cell mass. The generally considered benign wavelengths (yellow and red) were further investigated by assessing pregnancy and fetal outcomes following transfer to recipient females and assessing the impact of irradiance on intracellular lipid stores within the embryo.

Methods

Unless otherwise stated, all chemicals were purchased from Sigma-Aldrich (St. Louis, MO, USA).

Animals and ethics

Female (21–23 days old) and male (6–8 weeks old) CBA × C57BL/6 first filial (F1) generation (CBAF1) mice as well as female (6–8 weeks old) Swiss mice were obtained from Laboratory Animal Services (LAS; University of Adelaide, SA, Australia) and maintained on a 12 h light:12 h dark cycle. Animals were provided rodent chow and water ad libitum. All experiments were approved by the University of Adelaide Animal Ethics Committee (M-2019–052) and conducted in accordance with the Australian Code of Practice for the Care and Use of Animals for Scientific Purposes.

Media for embryo handling and culture

Embryo handling and culture media were pre-equilibrated for 4 h at 37 °C in a humidified incubator of 5% O_2, 6% CO_2 with a balance of N_2. Oviducts were collected in filtered Research Wash medium (ART Lab Solutions, SA, Australia) supplemented with 4 mg/mL low fatty acid bovine serum albumin (BSA, MP Biomedicals, AlbumiNZ, Auckland, NZ). Embryos were cultured in filtered Research Cleave medium (ART Lab Solutions, SA, Australia) supplemented with 4 mg/mL BSA.

Collection of in vivo fertilized embryos and in vitro culture

Female CBAF1 mice were administered with an intraperitoneal (I.P.) injection of 5 IU equine chorionic gonadotrophin (eCG; Folligon, Braeside, VIC, Australia), followed by 5 IU of human chorionic gonadotrophin I.P. (hCG; Pregnyl, Kilsyth, VIC, Australia) 46 h later. Female mice were then mated with male mice of proven fertility. At 23 h post-hCG, females were culled via cervical dislocation, and oviducts dissected. Presumptive zygotes were harvested by puncturing the ampulla with a 29-gauge insulin needle. Presumptive zygotes were denuded using hyaluronidase (50 U/mL) diluted in in Research Wash medium for 2 min. Presumptive zygotes were then washed in Research Wash medium and screened for polar body extrusions to confirm successful fertilization. Zygotes were cultured within a 20 µL drop of Research Cleave medium overlaid with paraffin viscous oil (Merck Millipore, Darmstadt, Germany: 10 embryos per 20 µL; one centrally located drop per 35 mm dish). The size (4 mm) and positioning of the culture drops were standardized to reduce irradiance variation in embryo light exposure (< 10%; Supp Fig. 1). Embryos were cultured in vitro at 37 °C in a humidified incubator of 5% O_2, 6% CO_2 with a balance of N_2.

Exposure of developing preimplantation embryos to specific wavelengths of light using LEDs

To determine how visible light exposure impacts preimplantation embryo development, in vitro cultured embryos were irradiated with specific narrow-band wavelengths during development. On the day of exposure, culture dishes were removed from the incubator and placed on a 37 °C heating stage. Culture dishes were exposed to only one wavelength, while control, unexposed dishes were kept in the dark to limit ambient light exposure. Light-emitting diodes (LEDs) corresponding to blue (470 nm), green (520 nm), yellow (590 nm), and red (620 nm) wavelengths were placed under the culture dishes. Light from the LEDs passed through band pass filters (Thorlabs, NJ, USA), restricting the light to ± 10 nm around the center wavelength (Supp Fig. 1).

Light sources, including those on different microscopes, as well as different wavelengths, vary in power output. Duration is only one aspect of light exposure. For each of the narrow band light sources used in the current study, the power output was measured using an optical power meter (Thorlabs, NJ, USA) and calculated in Watts/cm^2. An equivalent energy dose of 25.5 mJ/cm^2 was calculated for each wavelength using the formula Time = Energy/Power (energy is in joules, power is in watts, and time is the seconds). By keeping the energy dose equivalent, it accurately quantifies the impact of the chosen wavelengths. To achieve this, the duration of exposure, per day, was calculated to be 17.2, 86.1, 96, and 26.7 s for the blue, green, yellow, and red wavelengths, respectively (Supp. Table 1). Importantly, duration was controlled for in all groups (including the unexposed control group) with all embryos spending equivalent duration outside the incubator. The energy dose used in the current study is broadly comparable with the dose used in other forms of microscopy such as confocal and multiphoton imaging or light microscopy used during standard IVF procedures in the laboratory [8, 23]. After LED exposure, all culture dishes were returned to the incubator and cultured in standard in vitro conditions until the following day of exposure. Following the last day of exposure, blastocyst-stage embryos were fixed and underwent immunohistochemistry for either γH2AX (DNA damage), OCT3/4 (allocation of cells to the inner cell mass), or staining with BODIPY (intracellular lipid).

Assessment of on-time morphological development

Embryos were assessed for on-time morphological development on day 2 (2-cell; 46 h post-hCG) and day 5 (blastocyst stage; 118 h post-hCG). The rate of development to the 2-cell and blastocyst stages was calculated from the initial number of zygotes. Two-cell-stage embryos were identified

by the presence of two regular blastomeres of equal size, while blastocysts were identified by the presence of a blastocoel cavity ≥ two-thirds the size of the embryo; or expanded; or hatching.

Immunohistochemistry for DNA damage (γH2AX)

All immunostaining procedures were carried out at room temperature. Immunofluorescence for phosphorylated gamma-H2AX (γH2AX) was used to assess for double-stranded DNA breaks [24]. Blastocysts were fixed for 30 min in 200 µL of 4% paraformaldehyde (PFA) diluted in phosphate buffer saline (PBS). After fixation, embryos were washed with 200 µL of 0.3 mg/mL polyvinyl alcohol in PBS (PBV) and permeabilized for 30 min in 0.25% Triton-X in PBS. To prevent non-specific binding, embryos were blocked for 1 h in 10% goat serum (Jackson Immuno, Philadelphia, PA, USA) diluted in PBV. Embryos were then incubated for 24 h with anti-γH2AX rabbit monoclonal Alexa Fluor® 488-conjugated primary antibody (Ser139, 20E3, Cell Signaling Technology, Danvers, MA, USA) at 1:200 dilution in 10% goat serum. A negative control without primary antibody was also included. Following incubation, embryos were washed with PBV three times before incubation for 2 h in the dark with a goat anti-rabbit, Alexa Fluor® 594-conjugated secondary antibody (Life Technologies, Carlsbad, CA, USA) at 1:500 dilution in 10% goat serum. Embryos were also counterstained with 3 mM of 4,6-diamidino-2-phenylindole (DAPI) for 1 h in the dark to visualize nuclei. After secondary antibody incubation, embryos were washed with PBV three times and mounted on glass slides using DAKO mounting medium (Dako Inc., Carpinteria, CA, USA) before proceeding to imaging and analysis.

Immunohistochemistry for the inner cell mass (OCT-3/4)

All immunostaining procedures were carried out at room temperature. Immunofluorescence for octamer-binding transcription factor-3/4 (OCT-3/4) was used to assess the number of cells within the inner cell mass lineage of the blastocyst-stage embryo. Embryos were fixed in PFA as described for γH2AX immunohistochemistry. After fixation, embryos were incubated with 0.1 M glycine at room temperature for 5 min and washed with PBV prior to permeabilization with 0.5% Triton X-100 for 30 min. Embryos were then blocked with 10% goat serum for 1 h prior to incubation in anti-OCT-3/4 mouse primary antibody for 24 h (Santa Cruz Biotech, Dallas, TX, USA) at 1:200 dilution in 10% goat serum. Following incubation, embryos were washed in PBV and incubated for 2 h in anti-mouse Alexa Fluor 488-conjugated secondary antibody (ThermoFisher, Waltham, MA, USA) at 1:500 dilution in 10% goat serum. Embryos were then counterstained with DAPI and mounted as described for γH2AX staining.

BODIPY 493/503 staining

Blastocyst-stage embryos from unexposed and exposed groups (Supp. Table 2) were fixed in 4% paraformaldehyde-PBS for 30 min and rinsed thoroughly in PBV. Embryos were then incubated with BODIPY 493/503 (1 µg/mL; ThermoFisher) and DAPI (1.5 µM) in PBV for 1 h at room temperature in the dark. Embryos were thoroughly washed in PBV and mounted on glass slides in PBV before proceeding to imaging and analysis.

Image acquisition and analysis

All images of γH2AX and OCT-3/4 immunostaining were captured on an Olympus FV3000 confocal laser scanning microscope (Olympus, Tokyo, Japan). Images were collected at 60 × magnification with an immersion oil compatible objective (Olympus, NA = 1.4). Images were captured at 4-µm intervals through the entire embryo and a final z-stack projection generated. Samples were excited at a laser wavelength of 405 nm (emission wavelength detection range: 430–470 nm) for DAPI, 594 nm (emission detection wavelength: 499–520 nm) for γH2AX, and 488 nm (emission detection wavelength: 490–525 nm) for OCT-3/4.

BODIPY 493/503-stained blastocysts were captured on an Olympus FluoView FV10i confocal laser scanning microscope (Olympus, Tokyo, Japan). Images were acquired at 60 × magnification with a water-immersion compatible objective (Olympus, NA = 1.2). Images were captured at 2-µm intervals through the entire embryo and a final z-stack projection generated. Samples were excited at 405 nm (emission wavelength detection range: 430–470 nm) and 488 nm (emission detection wavelength: 490–525 nm) to detect DAPI- and BODIPY-stained cells, respectively.

All image analysis was performed using ImageJ for Windows 10 (Fiji, MD, USA). For image analysis of γH2AX, z-stack images of DAPI and γH2AX were first merged, and then the number of nuclei containing γH2AX-positive foci counted manually. The number of inner cell mass (ICM) cells and total cell number (TCN) were quantified using OCT-3/4-positive and DAPI-stained cells, respectively. The percentage of ICM/TCN was also calculated for each blastocyst. Lipid abundance was quantified by fluorescence intensity of BODIPY staining in a z-stack projection for each embryo.

Embryo vitrification and warming

To investigate the impact of light irradiation on subsequent pregnancy and post-natal outcomes, exposed and

non-exposed embryos were vitrified and then warmed on the day of transfer. This was to ensure that both embryos and pseudopregnant females were at the developmentally appropriate stage on the day of transfer (blastocyst stage and 2.5 days post-coitum, respectively). For embryo vitrification, the base medium used for handling and vitrification was Research Wash medium (ART Lab Solutions, Australia). Handling medium consisted of Research Wash medium supplemented with 5 mg/mL low fatty acid bovine serum albumin (BSA, MP Biomedicals, AlbumiNZ, Auckland, NZ). The handling medium described above constituted the base for all embryo vitrification media.

The equilibration solution comprised of handling medium with 10% ethylene glycol and 10% dimethyl sulfoxide (DMSO). The vitrification solution comprised of 1 M sucrose dissolved in handling medium with 16.6% ethylene glycol and 16.6% DMSO. Warming solutions comprised of decreasing concentrations of sucrose (0.3 M, 0.25 M, and 0.15 M) diluted in handling medium. Embryos were warmed in Research Cleave medium (ART Lab Solutions, SA, Australia) supplemented with 4 mg/mL BSA.

Morula-stage embryos (96 h post-hCG) were vitrified with the CryoLogic vitrification method (CVM). A NUNC four-well dish (ThermoFisher Scientific, Waltham, MA, USA) was set up with 600 µL of handling medium, equilibration solution, and vitrification solution. Once media were warmed to 37 °C, embryos were rinsed twice in handling medium, followed by transfer into equilibration solution for 3 min. Embryos were then transferred into vitrification solution for 30 s and then loaded onto a Fibreplug (CryoLogic, Pty. Ltd, VIC, Australia). Once loaded, the Fibreplug was immediately vitrified in the vapor phase of liquid nitrogen, followed by storage in a Fibreplug straw within liquid nitrogen.

For embryo warming, 600 µL of handling medium supplemented with decreasing concentrations of sucrose (0.3, 0.25, and 0.15 M) was pre-warmed to 37 °C. Fibreplugs containing embryos were removed from their straws and immediately submerged in 0.3 M sucrose for 30 s, and then transferred into a well containing 0.25 M sucrose for 5 min. Next, embryos were transferred into 0.15 M sucrose for 5 min prior to incubation in handling medium for 5 min. Lastly, embryos were transferred into Research Cleave medium and cultured to the blastocyst stage. The post-warming survival rate was 80–85% for all groups (data not shown).

Embryo transfer and postnatal outcomes

Blastocyst-stage embryos that were unexposed or exposed to yellow or red wavelength light were transferred into the uterine horns of pseudopregnant Swiss mice 2.5 days post-coitum. Embryo transfers were performed on mice under anesthesia with 1.5% isoflurane. Sixteen embryos were transferred per mouse, 8 embryos per uterine horn. Mice that underwent the embryo transfer procedure were monitored daily, with the number of pups from each female recipient recorded on delivery. At post-natal day 21, offspring were weighed and assessed for gross facial deformities.

Statistical analysis

All statistical analyses were performed using GraphPad Prism version 9 for Windows 10 (GraphPad Holdings LLC, CA, USA). Data were checked for normality and appropriate statistical tests carried out as described in the figure legends. Proportional data were arcsine transformed prior to statistical analysis. P values < 0.05 indicated statistically significant differences.

Results

The energy dose from optical microscopy can vary depending upon the exact type of imaging modality used. We chose a dose that was comparable with other forms of microscopy that are used during IVF treatments or for imaging the embryo to investigate the developmental and cellular impact of different wavelengths on the preimplantation embryo [8, 23].

The impact of specific wavelengths on embryo development

To assess whether exposure to varying wavelengths of light inhibits preimplantation embryo development, we first determined whether development to the 2-cell stage was affected following exposure at the 1-cell stage. Compared to the unexposed control group, no significant difference was observed in the 2-cell cleavage rates for blue (470 ± 10 nm), green (520 ± 10 nm), yellow (590 ± 10 nm), or red (620 ± 10 nm) wavelength exposed embryos (Supp. Fig. 2; $P > 0.05$). Similarly, there was no observable effect on development to the blastocyst stage when embryos were exposed blue, green, or red wavelengths daily (Fig. 1a, b, d, respectively; $P > 0.05$). In contrast, exposure to yellow wavelength resulted in significantly fewer embryos reaching the blastocyst stage of development compared to unexposed embryos (Fig. 1c; $P < 0.05$).

The impact of specific wavelengths on DNA integrity within the developing embryo

We next sought to determine whether irradiation with specific wavelengths during preimplantation development

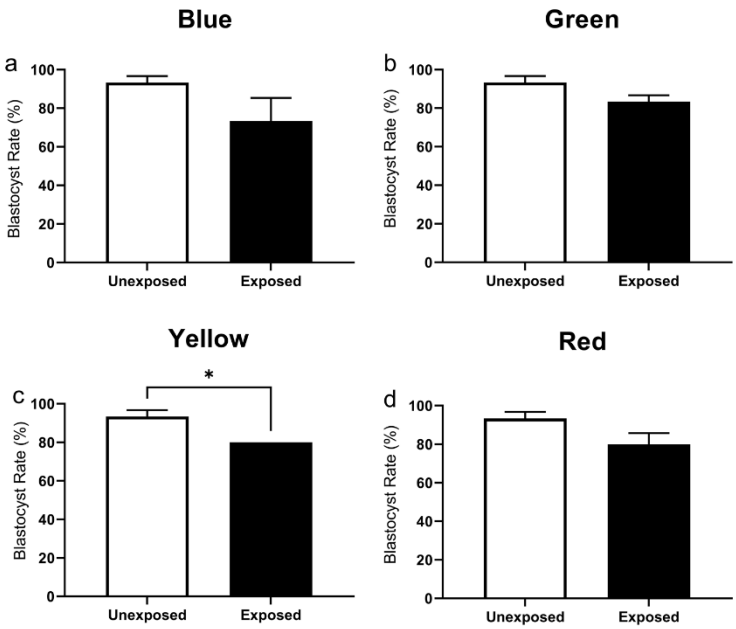

Fig. 1 Exposure to yellow wavelength (590 nm) negatively impacted development to the blastocyst stage. Embryos were exposed daily to blue (**a**; 470 ± 10 nm), green (**b**; 520 ± 10 nm), yellow (**c**; 590 ± 10 nm), or red (**d**; 620 ± 10 nm) wavelengths during preimplantation development and compared to an unexposed control group. Blastocyst rate was calculated from the starting number of zygotes. Data are presented as mean ± SEM, from 3 independent experimental replicates; $n = 21–28$ embryos per group. Data were analyzed using a Mann–Whitney test (**a**, **b**, and **d**) or unpaired *t*-test (**c**). $^*P < 0.05$

affected the level of DNA damage within resultant blastocyst-stage embryos (Fig. 2a, b). When compared to the unexposed control, we observed a significantly higher levels of DNA damage within blastocysts following daily exposure to blue, green, or red wavelengths (Fig. 2c, d, and f, respectively; $P < 0.05$). In contrast, exposure to the yellow wavelength during preimplantation development did not affect the level of DNA damage compared to the unexposed control group (Fig. 2e; $P > 0.05$).

The effect of specific wavelengths on the number of cells and allocation to the inner cell mass within resultant blastocyst-stage embryos

To further characterize the impact of specific wavelengths on the developing preimplantation embryo, we quantified the number of inner cell mass (ICM) cells and the total cell number (TCN) in blastocyst-stage embryos. There was no impact on either the total cell number or allocation to the inner cell mass when embryos were exposed to the blue (Fig. 3a–c), green (Fig. 3d–e), or yellow (Fig. 3g–h) wavelengths compared to the unexposed control group. Interestingly, exposure to the red wavelength every day of preimplantation development resulted in blastocyst-stage embryos with significantly fewer cells, but comparable number of inner cell mass cells compared to unexposed embryos (Fig. 3j and k). This difference did not impact the inner cell mass/total cell number ratio (Fig. 3l).

The impact of longer wavelengths on pregnancy rate and post-natal outcomes

It is generally accepted that longer wavelengths are safe for the developing preimplantation embryo [13, 14]. As exposure to longer wavelengths in the current study led to decreased numbers of embryos reaching the blastocyst stage (yellow), increased levels of DNA damage (yellow and red), and fewer cells within the blastocyst (red), we further explored whether these wavelengths impacted pregnancy success or post-natal outcomes. Following transfer to recipient females, there was a significant reduction in pregnancy rate when embryos were exposed to the red wavelength compared to unexposed control embryos (Fig. 4a; $P < 0.05$). In contrast, exposure to the yellow wavelength during preimplantation development did not affect pregnancy rate (Fig. 4a; $P > 0.05$). Exposure of embryos to either yellow or red wavelengths did not affect live birth rate compared to the unexposed control (Fig. 4b; $P > 0.05$). Interestingly, exposure to either yellow or red wavelengths during preimplantation development led to a significant increase in body weight at weaning compared to pups derived from unexposed control embryos (Fig. 4c; $P < 0.01$; Supp. Table 3).

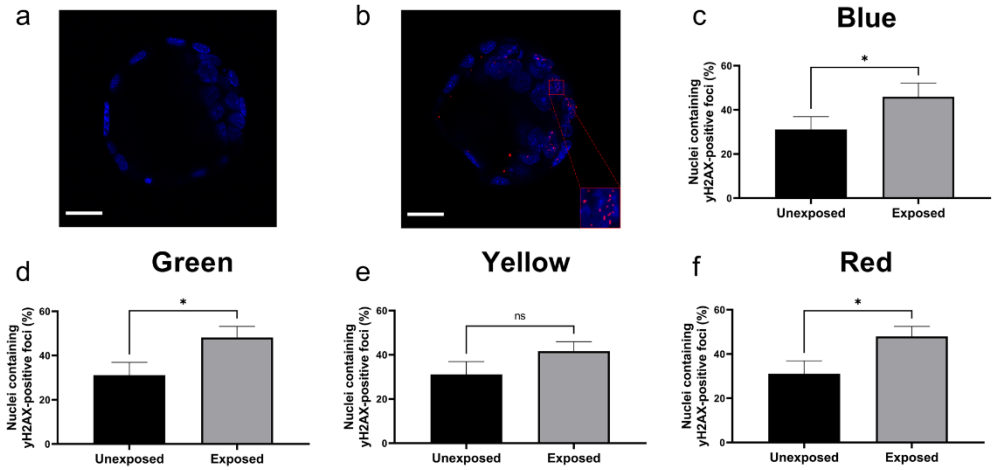

Fig. 2 Exposure to blue (470 nm), green (520 nm), or red (620 nm) wavelength led to significantly increased DNA damage within resultant blastocyst. Double-stranded DNA damage in unexposed (**a**) vs exposed (**b**) blastocyst-stage embryos was assessed using γH2AX immunohistochemistry. Inset in (**b**) shows multiple γH2AX-positive puncta within a nucleus. Percentage of nuclei containing γH2AX-positive punctum was quantified within blastocysts following exposure to blue (**c**; 470 ± 10 nm), green (**d**; 520 ± 10 nm), yellow (**e**; 590 ± 10 nm), or red (**f**; 620 ± 10 nm) wavelengths during preimplantation embryo development. These were compared to an unexposed control group. Data are presented as mean ± SEM, from 3 independent experimental replicates, $n = 9–16$ embryos per group. Data were analyzed using a Mann–Whitney test. *$P < 0.05$. Scale bar = 25 µm

No gross facial deformities were observed in any treatment group.

The effect of longer wavelengths on lipid abundance within resultant blastocyst-stage embryos

Previous work has shown that exposure of adipocytes to yellow or red wavelengths reduces intracellular lipid via lipolysis [25]. Lipids form an important energy source for the embryo, but an excess of lipid is damaging to developmental competence [26–28]. Thus, to investigate the mechanism by which longer wavelengths elicited a negative impact on the developing embryo, we quantified the abundance of intracellular lipid. Additionally, we explored whether any impact on lipid abundance was dose-dependent by exposing embryos to the same energy used in the experiments described above or to double the energy (Supp. Table 2). There was a visible increase in lipid abundance within embryos that were exposed to the yellow wavelength compared to unexposed controls (Fig. 5a-i). In contrast, there was no observable difference in lipid abundance when embryos were exposed to the red wavelength (Fig. 5j-r). The observable and contrasting impact of yellow and red wavelengths on lipid abundance were confirmed following quantification. Compared to unexposed embryos, there was a 1.3-fold increase in lipid abundance in embryos exposed to the yellow wavelength daily, although this did not reach statistical significance (Fig. 5s; single exposure vs unexposed). When exposure to the yellow light was doubled, there was a significant 1.8-fold increase in lipid abundance compared to the unexposed control group (Fig. 5s; double exposure vs unexposed; $P < 0.0001$). In contrast, exposure to the red wavelength did not affect levels of intracellular lipid compared to unexposed control embryos (Fig. 5t).

Discussion

There has been an increase in popularity in using various forms of optical imaging to study the preimplantation embryo both from a clinical and a research standpoint. Such studies expose embryos to light, varying in intensity and wavelength [9, 10, 17]. This, however, may have damaging effects on the embryo [2, 12]. Previous investigations with embryos either focus on specific wavelength ranges [13, 14] or use broadband light sources [2, 8, 11–13, 16, 20], but there is no detailed consideration of the uniformity of illumination across all embryos and an absence of controlling the energy dose given for each wavelength range. In the current study, we address these shortcomings of previous work and conduct a thorough

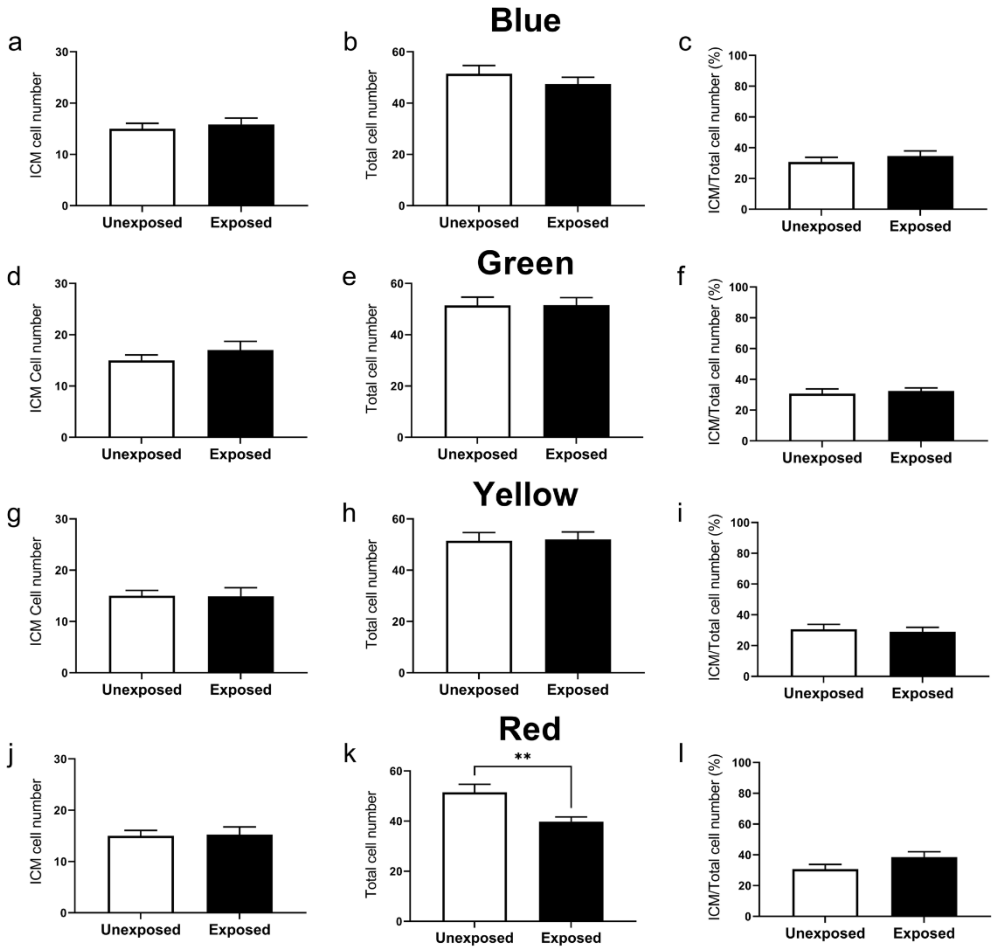

Fig. 3 Exposure to red wavelength (620 nm) during preimplantation development significantly reduced total cell number within resultant blastocysts. The impact of wavelength-specific exposure on the number of cells within the inner cell mass (ICM; **a**, **d**, **g**, **j**), the total cell number (TCN; **b**, **e**, **h**, **k**), and the ratio of ICM/TCN (expressed as a percentage; **c**, **f**, **i**, **l**) of resultant blastocyst was assessed using Oct-3/4 (ICM) and DAPI (TCN). Embryos were either unexposed or exposed daily to blue (**a**, **b**, **c**; 470 ± 10 nm), green (**d**, **e**, **f**; 520 ± 10 nm), yellow (**g**, **h**, **i**; 590 ± 10 nm), or red (**j**, **k**, **l**; 620 ± 10 nm) wavelengths. Data are presented as mean ± SEM, from 3 independent experimental replicates; $n = 11–13$ embryos per group. Data were analyzed using a two-tailed unpaired *t*-test. $^{**}P < 0.01$

examination by exposing developing preimplantation murine embryos to specific wavelengths of light and controlled energy doses. We assess the impact on embryo viability, DNA damage, pregnancy/fetal outcomes, and the abundance of intracellular lipid. Therefore—as we discuss below—it is perhaps not too surprising that our conclusions contrast at times with previous literature. We contend that our approach adds key new knowledge to this burgeoning area and our conclusions are supported by additional analyses that reinforce our outcomes.

Light-induced damage on the developing preimplantation embryo has been the focus of previous studies. However, most of these have described irradiance intensity as lux only [2, 13–15, 20]. This has made direct comparison of results within and between studies challenging, and at times imprecise. In the current study, light was measured as a function

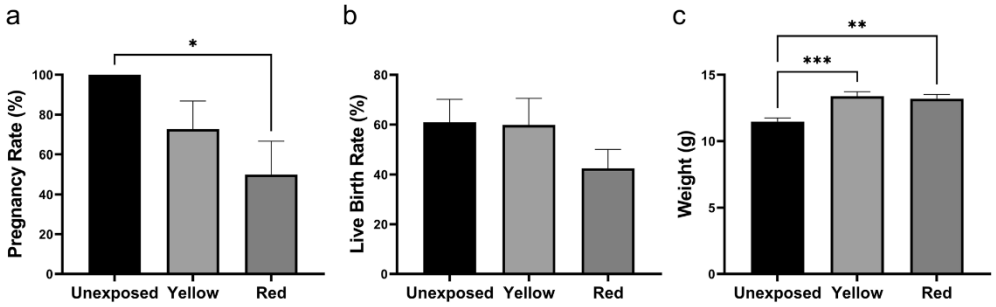

Fig. 4 Exposure to longer wavelengths during preimplantation development reduces pregnancy rate (red; 620 nm) and leads to significantly higher weights at weaning (red and yellow; 590). The effect of red and yellow wavelengths on pregnancy rate (**a**), live birth rate (**b**), and the weight of offspring at weaning (**c**) was assessed following embryo transfer of blastocyst-stage embryos to pseudopregnant mice. Data are presented as mean ± SEM, $n = 9–11$ pseudopregnant females per group for pregnancy rate, $n = 35–58$ pups per group for live birth rate, $n = 18–35$ pups for weight at weaning. Normally distributed data were analyzed using a one-way ANOVA with Holm-Šídák post hoc test (**a**). A Kruskal–Wallis with Dunn's multiple comparisons test was applied to data which did not follow a normal distribution (**b**). $^{*}P < 0.05$, $^{**}P < 0.01$, $^{***}P < 0.001$

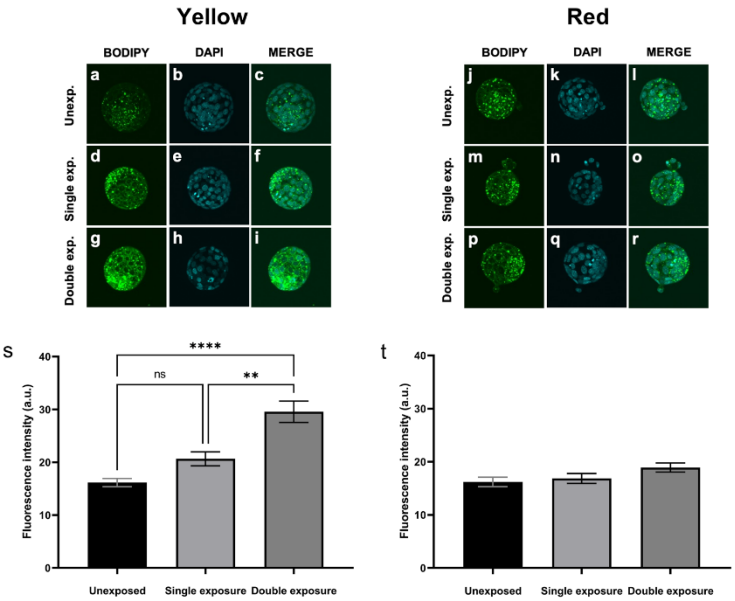

Fig. 5 Yellow wavelength (590 nm) exposure during preimplantation development significantly increased lipid abundance within resultant blastocysts. Lipid abundance in blastocyst-stage embryos was assessed using BODIPY 493/503. Embryos were either unexposed (**a–c**; **j–l**) or exposed to yellow (**d–i**; 590 ± 10 nm) or red (**m–r**; 620 ± 10 nm) wavelengths during preimplantation embryo development. Exposed embryos were irradiated for a single (**d–f**; **m–o**) or double dose (**g–i**; **p–r**; see Supp. Table 2). Fluorescence intensity was quantified for embryos that were unexposed or exposed to yellow (**s**) or red (**t**) wavelength exposed embryos. Data are presented as mean ± SEM, from 4 independent experimental replicates, $n = 26–37$ embryos per group. Data were analyzed using a Kruskal–Wallis with Dunn's multiple comparisons test. Images were captured at × 60 magnification. $^{**}P < 0.01$; $^{****}P < 0.0001$

of intensity and area. To accurately characterize wavelength-specific damage, we implemented an experimental design which accounted for irradiance intensity variation along the beam width by housing embryos within a 4 mm diameter drop of culture media where intensity variation was ≤ 10%. Additionally, a band pass filter was used to attenuate light to frequencies ± 10 nm around the center wavelength. Furthermore, as all wavelengths exert varying energy doses upon exposure, our experimental design tailored both the time and uniformity of exposure to ensure that the energy exposed to embryos was equivalent for each wavelength—a variable not accounted for in previous studies.

Across all wavelengths, only embryos exposed to the yellow wavelength (590 nm) daily had a significantly lower blastocyst rate compared to unexposed control embryos. To the best of our knowledge, our study is the first to show a negative impact of a long wavelength, rather than short [14], on development to the blastocyst stage. A previous study using differentiated adipocytes showed that amber light (590 nm) led to increased breakdown of lipid droplets [29]. In the current study, we investigated whether yellow light had a similar impact on the embryo. In contrast with the effect on adipocytes, exposure of embryos to the yellow wavelength led to an increase in lipid abundance. We also showed that the effect of the yellow wavelength was dose-dependent with delivery of increasing levels of energy correlating with increasing lipid within the embryo. Although lipid droplets have been found to be crucial for preimplantation embryo development, overabundance is harmful [28] which may explain the decreased blastocyst rate following irradiation with the yellow wavelength. Elevated levels of intracellular lipid within the embryo may have also contributed to the higher weight at weaning observed following transfer of yellow wavelength exposed embryos. The mechanism by which the yellow wavelength led to elevated lipid abundance and a higher weaning weight requires further investigation.

Analysis of γH2AX phosphorylation in blastocyst-stage embryos revealed unique impacts of specific wavelengths on DNA integrity. Embryos exposed daily to the blue, green, or red wavelengths had significantly higher levels of DNA damage. The effect of the blue wavelength is supported by a previous study showing elevated DNA damage following light (470 nm) exposure [2]. Intriguingly, however, are our outcomes for the red wavelength which contrast with previous work. Elevated DNA damage outcomes for red wavelength light were unexpected as a previous study showed lower hydrogen peroxide levels and HSP70 protein abundance after light (620–750 nm) exposure [14]. In the clinical setting, this outcome contrasts the claims of some time-lapse imaging systems that utilize red wavelength light to bypass the detrimental effects of short wavelength light [13, 30]. The negative effect of the blue and green wavelengths, resulting in elevated DNA damage, concurs with previous work where the same wavelengths led to increased reactive oxygen species (ROS) formation and HSP70 expression [12, 14], both indicators of cellular stress. Although certain wavelengths appeared more damaging to DNA, caution should still be exercised when using any visible light wavelengths.

Inner cell mass and trophectoderm populations at the blastocyst stage are predictive of pregnancy and live birth outcomes [31–33]. In this study, we showed no impact on the ICM or total cell number for blastocysts exposed to the blue, green, and yellow wavelengths. For blue wavelength light, our observations are inconsistent with previous findings [14], where the authors observed increased incidence of cell apoptosis. Though ICM numbers were comparable with unexposed embryos, TE numbers may have declined following red wavelength exposure as observed by significantly lower total cell number. This contrasts with earlier studies, where exposure of developing embryos to red wavelength light (620–750 nm) did not impact ICM, TE, or total cell numbers [13, 14]. Although our findings suggest no wavelength-specific impact on cell counts for blue, green, and yellow wavelength exposed embryos, caution should still be exercised as our DNA damage results may suggest increased ROS formation which may promote cell apoptosis [34].

Unique to the longer wavelengths was the negative effect of red wavelength exposure on pregnancy rate. This finding suggests that implantation was significantly impaired in red wavelength exposed embryos—an outcome that may be associated with the observed reduction in TE cells. In contrast, lipid droplet abundance was similar in red wavelength exposed groups relative to unexposed embryos. This result contrasts with the previous study on differentiated adipocytes where intracellular lipid was decreased following irradiation with a red wavelength (660 nm [25]). This suggests a difference in wavelength-specific tolerance between cells—an outcome alluded to in previous studies [8, 14, 19]. Further investigation into the mechanisms underlying these effects of the red wavelength on the preimplantation embryo is warranted.

Also pertinent to this present paper, a previous study showed that following spinning disk confocal imaging there was no impact on embryo development but the authors acknowledge that they did not use laser illumination and used very short exposure times [35]. Closest to the present work is the study by Squirrell et al. [23] who studied the dynamics of mitochondrial distribution in hamster embryos over 24 h using two-photon microscopy (operating at a wavelength of 1047 nm). This study showed that imaging did not affect development to blastocyst nor fetal developmental following transfer. In contrast, their study showed

that confocal imaging (at wavelengths of 514 nm, 532 nm, and 568 nm) for only 8 h inhibits development. However, it is to be noted that this study explored labeled samples and worked on three narrow band, closely spaced wavelengths in the blue to green range of the spectrum.

Our study thus adds significant value to the field as we concentrate on the effects on embryo development upon irradiation of narrowband (± 10 nm) light centered around the blue (470 nm), green (520 nm), yellow (590 nm), and red (620 nm) regions of the spectrum. Importantly, this widely varying range of wavelengths captures some of the key ones used in confocal imaging as well as being aligned to other more advanced forms of optical imaging such as fluorescence lifetime studies, hyperspectral imaging, and light sheet microscopy. This is coupled with the fact that our study is carefully designed to ensure equivalent energy dose for all samples regardless of wavelength used, a feature not seen in previous studies. This makes our study robust and highly informative to users of such imaging modalities for embryo analysis. It is, however, important to note that the murine embryo was used as a model in the current study. Thus, any direct correlation with human embryos based on these results warrants caution and requires further investigation.

In the current study, we observed that the yellow wavelength led to increased lipid abundance within the blastocyst-stage embryo which may explain the decreased rate of development to the blastocyst stage and heavier weight of resultant offspring at weaning. Furthermore, in exposing embryos to the red wavelength we observed higher levels of DNA damage at the blastocyst stage which may explain the reduced number of trophectoderm cells and the lower pregnancy rate post-transfer. These findings suggest that wavelength-specific impact is multifaceted and analyses of embryo health after light exposure require both spatial (i.e., development to the blastocyst stage and pregnancy/postnatal outcomes) and molecular (i.e., DNA damage; lipid abundance) assessments. Our findings will inform future studies of the potential damage of visible light, particularly those in the long wavelength spectrum. Further investigations into the source of cell damage and the mechanisms underlying effects on lipid as well as pregnancy and fetal weights will aid in understanding the implications of this research to clinical embryology.

Supplementary Information The online version contains supplementary material available at https://doi.org/10.1007/s10815-022-02555-4.

Author contribution Kylie Dunning, Kishan Dholakia, Jeremy Thompson, Antony Orth, and Philipp Reineck contributed to the study conception and design. Material preparation, data collection, and analysis were performed by Carl Campugan, Tiffany Tan, Darren Chow, Megan Lim, Tong Li, Philip Reineck, and Avishkar Saini. The first draft of the manuscript was written by Carl Campugan, Darren Chow, Megan Lim, Kishan Dholakia, and Kylie Dunning. Kylie Dunning and Kishan Dholakia provided critical feedback on the final manuscript. All authors commented on previous versions of the manuscript. All authors critically reviewed and approved the final manuscript.

Funding Open Access funding enabled and organized by CAUL and its Member Institutions KRD is supported by a Mid-Career Fellowship from the Hospital Research Foundation (C-MCF-58–2019). KD is supported by funding from the UK Engineering and Physical Sciences Research Council (EP/P030017/1) and the Australian Research Council (FL210100099). CC acknowledges the support of a PhD scholarship jointly from the University of Adelaide and University of Nottingham. This study was funded by the Australian Research Council Centre of Excellence for Nanoscale BioPhotonics (CE140100003). PR acknowledges funding through the RMIT Vice-Chancellor's Research Fellowship and ARC DECRA Fellowship scheme (DE200100279).

Data availability All data generated or analyzed during this study are included in this published article and are available from the corresponding author on reasonable request.

Code availability N/A.

Declarations

Ethics approval Ethics approval for the study was obtained from the University of Adelaide Animal Ethics Committee (M-2019–052).

Consent to participate N/A.

Consent for publication The authors consent for publication of this article.

Competing interests The authors declare no competing interests.

References

1. Niemann H, Wrenzycki C. Alterations of expression of developmentally important genes in preimplantation bovine embryos by in vitro culture conditions: implications for subsequent development. Theriogenology. 2000;53(1):21–34. https://doi.org/10.1016/s0093-691x(99)00237-x.
2. Lv B, Liu C, Chen Y, Qi L, Wang L, Ji Y, Xue Z. Light-induced injury in mouse embryos revealed by single-cell RNA sequencing. Biol Res. 2019;52(1):48. https://doi.org/10.1186/s40659-019-0256-1.
3. Wale PL, Gardner DK. Time-lapse analysis of mouse embryo development in oxygen gradients. Reprod Biomed Online. 2010;21(3):402–10. https://doi.org/10.1016/j.rbmo.2010.04.028.

4. Walters EA, Brown JL, Krisher R, Voelkel S, Swain JE. Impact of a controlled culture temperature gradient on mouse embryo development and morphokinetics. Reprod Biomed Online. 2020;40(4):494–9. https://doi.org/10.1016/j.rbmo.2019.12.015.
5. Swain JE. Optimizing the culture environment in the IVF laboratory: impact of pH and buffer capacity on gamete and embryo quality. Reprod Biomed Online. 2010;21(1):6–16. https://doi.org/10.1016/j.rbmo.2010.03.012.
6. Gardner DK, Kelley RL. Impact of the IVF laboratory environment on human preimplantation embryo phenotype. J Dev Orig Health Dis. 2017;8(4):418–35. https://doi.org/10.1017/S2040174417000368.
7. Santos JT, Soobrian L, Kashyap S. Off-gassing plasticware to decrease the toxicity effect in embryo culture. Jornal Brasileiro De Reproducao Assistida. 2021;25(3):428–33. https://doi.org/10.5935/1518-0557.20210005.
8. Ottosen LD, Hindkjaer J, Ingerslev J. Light exposure of the ovum and preimplantation embryo during ART procedures. J Assist Reprod Genet. 2007;24(2–3):99–103. https://doi.org/10.1007/s10815-006-9081-x.
9. Jacques SL, Weaver DR, Reppert SM. Penetration of light into the uterus of pregnant mammals. Photochem Photobiol. 1987;45(5):637–41. https://doi.org/10.1111/j.1751-1097.1987.tb07391.x.
10. Del Giudice M. Alone in the dark? Modeling the conditions for visual experience in human fetuses. Dev Psychobiol. 2011;53(2):214–9. https://doi.org/10.1002/dev.20506.
11. Bognar Z, Csabai TJ, Pallinger E, Balassa T, Farkas N, Schmidt J, Gorgey E, Berta G, Szekeres-Bartho J, Bodis J. The effect of light exposure on the cleavage rate and implantation capacity of preimplantation murine embryos. J Reprod Immunol. 2019;132:21–8. https://doi.org/10.1016/j.jri.2019.02.003.
12. Korhonen K, Sjovall S, Viitanen J, Ketoja E, Makarevich A, Peippo J. Viability of bovine embryos following exposure to the green filtered or wider bandwidth light during in vitro embryo production. Hum Reprod. 2009;24(2):308–14. https://doi.org/10.1093/humrep/den432.
13. Li R, Pedersen KS, Liu Y, Pedersen HS, Laegdsmand M, Rickelt LF, Kuhl M, Callesen H. Effect of red light on the development and quality of mammalian embryos. J Assist Reprod Genet. 2014;31(7):795–801. https://doi.org/10.1007/s10815-014-0247-7.
14. Oh SJ, Gong SP, Lee ST, Lee EJ, Lim JM. Light intensity and wavelength during embryo manipulation are important factors for maintaining viability of preimplantation embryos in vitro. Fertil Steril. 2007;88(4 Suppl):1150–7. https://doi.org/10.1016/j.fertnstert.2007.01.036.
15. Takahashi M, Saka N, Takahashi H, Kanai Y, Schultz RM, Okano A. Assessment of DNA damage in individual hamster embryos by comet assay. Mol Reprod Dev. 1999;54(1):1–7. https://doi.org/10.1002/(SICI)1098-2795(199909)54:1%3c1::AID-MRD1%3e3.0.CO;2-0.
16. Takenaka M, Horiuchi T, Yanagimachi R. Effects of light on development of mammalian zygotes. Proc Natl Acad Sci USA. 2007;104(36):14289–93. https://doi.org/10.1073/pnas.0706687104.
17. Sanchez T, Venturas M, Aghvami SA, Yang X, Fraden S, Sakkas D, Needleman DJ. Combined noninvasive metabolic and spindle imaging as potential tools for embryo and oocyte assessment. Hum Reprod. 2019;34(12):2349–61. https://doi.org/10.1093/humrep/dez210.
18. Khodavirdilou R, Pournaghi M, Oghbaei H, Rastgar Rezaei Y, Javid F, Khodavirdilou L, Shakibfar F, Latifi Z, Hakimi P, Nouri M, Fattahi A, Dittrich R. Toxic effect of light on oocyte and pre-implantation embryo: a systematic review. Arch Toxicol. 2021;95(10):3161–9. https://doi.org/10.1007/s00204-021-03139-4.
19. Pomeroy KO, Reed ML. The effect of light on embryos and embryo culture. J Reproductive Stem Cell Biotech 2012;3(2):46–54. https://doi.org/10.1177/20589158120300203.
20. Umaoka Y, Noda Y, Nakayama T, Narimoto K, Mori T, Iritani A. Effect of visual light on in vitro embryonic development in the hamster. Theriogenology. 1992;38(6):1043–54. https://doi.org/10.1016/0093-691x(92)90118-b.
21. Tan TCY, Mahbub SB, Campbell JM, Habibalahi A, Campugan CA, Rose RD, Chow DJX, Mustafa S, Goldys EM, Dunning KR. Non-invasive, label-free optical analysis to detect aneuploidy within the inner cell mass of the preimplantation embryo. Hum Reprod. 2022;37(1):14–29. https://doi.org/10.1093/humrep/deab233.
22. Shah JS, Venturas M, Sanchez TH, Penzias AS, Needleman DJ, Sakkas D. Fluorescence lifetime imaging microscopy (FLIM) detects differences in metabolic signatures between euploid and aneuploid human blastocysts. Hum Reprod. 2022;37(3):400–10. https://doi.org/10.1093/humrep/deac016.
23. Squirrell JM, Wokosin DL, White JG, Bavister BD. Long-term two-photon fluorescence imaging of mammalian embryos without compromising viability. Nat Biotechnol. 1999;17(8):763–7. https://doi.org/10.1038/11698.
24. Yagoub SH, Thompson JG, Orth A, Dholakia K, Gibson BC, Dunning KR. Fabrication on the microscale: a two-photon polymerized device for oocyte microinjection. J Assist Reprod Genet. 2022. https://doi.org/10.1007/s10815-022-02485-1.
25. Choi MS, Kim H-J, Ham M, Choi D-H, Lee TR, Shin DW. Amber light (590 nm) induces the breakdown of lipid droplets through autophagy-related lysosomal degradation in differentiated adipocytes. Sci Rep. 2016;6(1):28476. https://doi.org/10.1038/srep28476.
26. Dunning KR, Cashman K, Russell DL, Thompson JG, Norman RJ, Robker RL. Beta-oxidation is essential for mouse oocyte developmental competence and early embryo development1. Biol Reprod. 2010;83(6):909–18. https://doi.org/10.1095/biolreprod.110.084145.
27 Sutton-McDowall ML, Feil D, Robker RL, Thompson JG, Dunning KR. Utilization of endogenous fatty acid stores for energy production in bovine preimplantation embryos. Theriogenology. 2012;77(8):1632-1641. https://doi.org/10.1016/j.theriogenology.2011.12.008.
28. Aizawa R, Ibayashi M, Tatsumi T, Yamamoto A, Kokubo T, Miyasaka N, Sato K, Ikeda S, Minami N, Tsukamoto S. Synthesis and maintenance of lipid droplets are essential for mouse preimplantation embryonic development. Development. 2019;146(22):dev181925. https://doi.org/10.1242/dev.181925.
29. Choi MS, Kim HJ, Ham M, Choi DH, Lee TR, Shin DW. Amber light (590 nm) induces the breakdown of lipid droplets through autophagy-related lysosomal degradation in differentiated adipocytes. Sci Rep. 2016;6:28476. https://doi.org/10.1038/srep28476.
30. Kovacs P. Embryo selection: the role of time-lapse monitoring. Reprod Biol Endocrinol. 2014;12(1):124. https://doi.org/10.1186/1477-7827-12-124.
31. Ebner T, Tritscher K, Mayer RB, Oppelt P, Duba HC, Maurer M, Schappacher-Tilp G, Petek E, Shebl O. Quantitative and qualitative trophectoderm grading allows for prediction of live birth and gender. J Assist Reprod Genet. 2016;33(1):49–57. https://doi.org/10.1007/s10815-015-0609-9.
32. Zhao YY, Yu Y, Zhang XW. Overall blastocyst quality, trophectoderm grade, and inner cell mass grade predict pregnancy outcome in euploid blastocyst Transfer Cycles. Chin Med J. 2018;131(11):1261–7. https://doi.org/10.4103/0366-6999.232808.

33. Ai JH, Jin L, Zheng Y, Yang PW, Huang B, Dong XY. The morphology of inner cell mass is the strongest predictor of live birth after a frozen-thawed single embryo transfer. Front Endocrinol. 2021;12:46. https://doi.org/10.3389/fendo.2021.621221.
34. Yang HW, Hwang KJ, Kwon HC, Kim HS, Choi KW, Oh KS. Detection of reactive oxygen species (ROS) and apoptosis in human fragmented embryos. Hum Reprod. 1998;13(4):998–1002. https://doi.org/10.1093/humrep/13.4.998.
35. Ross PJ, Perez GI, Ko T, Yoo MS, Cibelli JB. Full developmental potential of mammalian preimplantation embryos is maintained after imaging using a spinning-disk confocal microscope. Biotechniques. 2006;41(6):741–50. https://doi.org/10.2144/000112310.

Chapter 5
General Discussion and Future directions

5.1 Significance and clinical relevance

Infertility, defined as the inability to successfully conceive after one year of regular, unprotected intercourse, has become an increasingly prevalent global issue, affecting approximately 17.5% of the adult population worldwide [1, 2]. In response to this rising prevalence, assisted reproductive technologies (ART), like in vitro fertilisation (IVF), have become key solutions for overcoming infertility. This increasing reliance on IVF is most evident in the consistent annual growth in initiated IVF cycles, which have risen by approximately 8% each year since 1999, resulting in a fourfold increase between 1999 and 2021 [3]. Despite the increasing use of IVF, success rates have stagnated, with live birth rates per initiated cycle persisting at ~20% for more than a decade [3]. A fundamental pillar for improving IVF outcomes lies in the accurate assessment of oocyte and embryo quality. As multiple oocytes and embryos are generated during an IVF cycle, ranking these based on developmental potential could enable patients to achieve pregnancy sooner, reducing the financial and emotional burdens of repeated attempts. Currently, morphological evaluations are the primary method of assessment, focusing on the appearance and size of various cellular structures, such as the zona pellucida or blastomere symmetry in oocytes and embryos, respectively. However, these approaches are subject to limitations attributed to the variability in grading systems across clinics and grading subjectivity between embryologists. Furthermore, correlation between morphological features and actual quality remains contentious, with conflicting evidence suggesting that these features are unable to accurately predict viability. These limitations highlight the need for objective and reliable methods for assessing oocyte and embryo quality and light-based technologies may offer a solution.

Currently, light-based technologies, such as those used for label-free fluorescent imaging, offer a promising approach for the objective assessment of intrinsic properties that are reflective of cellular health. Although these techniques are powerful in their ability to view these properties in a label free manner, they are unable to directly measure the physical properties of the cell microenvironment. In other cell types, the mechanical property of their microenvironment is correlated with viability [41, 42, 46].

Whether this applies to oocytes and embryos remains to be determined. The studies described in this thesis explore the use of light-based techniques, specifically optical tweezers for passive microrheology, to reveal that the viscosity of the microenvironment provides valuable insights into oocyte viability and embryo development. The promising results of these studies highlight a potential non-invasive method to objectively evaluate oocyte and embryo viability, which would be highly beneficial in improving IVF success. As light-based technologies, such as optical tweezers and optical imaging methods, gain prominence in ART, it is critical to understand how light exposure impacts embryo health. In standardising exposure and accounting for energy differences, my results demonstrate that exposure to different wavelengths across the visible range, has varying effects on the developing embryo. This section of my thesis highlights the importance of judicious selection of light exposure parameters for optimising embryo health.

5.2 Optical tweezers for the objective measurement of the oocyte and embryo microenvironment

In **Chapter 2**, I used the optical tweezers for passive microrheology to quantify the viscosity of the oocyte microenvironment. I observed differences in viscosity that were associated with developmental potential. While simply tracking particle motion without the tweezers can be performed to measure viscosity, the use of optical tweezers in this study enabled maintenance of particle motion within a defined region, which allowed for measurements to occur over an extended period. This enabled precise characterisation of the viscosity of the extracellular matrix (ECM) within a microlitre volume. My results demonstrated that the viscosity of the cumulus-oocyte matrix following maturation was positively correlated with its developmental competence post-fertilisation. To the best of my knowledge, these results are the first to show an association between cumulus matrix viscosity and oocyte developmental potential. Thus, measuring the viscosity of the cumulus-oocyte matrix has the potential to become a non-invasive, and objective predictor of oocyte viability. As this matrix and associated cumulus cells are typically trimmed

and discarded prior to fertilisation, my approach to measuring the viscosity of this isolated cumulus matrix is also clinically viable. Future studies could extend this work by investigating whether the viscosity of the ECM is (1) directly correlated with oocyte developmental potential (taking measurements of cumulus matrix from a single oocyte and correlating with development post-fertilisation) and (2) extending this assessment by taking resultant embryos and recording developmental outcomes post-embryo transfer (e.g., implantation success, pregnancy success, and foetal health). Although my results demonstrate the potential of cumulus matrix viscosity as a predictor of oocyte developmental competence, a positive correlation between cumulus matrix viscosity and pregnancy outcomes would further strengthen the potential of this approach to become an objective method of predicting IVF success.

Building on the promising results in **Chapter 2**, **Chapter 3** describes my use of the optical tweezers to measure the viscosity of the microenvironment surrounding pre-implantation embryos. This microenvironment is highly dynamic, comprising of several factors that are essential to embryo development. Amongst the substrates present in this microenvironment is lactate, a metabolic byproduct of glycolysis. As the embryo's metabolic demands increase with development, its primary metabolic pathway shifts from predominantly oxidative phosphorylation to glycolysis, leading to a significant increase in lactate concentrations within the surrounding microenvironment. While a previous study in blood has shown that high concentrations of lactate increase its viscosity, whether the same phenomena occurs in the embryo microenvironment has yet to be determined. Building on this foundational knowledge, I applied optical tweezers to measure the viscosity of the surrounding microenvironment in 4 cell- and blastocyst-stage embryos. Excitingly, I identified a viscous microenvironment in both embryos, with viscosity being significantly higher in the microenvironment surrounding blastocyst-stage embryos. Further measurements on an isolated 4 cell or blastocyst embryo revealed that this microenvironment was heterogeneous, and that viscosity generally decreased with increasing measurement distance from the embryo. This study was the first of its kind to identify a viscous microenvironment surrounding the pre-implantation embryo. Additionally, similar to oocytes, this study was the first to employ optical

tweezers as a method to measure the viscosity of the microenvironment surrounding pre-implantation embryos. However, in contrast to the oocyte measurements of **Chapter 2**, where the ECM was isolated, the measurements here were performed adjacent to the embryo. I observed a notable influence of the zona pellucida when such measurements occurred close to the embryo. Although insightful, the role of hydrodynamics (Faxén's correction) that accounts for this effect may to be investigated in more detail due to the assumptions on the lack of curvature and rigidity of the embryo zona pellucida, which is both curved and softens during development. Future studies should first aim to identify an accurate method to account for the observed effect of surface proximity on the viscosity measurements performed on the embryo. Potential methods to obviate this interaction between the particle and the zona pellucida are discussed further in **Chapter 5.4.4**. Future studies should employ a component analysis method to identify the composition of this microenvironment through specific dyes or techniques like mass spectrometry. This measurement could provide complementary biochemical information on the specific concentration of lactate, which could also be corroborated with embryo developmental competence, implantation, and pregnancy outcomes. The results from these studies would strengthen the existing results, enhancing our current understanding on how (1) the viscosity of the microenvironment changes during development, and (2) whether the viscosity of this microenvironment can be an objective predictor of IVF success.

5.3 Implications of light exposure on pre-implantation embryo development

Chapters 2 and **3** demonstrates the potential of light-based technologies for advancing ART, particularly in providing a means to objectively quantify the viscosity of the microenvironment surrounding oocytes and embryos. However, despite the increasing implementation of light-based technologies in ART, the effects of light exposure on in vitro embryo development remains poorly understood. Though previous studies have sought to identify the impact of light exposure on embryos, significant variations in

experimental parameters led to large discrepancies in results between studies. As a result, there remained a lack of clinically relevant conclusion on (1) the impact of light and (2) the specific impact of discrete wavelengths of light exposure on the developing embryo. In **Chapter 4**, I addressed this gap by investigating the influence of four discrete wavelengths, that are typical in imaging modalities such as confocal or hyperspectral microscopy, on the development and health of pre-implantation embryos. My results revealed wavelength-specific effects following daily exposure on several key developmental outcomes, including blastocyst formation, DNA integrity, cellular lineage allocation, lipid abundance, pregnancy rates, and pre-natal outcomes. Interestingly, my findings contrast current beliefs that longer wavelengths are safer. My results showed that longer wavelengths (yellow and red) were as damaging to embryo health as the shorter wavelengths (blue and green). This work emphasises the need for careful consideration of light exposure in ART, as different wavelengths can exert multifaceted, and at times damaging effects on the embryo and resultant offspring. Given that this thesis uses Near-Infrared (NIR) light for optical trapping, a logical progression of this work would be to investigate how exposure to NIR light impacts the developing embryo. Characterising the impact of NIR exposure, in a manner similar to what was performed in **Chapter 4**, would provide crucial insight on the parameters required for the safe use of optical tweezers within the IVF clinic.

5.4 Future directions:

5.4.1 Investigating the impact of different in vitro maturation conditions on oocyte viability using optical tweezers

During oocyte maturation, cumulus cells surrounding the oocyte synthesise and release an extracellular matrix (ECM), which is important for oocyte viability. In this thesis, I demonstrated the capability of the optical tweezers to measure significant differences in viscosity between high- and low-viability oocytes, providing a non-invasive and objective method to measure embryo developmental competence. This study was the first to showcase the use ECM viscosity as a predictor for embryo developmental competence. While the study uses two distinct maturation models to generate oocytes of varying viability,

a future direction of this work could look to employ a third maturation method. Specifically, a compromised in vitro model that uses different additives to generate an oocyte of even lower viability would be beneficial in identifying whether the same correlation exists between three maturation models. As the current in vitro model utilised additives like epidermal growth factor, fetal calf serum and follicle stimulating hormone to promote cumulus expansion, potentially enhancing embryo developmental competence, culturing oocytes without these additives would provide a model for reduced viability [160-164]. The result from such a study would be highly informative in assessing the sensitivity of the optical tweezers in distinguishing between the ECM of oocytes matured under different in vitro conditions. Establishing its sensitivity would also help determine its potential as an objective method for assessing oocyte viability following in vitro maturation in the IVF clinic. Longitudinally, this result could reduce the number of IVF cycles required for a successful IVF outcome.

It is interesting to consider whether optical tweezers might ultimately be used in the IVF clinic. My data shows promise for detailed and informative microrheology measurements on the ECM. Whilst our lab based optical tweezers had typical dimensions of around 1m x 0.5m x 0.5 m (w x h x d), the optical path and system may readily be compacted down to a monolithic footprint of approxmately 30cm x 30cm x 20cm, making it a benchtop device. The advances in solid state lasers in the near infra-red mean the laser itself would be incorporated into this footprint. In terms of practicality, there would be a need for a trained operator/user to load particles and take measurements, the overall workflow would mean measurements could be performed within a timeframe of 10-20 minutes making it an attractive proposition for inclusion in a clinical setting.

5.4.2 Correlating cumulus-oocyte matrix viscosity with reproductive outcomes

While **Chapter 2** demonstrated that the viscosity of the cumulus-oocyte matrix is correlated with oocyte viability, additional studies are required to further elucidate how ECM viscosity may be predictive of broader reproductive outcomes. A natural progression of this study would be to assess how ECM viscosity correlates with pregnancy success, live birth rates, and post-natal outcomes of oocytes matured

under the two conditions described in **Chapter 2**. Considering the established importance of specific genes, such as HAS2, in influencing implantation success [62, 63], this study would provide substantial insights into how matrix viscosity might serve as a predictive marker for oocyte competence beyond embryo development. The outcomes of this study would not only enhance current understanding of the relationship between oocyte viability and ECM viscosity, but also position the optical tweezers as a key tool for assessing oocyte quality, with the potential to improve IVF outcomes.

5.4.3 Measuring the ECM from the same oocyte to be fertilised

To further enhance the clinical applicability of optical tweezers for oocyte viability assessments**,** the proposed studies in **Sections 5.4.1** and **5.4.2** could also modify the current experimental parameters by performing a longitudinal study of taking single oocytes, removing and measuring the oocyte ECM, fertilising the oocyte, assess its embryo developmental competence, and then implant it into pseudopregnant females to assess post-natal outcomes. If successful, such a study would solidify the connection established in **Chapter 2**, creating a cohesive link between ECM viscosity and IVF outcomes.

5.4.4 Reducing the hydrodynamic interactions between the trapped particle and the embryo zona

In **Chapter 3**, I demonstrated that the optical tweezers was capable of identifying a viscous microenvironment surrounding the embryo at different developmental stages. As these measurements were performed adjacent to the embryo, I investigated whether proximity to the zona pellucida surrounding embryos influenced my results by comparing the mean viscosity with Faxén's corrected viscosity for both parallel and perpendicular measurements. This comparison showed that the microenvironment immediately adjacent to the embryo (5 μm) was unexpectedly more viscous, leading to lower viscosity measurements than what was expected in the corrected viscosity. This suggests that the embryo zona at this distance interfered with the viscosity measurements. While these results provide insight into the potential influence of the zona pellucida, they should be interpreted with caution due to assumptions in Faxén's correction, particularly regarding the lack of curvature and rigidity of the zona

pellucida, which is inaccurate given its curved and non-rigid nature. The rigidity of the zona pellucida has been observed to soften with development [157]. Previous characterisation of the zona pellucida revealed that it initially hardens following fertilisation, but softens as embryo development progresses [165]. The degree to which this softening impacts the measurement of viscosity with optical tweezers is yet to be determined. Additionally, to minimise any impact of the zona pellucida on viscosity measurements, future studies could measure viscosity at greater distances from the embryo, starting at 10 and increasing by 1 um to precisely characterise the optimal measurement distance. Finally, as my viscosity measurements in **Chapter 3** were based on *x* axis particle motion, future studies should also assess viscosity in both the *x* and *y* axis to improve the accuracy of measurements. Building on the exciting findings in **Chapter 3,** future research should address the experimental limitations and optimise methods to enable precise microrheological measurement of the embryo microenvironment as it may offer valuable insights for predicting IVF outcomes.

5.4.4 Corroborating concentrations of lactate with embryo development and pregnancy outcomes

In **Chapter 3**, I observed a significantly higher microenvironment viscosity in the blastocyst-stage embryo, which may be attributed to increased lactate concentrations, an byproduct of glycolysis [75, 116]. This study is the first to show developmental-stage differences in the viscosity of the embryo microenvironment, which we attributed to increased lactate secretions reported previously [74]. However, whether lactate is the sole contributor this viscosity and whether elevated lactate levels in the microenvironment is a predictor for embryo developmental competence, implantation success, and pregnancy success remains to be determined. Future experiments could thus quantify lactate levels at various developmental stages using assays or mass spectrometry, correlating the quantified concentrations with developmental outcomes and viscosdity. Additionally, inhibition of glycolysis, through treatment with YZ9, could also be used to assess how reduced lactate production affects viability and the viscosity of the microenvironment. Embryos with inhibited lactate production could be transferred into

pseudopregnant mice in these experiments to evaluate the impact of lactate levels on implantation and pregnancy success. These studies would aid in establishing whether the increased microenvironment viscosity that I measured in **Chapter 3**, can serve as a predictive marker for clinical outcomes.

5.4.5 Measuring the elastic property of the oocyte and embryo microenvironment

In both **Chapters 2** and **3**, I demonstrated that optical tweezers were effective in measuring the viscosity of the microenvironment surrounding oocytes and embryos. Although quantifying viscosity provides valuable insights into the fluid-like property of the microenvironment, it is equally important to assess its elasticity, which determines its stiffness and resistance to forces. Several microrheological studies have highlighted that cell microenvironments demonstrate a unique combination of viscosity and elasticity, referred to as viscoelasticity, which influences cell processes like spreading and differentiation [166, 167]. A future direction of the studies in this thesis would be to also assess the elasticity of the oocyte ECM and the embryo microenvironment to determine whether the same correlations/trends exist. The results from this study would provide a more comprehensive understanding of the properties that are present in the oocyte and embryo microenvironments and their correlation with viability and quality. Additionally, the elastic responses may also complement the insights gained from the viscosity measurements performed in this thesis further enhancing the importance of the optical tweezers as a novel tool in ART.

5.4.6 Investigating the safety of near-infrared light exposure on developing embryos

Chapters 2 and **3** demonstrate the potential of optical tweezers as a novel tool for the objective measurement of viability. To further enhance whether this technique may be applicable to the clinic, analysis on the potential effects of near-infrared (NIR) light exposure on embryo development, specifically within the 700 – 1400 nm range, should be performed in a manner similar to that conducted in **Chapter 4**. Specifically, a comprehensive safety study, measuring both the direct phototoxic effects and indirect thermal effects NIR light exposure has on blastocyst development, DNA integrity, cellular metabolism, and cell lineage allocation would be informative on addressing the safety of NIR light exposure. This work

would not only be useful in establishing safety guidelines for the clinical application of optical tweezers in ART, but also provide a foundation for further optimisation of NIR light exposure parameters in IVF protocols to mitigate light induced damage.

5.5 Summary

In summary, the work in this thesis highlights the potential of optical tweezers for assessing the microenvironment as a predictor of oocyte viability, embryo development, and IVF success. By enabling objective measurements of viscosity, microrheology with optical tweezers presents a novel approach to directly measure physical properties that may be indicative of oocyte viability and embryo development, obviating the limitations associated with current morphological assessments. The work in this thesis also underscores the importance of judicious choice of wavelength, given that I found wavelength-specific impacts on embryos following exposure. Collectively, this work demonstrates the promise of light-based technologies in ART and that further efforts in this area are warranted. Future studies would also advance our understanding of how the microenvironment affects oocyte and embryo development. Further research is essential in moving toward developing this technique for future clinical implementation to improve patient outcomes.

5.6 References

1. Organization, W.H., *WHO fact sheet on infertility*. 2021, LWW. p. e52.
2. Organization, W.H., *Infertility prevalence estimates, 1990–2021*. 2023: World Health Organization.
3. Newman, J.E., Paul, R.C., and Chambers G.M., *Assisted reproductive technology in Australia and New Zealand 2021.* National Perinatal Epidemiology and Statistics Unit, The University of New South Wales: Sydney., 2023.
4. Dzamba, B.J. and D.W. DeSimone, *Extracellular matrix (ECM) and the sculpting of embryonic tissues.* Current Topics in Developmental Biology, 2018. **130**: p. 245-274.
5. Elosegui-Artola, A., *The extracellular matrix viscoelasticity as a regulator of cell and tissue dynamics.* Current Opinion in Cell Biology, 2021. **72**: p. 10-18.
6. Wilems, T., S. Vardhan, S. Wu, and S. Sakiyama-Elbert, *The influence of microenvironment and extracellular matrix molecules in driving neural stem cell fate within biomaterials.* Brain research bulletin, 2019. **148**: p. 25-33.
7. Downs, S.M., *Specificity of epidermal growth factor action on maturation of the murine oocyte and cumulus oophorus in vitro.* Biology of reproduction, 1989. **41**(2): p. 371-379.
8. Das, K., W.R. Phipps, H.C. Hensleigh, and G.E. Tagatz, *Epidermal growth factor in human follicular fluid stimulates mouse oocyte maturation in vitro.* Fertility and sterility, 1992. **57**(4): p. 895-901.
9. De La Fuente, R., M.J. O'Brien, and J.J. Eppig, *Epidermal growth factor enhances preimplantation developmental competence of maturing mouse oocytes.* Human Reproduction, 1999. **14**(12): p. 3060-3068.
10. Buccione, R., B.C. Vanderhyden, P.J. Caron, and J.J. Eppig, *FSH-induced expansion of the mouse cumulus oophorus in vitro is dependent upon a specific factor (s) secreted by the oocyte.* Developmental biology, 1990. **138**(1): p. 16-25.

11. Chen, L., S. Mao, and W.J. Larsen, *Identification of a factor in fetal bovine serum that stabilizes the cumulus extracellular matrix. A role for a member of the inter-alpha-trypsin inhibitor family.* Journal of Biological Chemistry, 1992. **267**(17): p. 12380-12386.

12. Gebhardt, K.M., D.K. Feil, K.R. Dunning, et al., *Human cumulus cell gene expression as a biomarker of pregnancy outcome after single embryo transfer.* Fertility and sterility, 2011. **96**(1): p. 47-52. e42.

13. Wathlet, S., T. Adriaenssens, I. Segers, et al., *Cumulus cell gene expression predicts better cleavage-stage embryo or blastocyst development and pregnancy for ICSI patients.* Human Reproduction, 2011. **26**(5): p. 1035-1051.

14. Murayama, Y., J. Mizuno, H. Kamakura, et al., *Mouse zona pellucida dynamically changes its elasticity during oocyte maturation, fertilization and early embryo development.* Human cell, 2006. **19**: p. 119-125.

15. Kim, J. and J. Kim, *Viscoelastic characterization of mouse zona pellucida.* IEEE Transactions on Biomedical Engineering, 2012. **60**(2): p. 569-575.

16. Clough, J. and D. Whittingham, *Metabolism of [14C] glucose by postimplantation mouse embryos in vitro.* Development, 1983. **74**(1): p. 133-142.

17. Gardner, D.K. and A.J. Harvey, *Blastocyst metabolism.* Reproduction, Fertility and Development, 2015. **27**(4): p. 638-654.

18. Gott, A., K. Hardy, R. Winston, and H. Leese, *Non-invasive measurement of pyruvate and glucose uptake and lactate production by sigle human preimplantation embryos.* Human Reproduction, 1990. **5**(1): p. 104-108.

19. Chaudhuri, O., L. Gu, M. Darnell, et al., *Substrate stress relaxation regulates cell spreading.* Nature communications, 2015. **6**(1): p. 6365.

20. Nam, S., R. Stowers, J. Lou, et al., *Varying PEG density to control stress relaxation in alginate-PEG hydrogels for 3D cell culture studies.* Biomaterials, 2019. **200**: p. 15-24.

Chapter 6
Appendix

6.1 Adelaide Optical Tweezers system

6.1.1 Diagram of the optical tweezers instrument

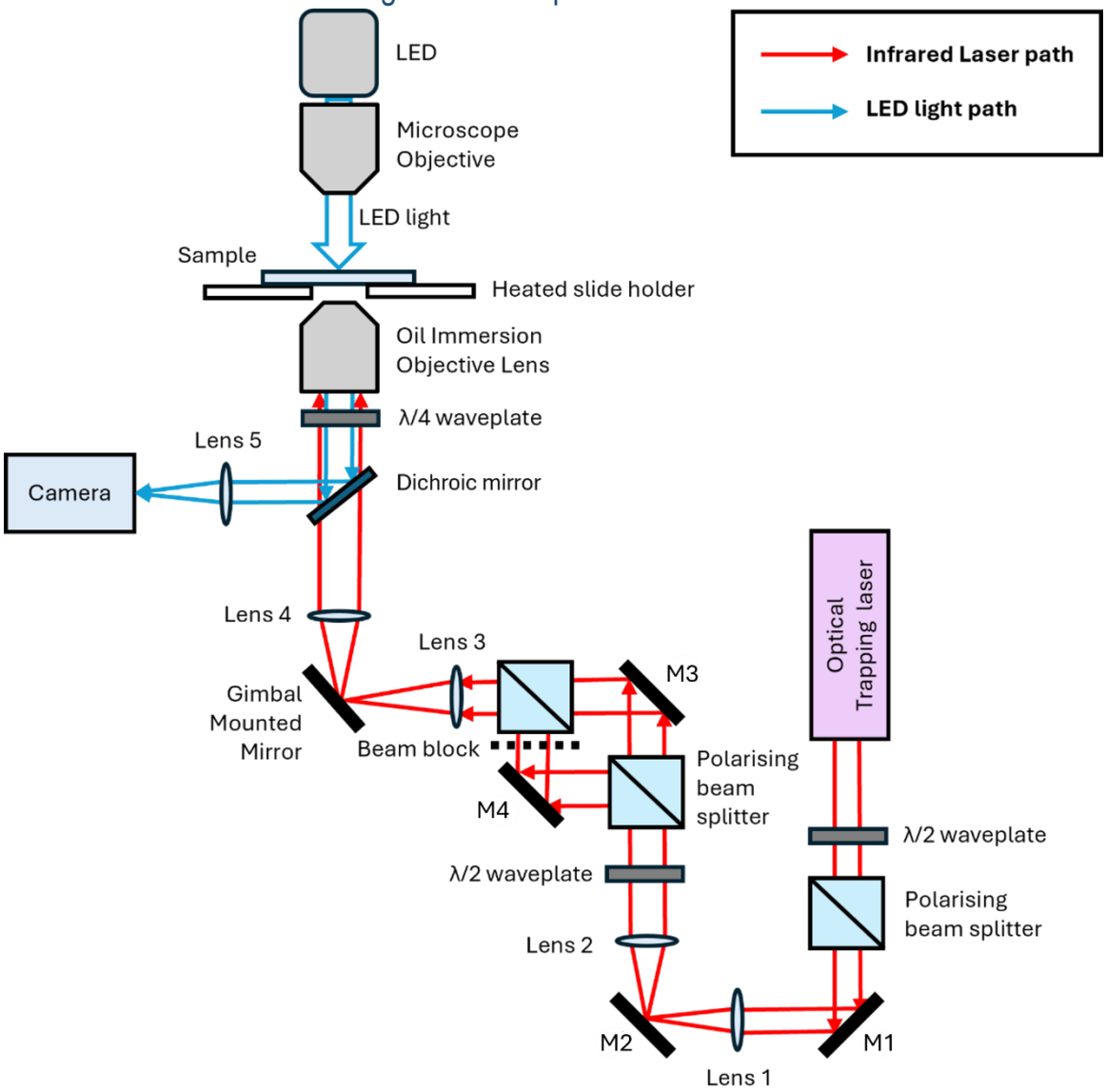

Figure 1. Schematic diagram of the optical tweezers system used in Chapter 2. A 100x oil immersion microscope objective collects transmitted light (green) and directs the trapping laser (red) to the sample. Lenses 1-4 (L1 (75mm) and L2 (150mm)) and (L3 (75mm) and L4 (100mm)) function as a beam expander, allowing over-filling of the back aperture of the 100x objective. To restrict the system to a single optical trap, a beam blocker (dashed line) was applied. A gimbal-mounted mirror between Lens 3 and 4 allowed for the adjustment of the optical trap's position along the *x*- and *y*-axes. Dimensions are not to scale.

6.1.2 Optical tweezers setup for the microrheology of the cumulus-oocyte matrix

Figure 1 shows a schematic of the optical tweezers system used to measure the viscosity of the cumulus-oocyte matrix, based on the setup described in Fallman and Axner (1996) [168].The optical trap was generated using a 1064-nm continuous wave laser (Coherent Mephisto) with a maximum power output of 2 W, passing through a high NA oil-immersion objective lens (Nikon CF1 E Plan Achromat, 100x, NA 1.25; Nikon) creating a laser spot size of approximately $1/_{(2A)}$ = 0.4 µm. The laser was set to be linearly polarised using a polarising beam splitter (PBS), with fine tuning of the laser power achieved using a half-waveplate (½) and second PBS. To ensure the trapping laser overfills the back aperture of the objective, two beam expander systems consisting of four lenses (L1 (75mm) and L2 (150mm)) and (L3 (75mm) and L4 (100mm)) were used. As this optical tweezers system can generate two optical traps, we applied a beam blocker (dashed line) on one arm of the Mach Zender-like arrangement resulting in only a single optical trap at the site of the sample. A 4f relay system, comprised of a mounted mirror and two lenses (L3 and L4), functions as a telescope. In this setup, the distance between L3 and L4 was equal to the sum of their focal lengths (75mm and 100mm, respectively), with a mounted mirror positioned between the lenses. This configuration makes the back aperture conjugate to the optical trap where tilting the mirror changes the x and y position of the trap within the sample plane while also maintaining the same degree of overfilling at the back aperture of the microscope objective. To image the particle, a 400-700nm, white light LED (Thorlabs MWWHL4) illuminated the sample from above through a long working distance 20x magnification microscope objective (Mitutoyo M Plan Apo NIR) with NA = 0.4. The sample imaging path consisted of the white light passing through: the 100x magnification microscope objective that created the optical trap, a longpass dichroic filter (900nm) which separated the white light from the 1064nm trapping laser, and an imaging lens (L5 (100mm)) which focused the white light into the Basler ace U camera (Basler ACA1440-220um). Image magnification was determined using a 1951 USAF resolution test target, which defined how well our camera could distinguish fine details between calibrated lines at each magnification. The Basler ace U camera acquired images at a magnification of 49x, or 69.5 nm/pixel scaling. By confining the region of interest to a 36 x 36 pixel, data transfer requirements were

reduced allowing the camera to acquire images at a rate of approximately 3,000 frames per second. Indirect damage caused by laser heating on the sample was minimised by using a 1064 nm laser, which is weakly absorbed by water, and a low trap power (0.4 mW at the sample) was used throughout data collection. A heated three-axis translation stage (set at of 37°C) was used to: control both the lateral and axial trapped particle position and maintain the biological viability of the matrix sample. To determine trap stiffness and the viscosity of our samples, an autocorrelation analysis of particle position was performed, and this is thoroughly described in **Chapter 2**.

Chapter 2.4 Figure 1 (page 52) presents a visual render of the imaging path components, including lens L3, the gimbal-mounted mirror, lens L4, lens L5, and the Basler ace U camera. This schematic focuses on the path relevant to sample imaging. A more complete and updated optical diagram, including the full telescope arrangement that makes the mirror (labelled M3) conjugate with the back focal plane of the objective (as standard in optical trapping systems), is provided in **Chapter 6.1.1.**

6.1.3 Definition and Rationale for 2D Gaussian Fitting Method used in Chapter 2.4

Gaussian Fitting Method – University of Adelaide

At the University of Adelaide, particle tracking was achieved through fitting a two-dimensional (2D) Gaussian function to the bright-field image of the bead in each video frame. The Gaussian took the following form:

$$I(x,y) = z_0 - A \cdot \exp\left(-\frac{(x-x_0)^2 + (y-y_0)^2}{2\sigma^2}\right) \quad (1)$$

In this equation, z_0 describes the background intensity or the baseline bright-field illumination; A describes the shadow depth, which indicates the darkness of the bead relative to the background; σ depicts the width of the Gaussian, approximating the bead size within the region of interest; and x_0, y_0 represent the

coordinates of the particle centre. The primary parameters of interest were x_0 and y_0, which represent the particle's position and were used in microrheological analysis. The remaining parameters were fixed following an initial calibration. This reduction in free parameters substantially improved computational speed and reduced overfitting, while preserving the sub-pixel resolution accuracy of particle localisation. Gaussian fitting is particularly advantageous in bright-field imaging, where edges are diffuse and conventional thresholding may lead to greater positional uncertainty.

Centre-of-Mass Tracking – University of Nottingham

In contrast, the setup at the University of Nottingham, described in **Chapter 3** employed a centre-of-mass tracking approach. Prior to acquisition, a manual threshold was applied to isolate the foreground (the particle) from the background within a tightly defined region of interest. The particle's centre became the only high-intensity feature within the frame, enabling calculation of its position based on the intensity-weighted centroid. This method allowed for high-throughput processing and real-time tracking of particle motion over prolonged videos (up to 300,000 frames at ~300 fps) using a custom tracking script in Micro-Manager software.

Comparative Assessment

Both methods ultimately derive viscosity from Brownian particle motion and apply standard microrheological analysis (e.g., autocorrelation, Normalised Position Autocorrelation Function. The Gaussian fitting method offers improved localisation precision and robustness to noise, especially in bright-field conditions, but at the cost of increased computational demand. The centre-of-mass method, while faster and simpler, may be more sensitive to illumination artefacts or uneven contrast, as indeed seen in the Nottingham setup. Importantly, both approaches were validated independently using standard fluids, and measurements were internally consistent within each setup. Therefore, despite differences in localisation methodology, the overall viscosity measurements remain methodologically comparable.

6.1.4 References

1. Fällman, E. and O. Axner, Design for fully steerable dual-trap optical tweezers. Applied Optics, 1997. 36(10): p. 2107-2113

6.2 Supplementary Materials

6.2.1 Supplementary Material: The effect of discrete wavelengths of visible light on the developing murine embryo

Carl A. Campugan[1,2,3], Megan Lim[1,2,3], Darren J. X. Chow[1,2,3], Tiffany C. Y. Tan[1,2,3], Tong Li[1], Avishkar A. Saini[1,2,3], Antony Orth[4], Philipp Reineck[5], Erik P. Schartner[2,3,6], Jeremy G. Thompson[1,2,3,7], Kishan Dholakia[8,9,10], Kylie R. Dunning[1,2,3]

[1]School of Biomedicine, Robinson Research Institute, The University of Adelaide, Adelaide, SA 5005, Australia

[2]Australian Research Council Centre of Excellence for Nanoscale BioPhotonics, The University of Adelaide, Adelaide, SA 5005, Australia

[3]Institute for Photonics and Advanced Sensing, The University of Adelaide, Adelaide, South Australia, Australia

[4]National Research Council of Canada, Ottawa, Ontario, Canada

[5]Australian Research Council Centre of Excellence for Nanoscale BioPhotonics, School of Science, Royal Melbourne Institute of Technology, Melbourne, VIC 3000, Australia

[6]School of Physical Sciences, The University of Adelaide, Adelaide, SA 5005, Australia

[7]Fertilis Pty Ltd, Adelaide, South Australia 5005, Australia

[8]School of Physics and Astronomy, University of St Andrews, North Haugh, Scotland KY16 9SS, UK

[9]School of Biological Sciences, The University of Adelaide, Adelaide, SA 5005, Australia

[10]Department of Physics, College of Science, Yonsei University, Seoul 03722, South Korea

Supplementary Figure 2. No impact on embryo cleavage rates following exposure at the 1-cell stage to (a) blue, (b) green, (c) yellow, and (d) red wavelengths. Data are presented as mean ± SEM, from 3 independent experimental replicates; n = 26-29 embryos per group. Data were analyzed using a Mann-Whitney test.

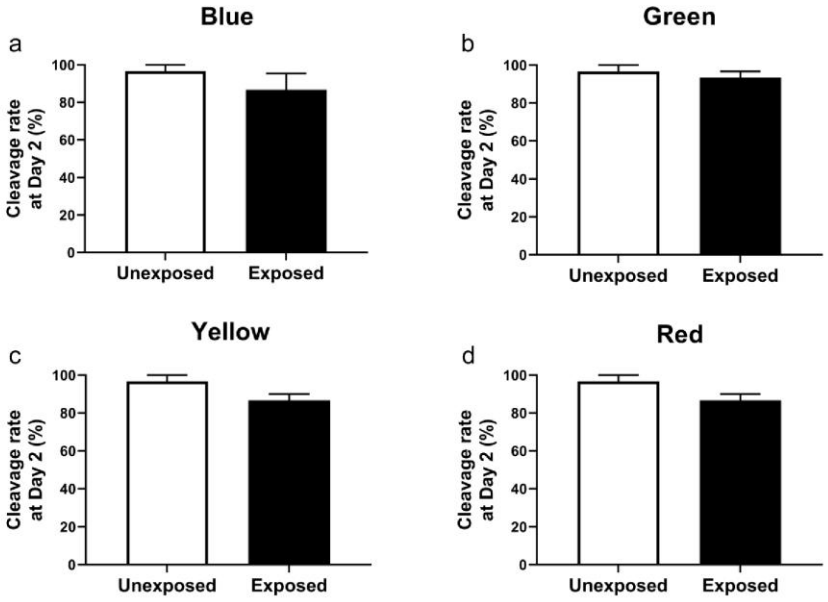

Supplementary Table 1. Duration of exposure for each wavelength to achieve uniform energy dose of 25.5 mJ/cm^2.

LED (wavelength)	Power (mW/cm^2)	Duration in secs
Blue (470 nm)	1.482	17.2
Green (520 nm)	0.296	86.1
Yellow (590 nm)	0.266	96.0
Red (620 nm)	0.955	26.7

Supplementary Table 2. Duration of exposure for yellow and red wavelengths to achieve a uniform energy dose of 25.5 mJ/cm^2 (single exposure) or 51 mJ/cm^2 (double exposure).

LED (wavelength)	Power (mW/cm^2)	Single exposure duration (sec)	Double exposure duration (sec)
Yellow (590 nm)	0.266	96.0	192
Red (620 nm)	0.955	26.7	53.4

Supplementary Table 3. Individual weight (g) of pups at weaning. Pups derived from blastocyst-stage embryos that were either unexposed, or exposed to red or yellow wavelength during preimplantation development.

	Weight of pups at weaning (g)		
Pup number	Unexposed	Yellow	Red
1	13	12	13
2	11	11	14
3	12	13	15
4	12	12	18
5	13	12	18
6	13	13	16
7	12	12	16
8	13	14	16
9	11	14	12
10	13	13	11
11	11	14	13
12	12	12	12
13	12	14	10
14	9	16	11
15	11	14	13
16	13	14	12
17	7	16	11
18	9	15	12
19	12		14
20	11		13
21	12		12
22	11		14
23	13		12
24	11		13
25	11		12
26	9		12
27	9		12
28	13		15
29	12		12
30	13		13
31			14
32			12
33			13
34			14
35			12